Department of Chemical Engineering

Catalysis Institute

Selective production of nitrogen-containing compounds via a modified Fischer-Tropsch process

Danielle Sympathie Goho

BSc Hons (Chemical Engineering), UCT

Supervisors:

Prof Michael Claeys

Associate Prof Nico Fischer

Dr. Mohamed Fadlalla

Key Words: Fischer-Tropsch synthesis, Iron-based catalysts, Oxygenates, Nitrogen-containing compounds

Thesis submitted to the University of Cape Town in partial fulfilment of the academic requirement for the degree of **Master of Science in Chemical Engineering**

October 2020

Plagiarism declaration

I, Danielle Sympathie Goho, know the meaning of plagiarism and declare that all the work in the document, save for that which is properly acknowledged, is my own. This thesis/dissertation has been submitted to the Turnitin module (or equivalent similarity and originality checking software) and I confirm that my supervisor has seen my report and any concerns revealed by such have been resolved with my supervisor.

Signed by candidate

_____

Danielle Sympathie Goho

Student Number: GHXDAN001

October 2020

Acknowledgements

I would like to thank my supervisors (Prof. Michael Claeys, A. Prof. Nico Fischer and Dr. Mohamed Fadlalla) for their guidance, advice and support throughout my project. A special word of thanks must go to Dr. Mohamed Fadlalla whose input, patience and help allowed me to learn so much throughout my master journey.

I would like to thank the Catalysis lab personal (Portia, Rachel, Chantal, Waldo and Edward) for their invaluable assistance and guidance in the lab and my research group members (Lindiwe, Khasu, Thulani, Shaine, Veroushia, Bongani, Dominic, Wiynand and Camila) for their support and advice.

I would like to express my sincere gratitude to the MasterCard Foundation Scholars Program for the financial support which allowed me to complete my master's degree and share my findings at the International Conference on Catalysis, Advanced Chemical Engineering and Technology, 2019, Valencia, Spain.

To my friends (Hermann, Othniel, Nogues, Stephane, Lesedi, Lennie and Lindiwe) and my siblings (Synthia, Sandrine, Stephanie and Eloge) a big thank for the moral support, encouragement and prayers.

Finally, I would like to dedicate this work to my Parents (Victor and Julienne Goho) for their love, kindness and trust. They have always been by my side believing in me and praying incessantly for my well-being and success. I will forever be gratefully to them.

Danielle Sympathie Goho

October 2020

Synopsis

The catalytic conversion of the syngas, *i.e.* carbon monoxide and hydrogen, known as the Fischer-Tropsch synthesis (FTS) process, has been widely used for the production of transportation fuels. In addition of the major products, *i.e.* olefins and paraffins, the FTS also leads to the formation of a small amount of oxygenates, considered as valuable chemicals used as feedstock in various industries processes. Due to the variety of products obtained from the FTS, several researches have been dedicated to the understanding of the FTS mechanisms, the development of new catalysts and the improvement of the process conditions for the production of valuable chemicals instead of transportation fuels.

The research led to the development of various catalysts allowing a high oxygenates selectivity. In addition, research on the addition of ammonia (NH_3) during the FTS, *i.e.* Nitrogen FTS (NFTS), pointed out that the co-feeding of NH_3 can result in the direct production of nitrogen-containing compounds (NCCs), *i.e.* nitriles, amines, amides, acetamides and formamides.

During further investigations on the NFTS performed over various iron (Fe) and cobalt (Co) based catalysts, a significant decrease in the oxygenates selectivity followed by the formation of NCCs were reported. Based on the correlation observed between the disappearance of oxygenates and the formation of NCCs, it has been speculated that oxygenates and/or their precursors are the precursors of NCCs during the NFTS. Based on this idea, it was further hypothesised that the use of a catalyst, yielding a high oxygenates selectivity under FTS conditions, will allow the selective production of NCCs under NFTS conditions.

The objectives of this study were to investigate the addition of NH_3 during the FTS over four catalysts which had been selected based on their relatively high oxygenates selectivity under FTS conditions. The investigation focused on the effects of the co-feeding of NH_3 on the catalytic activity, the formation and selectivity of both FTS products and NCCs.

The four selected catalysts, *i.e.* Fe,Mn-CuZnO; K,Al-Fe; 10 wt% Fe/Al_2O_3; K-CuFe/Silica catalysts were synthesised via a (co)precipitation and/or wet impregnation techniques described by Ding et al. (2013), Schaller et al. (2018), Pijolat & Perrichon (1985), and Ding et al. (2012b) respectively. The XRD and in-situ XRD analyses allowed to determine the different phases present in each of the catalysts in their calcined state and to investigate the phases reduction behaviour, respectively. In addition, the ICP-OES and BET analyses confirmed their actual composition and the presence of mesopores.

The catalyst testing was conducted in a fixed bed reactor at 240˚C with a total pressure of 20 bar, a space velocity of 6000 h^{-1}, a H_2/CO ratio of 2 and 10 vol% of the total flowrate being the

reference gas, argon. The catalyst testing was performed in three stages, *i.e.* 24 hours under normal FTS conditions (FTS-Before) followed by 6 hours of NH_3 co-feeding (NFTS) and 6 hours after returning to normal FTS conditions (FTS-after). To assess the effects of NH_3 co-feeding on the catalytic activity and the products formation, online GC-TCD analyses were performed continuously during all three stages while the product analysis was conducted via offline GC-FID and an online 2D-GC (TOF-MS & FID).

The co-feeding of NH_3 during the FTS over the four selected catalysts led to the formation of a variety of NCCs and a white solid, believed to be ammonium carbonate as confirmed by Alfred (1950) and Sango (2013). Moreover, it was observed that the type of catalyst used during the NFTS greatly affects the composition and nature of NCCs formed. Over the Fe,Mn-CuZnO catalyst, a selective production of nitriles with an overall selectivity of 17.9 C% was obtained while the formation of a mixture of NCCs made up of nitriles, amines, amides, acetamides and formamides with an overall selectivity of 3.2 C%, 3.3 C% and 3.8 C% was obtained during the NFTS over K,Al-Fe, 10 wt% Fe/Al_2O_3 and K-CuFe/Silica catalysts respectively. Additionally, the results obtained over all four catalysts pointed out that the co-feeding of NH_3 impacts on both the catalytic activity and the formation of the standard FTS products.

The co-feeding of NH_3, over the unsupported catalysts, *i.e.* Fe,Mn-CuZnO and K,Al-Fe, resulted in a significant deactivation of the catalysts while minimal changes in the CO conversion were observed over the supported catalysts, *i.e.* 10 wt% Fe/Al_2O_3 and K-CuFe/Silica. This indicated that the poisonous effect of NH_3 on the catalytic activity via the inhibition of the CO adsorption by the NH_3 species is less pronounced over the supported catalysts due to their stability compared to the unsupported catalysts. This may also be attributed to the interaction of the NH_3 species with the support leading to less effect on the reactions.

Additionally, the co-feeding of NH_3 resulted in a complete disappearance of CO_2 over all four selected catalysts, which suggested that the presence of NH_3 suppresses the formation of CO_2 via the water gas shift (WGS) reaction. However, the formation of a white solid and the occurrence of a pressure build-up during the NFTS, suggested that the CO_2, formed via WGS reaction, reacted further with the NH_3 species in presence of water to form ammonium carbonate as postulated by Alfred (1950) and Sango (2013).

The co-feeding of NH_3 also led to an increase in the CH_4 selectivity over the Fe,Mn-CuZnO and K-CuFe/Silica catalysts while a drop was obtained over the K,Al-Fe and 10 wt% Fe/Al_2O_3 catalysts. The increase in CH_4 selectivities observed over the Fe,Mn-CuZnO and K-CuFe/Silica catalysts suggested that the NH_3 species compete and limit the adsorption of the

CO while favouring the desorption of methyl surface species to form methane. From the drop in CH_4 selectivities observed over K,Al-Fe and 10 wt% Fe/Al_2O_3 catalysts, it can be assumed that the presence of NH_3 competes and limits the adsorption of both CO and H_2 species while restricting the desorption of methyl species and favouring their incorporation in the chain growth.

An increase in the olefin content was also observed as a result of the NH_3 co-feeding over the selected catalysts which suggested that the presence of NH_3 inhibits the hydrogenation reaction by reducing the amount of H_2 species available on the catalyst surface due to the competitive adsorption between NH_3 and H_2 species. Alternatively, the adsorption of the NH_3 species might have favoured the desorption and inhibited the re-adsorption of the olefins resulting in the inhibition of olefin secondary reactions and the high olefin content.

Over all four selected catalysts, the co-feeding of NH_3 during the FTS resulted in the significant decrease in the oxygenates selectivity followed by the formation of NCCs. It could then be assumed that the competitive adsorption between NH_3, CO and H_2 species limits the availability of CO and OH species, *i.e.* species responsible for the oxygenates formation, which inhibits the primary routes of oxygenates formation. Alternatively, the drop in the oxygenates selectivity could be attributed to the substitution of the CO and OH species by the NH_3 species into the final step of the oxygenates formation mechanism leading to the formation of NCCs while limiting the oxygenates formation. Furthermore, it could be assumed that the drop in the oxygenates selectivity might be due to the secondary reactions involving the oxygenates formed and the NH_3 species leading to the formation of NCCs as shown by De Vries (2017).

Table of contents

List of figures

List of tables

Nomenclature

Abbreviation/ Symbol	Description/Meaning
α-value	Chain growth probability
Al	Aluminium
ASF	Anderson-Schulz-Flory
BET	Brunauer-Emmett-Teller
CO	Carbon monoxide
CO2	Carbon dioxide
CH4	Methane
Cu	Copper
Co	Cobalt
Fe	Iron
FTS	Fischer-Tropsch synthesis
GC-TCD	Gas chromatography equipped with thermal conductivity detector
GC-FID	Gas chromatography equipped with flame ionization detector
2D-GC	Two-dimensional gas chromatography
GHSV	Gas hourly space velocity
H2	Hydrogen
H2O	Water
HTFT	High temperature Fischer-Tropsch
ICP	Inductively coupled plasma
K	Potassium
LTFT	Low temperature Fischer-Tropsch
Mn	Manganese
MS	Mass spectrometer
NCCs	Nitrogen-containing compounds

N2	Nitrogen
NFTS	Nitrogen Fischer-Tropsch Synthesis
NH3	Ammonia
O2	Oxygen
SiO	Silica
TOF-MS	Time-of-flight mass spectrometer
XRD	X-ray diffraction
Zn	Zinc

Chapter 1: Introduction

1.1. Background

The Fischer-Tropsch synthesis (FTS) process is a well-known process which consists of the catalytic conversion of the synthesis gas, *i.e.* hydrogen and carbon monoxide, into a wide range of valuable hydrocarbon-based products such as paraffins, olefins, oxygenates and aromatics (Claeys & Van Steen, 2004). These hydrocarbons are used as transportation fuels (gasoline, diesel and jet fuel) and the oxygenates as chemical feedstocks for various chemical processes in the petrochemical and pharmaceutic industries (Dry, 1981). Since its invention in the early 1900s by Franz Fischer and Hans Tropsch, the Fischer-Tropsch process has been dedicated to the production of transportation fuels (Schulz, 1999).

However, the production of transportation fuels and chemicals, is currently predominantly based on the crude oil refining process. Therefore, the economic viability of the FTS process is strongly dependent on the price of crude oil. In addition, due to the high capital and operating costs of the FTS process, the feasibility and profitability of this process are still questionable (Dry, 2002).

1.2. Context

In the attempt to make the FTS process more economically viable, over the past decades, several academic studies and industrial research have been dedicated to the development of new catalyst systems for a high production of valuable chemicals such as oxygenates, and nitrogen-containing compounds (NCCs).

On the industrial level, Sasol, known as the leader in the FTS field,has been developing and commercializing several iron-catalysed FTS processes over the past decades (Steynberg, 2004). The recent performance of the FTS refinery at Sasolburg, South Africa, after the switch in production from fuels to chemicals highlights the profitability of a FTS chemical refinery compared to a FTS fuels refinery (De Klerk et al., 2005). Synfuels China has also recently developed a new integrated FTS technology, *i.e.* high-temperature slurry-phase technology (HTSFTP^{TM}). This novel technology enhances thermal efficiency of the process and employs a highly active catalyst (Liu et al., 2010).

Intensive academic research performed on the production of oxygenates via the catalytic conversion of syngas, also led to the synthesis of various iron-based catalysts with high activity and oxygenate selectivity (Surisetty et al., 2011). Furthermore, the investigation of the addition of ammonia (NH_3) into the syngas during the FTS process revealed the possibility of producing

NCCs such as amides, amines and nitriles (Walter, 1958), (Kurtz, 1969), (Gredig et al., 1996), (Claeys et al., 2013). However, only a very limited number of studies focused on the co-feeding of NH_3 during the FTS process, *i.e.* Nitrogen Fischer-Tropsch synthesis (NFTS).

1.3. Problem statement

During the research on the NFTS, it had been reported that the production of NCCs was enhanced by the presence of oxygenates. Therefore, it is speculated that oxygenates and/or their precursors are the precursors of NCCs (Walter, 1958), (Kurtz, 1969), (Gredig et al., 1996), (Sango, 2013), (Rawoot, 2017), (De Vries, 2017). However, due to the complexity of the reactions occurring during the NFTS, a general gap in knowledge regarding the mechanisms of the NCCs formation is still existing. Thus, further investigations are required to confirm that the oxygenates are the main precursors for the NCCs formation during the NFTS and that higher NCCs selectivities can be achieved with catalysts which have high oxygenate selectivities in the absence of ammonia in the feed.

1.4. Overall objectives

The present project aimed to investigate the production of NCCs *via* the co-feeding of ammonia to the FTS process. The investigation focused on the correlation between the presence of oxygenates under the normal FTS conditions and the production of NCCs under the NFTS conditions. Additionally, this project investigated the suitability of various catalysts for the NFTS process.

1.5. Scope of project

In this project, four catalysts reported in literature to yield a relatively high percentage of oxygenates under FTS conditions, were synthesised and tested under both FTS and NFTS conditions. The scope of this project included the investigation of the effects of ammonia on the performance, *i.e.* catalytic activity and product selectivity, of the four selected catalysts. The selectivity of NCCs over these catalysts provided an indication of the suitability of these catalysts for the NFTS process and gave insights on the role of oxygenates in the formation of NCCs during the NFTS process.

The analysis of both FTS and NFTS products was performed via a state-of-the art two-dimensional gas chromatography (2D-GC) equipped with a Time-Of-Flight Mass Spectrometer (TOF-MS) and Flame Ionization Detector (FID) for accurate product identification and quantification, respectively.

Chapter 2: Literature review

2.1. Fischer-Tropsch synthesis

2.1.1. Evolution of the Fischer-Tropsch synthesis

In the 1920s, Franz Fischer and Hans Tropsch investigated the production of hydrocarbons from the hydrogenation of carbon monoxide (CO) over transition metal-based catalysts (Fischer & Tropsch, 1926). Further studies were performed to understand the mechanisms and improve the process which is now known as the Fischer-Tropsch synthesis (FTS) Process. The possibility to produce chemicals and transportation fuels from available resources such as coal, natural gas and biomass via the FTS, led to the process being considered as a potential alternative to the use of crude oil to produce these compounds. Thus, the FTS process has attracted a great attention as it limits the reliance on oil and fossils due to their declining availability and reduces the negative environmental impacts of these energy sources (Schulz, 1999).

The industrialization of the FTS process started in Germany in the early 1930s with the commission of the first industrial FTS plant by Ruhrchemie. The interest in the FTS process increased significantly in the 1970s due to the forecasted depletion of the world's oil reserves. The development of the process was then marked by the commission of several FTS plants across the world, *i.e.* in the United States of America, Britain, Japan, France and South Africa (Mahmoudi et al., 2017). However, the increase in the FTS operation was short lived due to an increase in the price of natural gas and the discovery of low cost and large volume crude oil reserves in the Middle East in 1955, which resulted in most of the FTS plants being decommissioned (Dry & Steynberg, 2004). Therefore, the FTS development and industrial application was found to be strongly dependent on the crude oil price and performance of the petroleum industry (Dry, 2002).

Despite the low price of crude oil over the past decade, a great interest in the FTS process has developed due to the availability of low-cost natural gas and coal and the environmental demands governed by the energy saving policies. The urgent need for the reduction of carbon dioxide (CO_2) emissions and the substitution of fossil fuels by renewable feedstocks to limit global warming has also been heightening interest in the FTS process. Thus, a considerable amount of research has been dedicated to the optimisation of the FTS process for the production of clean transportation fuels (Schulz, 1999).

Research focused on:

- the improvement of the understanding of the mechanisms and kinetics of the FTS reactions (Glasser et al., 2012),
- the development of catalysts and reactors (Zhang et al., 2013) and
- the optimisation of the FTS reaction conditions (Dry, 2002).

This research led to the development and commercialisation of several improved FTS technologies (van de Loosdrecht et al., 2013). As the pioneer in the FTS field, in the early 1950s, Sasol commercialised, the Fe-catalysed FTS based on the Ruhrchemie catalyst to produce synthetic petroleum using Arge tubular fixed bed reactor. The Arge tubular fixed bed reactor technology was later combined with a slurry-bed reactor to enhance the production of long chain hydrocarbons for the wax industry. To allow the production of short chain hydrocarbons used as fuel and chemical feedstock, an improved fixed fluidized bed technology based on a fused iron catalyst operating at high temperature, *i.e.* 330-350° C, was developed and commercialised by Sasol in the late 1990s (Steynberg, 2004). This technology largely replaced the circulating fluidized bed reactors. Most recently, an integrated FTS technology, named the high-temperature slurry-phase technology (HTSFTP^{TM}), which uses an iron-based catalyst, was developed and commercialised by Synfuel China (Liu et al., 2010).

In addition to transportation fuels, the FTS process can also be used to produce valuable chemicals, *i.e.* waxes, olefins and oxygenates, which can be further processed to *e.g.* polymers and surfactants. Thus, the FTS process has recently attracted more academic and industrial attention. Investigations on the production of methanol, higher alcohols and mixed alcohols from the hydrogenation of CO under FTS typical conditions have been performed (Surisetty et al., 2011). Regardless of the development of the commercialized FTS processes for the production and extraction of valuable chemicals such as olefins, alcohols, polymers and surfactants, very few plants across the world have been focusing on the production of chemicals as primary aim. However, the recent performance of the FTS refinery at Sasolburg, South Africa, after the switch in production from fuels to chemicals, highlights the profitability of a FTS chemical refinery compared to a FTS fuels refinery (De Klerk et al., 2005). Furthermore, the co-feeding of other compounds into the feed gas of the FTS process to produce alternative valuable chemicals has also been the subject of several academic research projects. For example, the addition of ammonia into the FTS process revealed the possibility for synthesising nitrogen-containing compounds such as amides, amines and nitriles in addition to the normal FTS products (Walter, 1958), (Kurtz, 1969), (Brown & Maselli, 1973), (Bartley, 1981), (Claeys et al., 2013).

2.1.2. Technology of the Fischer-Tropsch synthesis

Since its invention, the FTS technology comprises three key steps, namely syngas production, FT synthesis and FTS product upgrading (Davis, 2003).

The synthesis of the FTS feed gas, mainly comprising of carbon monoxide (CO) and hydrogen (H_2), occurs through either the gasification of coal and biomass or the autothermal reforming of natural gas or the catalytic partial oxidation of natural gas, as shown in Table 2. 1. Syngas generated from the gasification of coal or biomass has a low H_2/CO ratio compared to the one generated from the reforming or partial oxidation of natural gas processes (Dry, 1996).

Table 2. 1: Stoichiometric equations of reactions occurring during the production of syngas.

Natural gas	$1.11\ CH_4 + 0.72\ O_2 \rightarrow 2\ H_2 + 1\ CO + 0.11\ CO_2 + 0.22\ H_2O$	$Rxn.1$
Coal	$1.78\ CH_{0.5} + 0.5\ O_2 + 1.56\ H_2O \rightarrow 2\ H_2 + 1\ CO + 0.78\ CO_2$	$\mathrm{Rxn.}\,2$

The crude syngas, mainly composed of H_2, CO, CO_2 and H_2O, is further processed to obtain the purified syngas at the required H_2/CO ratio. Dry & Steynberg (2004) reported that the composition of the syngas is a significant factor affecting the overall FTS process performance.

Fischer-Tropsch synthesis reactions

The purified syngas is then fed into an FTS reactor where the catalytic conversions occur resulting in the formation of a wide range of products namely *n*-paraffins, *n*-olefins and a small amount of oxygenates. The FTS is generally performed at elevated pressures, *i.e.* between 20 to 30 bar, to enhance the formation of the desired FTS products (Steynberg et al., 2004). It is believed that the conversion of the syngas into various organic products occurs mainly through surface polymerization reactions presented in Table 2. 2. Additionally, side reactions such as the water gas shift (WGS) and Boudouard reactions also occur during the FTS and lead to the formation of carbon dioxide, hydrogen and carbon deposition as shown in the reaction equations presented in Table 2. 2 (Zhang et al., 2010).

Table 2. 2: Stoichiometric equations of reactions occurring during the Fischer-Tropsch synthesis.

Polymerization reactions		
1. Paraffins	$(2n+1)H_2 + nCO \rightarrow C_nH_{2n+2} + nH_2O$	$Rxn.3$
2. Olefins	$2nH_2 + nCO \rightarrow C_nH_{2n} + nH_2O$	$Rxn.4$
Side reactions		
3. Oxygenates	$2nH_2 + nCO \rightarrow C_nH_{2n+2}O + (n-1)\,H_2O$	$Rxn.5$
4. Water gas shift	$CO + H_2O \rightarrow CO_2 + H_2$	$Rxn.6$
5. Boudouard	$2\,CO \rightarrow C + CO_2$	$Rxn.7$

Fischer-Tropsch operation modes

The surface polymerization reactions leading to the formation of organic products during the FTS are highly exothermic. Therefore, the extent of these reactions and the FTS products spectrum were found to be strongly dependent on the operating temperature as it is thermodynamically expected for exothermic reactions. On this basis, the industrial FTS operations have been generally classified into two modes, namely the low temperature Fischer-Tropsch (LTFT) and the high temperature Fischer-Tropsch (HTFT). However, recent research on coal-to-liquids conversion in China led to the development of the medium temperature Fischer-Tropsch (MTFT) technology (Maitlis & de Klerk, 2013).

The LTFT process is generally operated at a temperature between 200˚C and 240˚C over either Co- or Fe-based catalysts in fixed bed or slurry phase reactors. Due to the low operating temperature, the LTFT process generates predominantly long chain hydrocarbons such as diesel and waxes (Dry, 2002). On the other hand, the HTFT process allows the production of short chain hydrocarbons such as gasoline and light olefins. The HTFT process is commonly performed in a fluidized bed over Fe-based catalysts at a temperature ranging between 300˚C and 350˚C (Steynberg, 2004). Furthermore, the recent research performed by Synfuels China led to the design of a Fe-based MTFT catalyst and a slurry reactor suitable for a high-performance FTS process operating at a temperature between 270˚C and 290˚C. In contrast to the conventional LTFT process, the newly developed MTFT process allows a higher hydrocarbons productivity while limiting the formation of methane (Xu et al., 2013), (Xu et al., 2015).

Fischer-Tropsch catalysts

In terms of catalysts used for the FTS, transition metal-based catalysts, *i.e.* iron (Fe), cobalt (Co), nickel (Ni), ruthenium (Ru) and rhodium (Rh) were found to be suitable to the FTS. However, due to the limited availability and high prices of Ru and Rh and the high methane selectivity obtained over Ni-based catalysts (essentially used as a methanation catalyst in industry), only Fe- and Co-based catalysts are industrially used for the FTS (Dry, 2002).

Precipitated Co-based catalysts were the first commercialized FTS catalysts during the second world war in Germany, due to their higher yields and longer lifetime in comparison to Fe-based catalysts. Co-based catalysts are generally more active at low operating temperature and more selective to long-chain linear alkanes, such as wax and diesel fuel (Chaumette et al., 1995). Additionally, the water gas shift (WGS) activity over Co-based catalysts was found to be very low, thus, the use of a syngas with a high H_2/CO ratio, *i.e.* 2.0-2.3, is recommended. This makes Co-based catalysts suitable for natural gas based FTS processes (Davis, 2003). Furthermore, Co-based catalysts have higher stability and a smaller negative effect of water on conversion which permit the operation of the FTS at high conversion levels (Lappas & Heracleous, 2016).

However, compared to Co-based catalysts, Fe-based catalysts have a higher resistance to poisons, *e.g.* sulphur, and are cheaper due to the abundance of iron metals. Additionally, the oxygen containing compounds produced with Co-based catalysts are predominantly water while carbon dioxide (CO_2), and oxygenates, *e.g.* alcohols and aldehydes, are formed over Fe-based catalysts (Davis, 2003). Fe-based catalysts allow a low methane selectivity even at high temperatures and favour the high activity of the WGS reaction which allows the formation of hydrogen during the FTS process (Claeys & Van Steen, 2004). Hence, a syngas with a low H_2/CO ratio, *i.e.* 0.5-1.3, typically syngas produced from coal or biomass, can be used over Fe-based catalysts (Dry, 2004a). However, Fe-based catalysts can also be used for natural gas based FTS as it is the case in Sasolburg, South Africa (Dry & Steynberg, 2004). In addition to a variety of linear paraffins, Fe-based catalysts are more suitable for the formation of olefins and oxygenates.

The Fe-based catalysts used for the FTS are generally promoted with alkali-metals, *e.g.* potassium (K), copper (Cu) and magnesium (Mg), which act as electronic promoters by affecting the electronic structure of Fe atoms. The alkali-metal promoters, therefore, affect the catalyst activity, the products selectivity as well as the WGS activity by enhancing the chemisorption of CO and reducing the H_2 chemisorption (Zhang et al., 2010). Additionally, it was found that the addition of potassium (K) promoter into Fe-based catalysts allows an increase in the catalytic activity and enhances the selectivity of olefins and oxygenates (Yang

et al., 2004). Furthermore, Herranz et al. (2006), Zhu et al. (2016) and Bradley et al. (2017) agreed that the stability, activation and structure of the Fe-based catalysts can be improved though the addition of a chemical promoter, *e.g.* copper (Cu), and a structural promoter, *e.g.* silica (SiO_2). Schulz (1999) reported that the addition of magnesium (Mg) into the Fe-based catalysts also permits the control of the product selectivity and results in a high olefins yield.

Fischer-Tropsch product distribution

The product spectrum of the FTS is typically described as a broad and complex spectrum as it consists of a mixture of different compounds of various carbon chain length, *i.e.* C_1 to C_{100}, and functional groups, *e.g.* alkanes, alkenes, alcohols, aldehydes, acids and ketones. Among the FTS products, the oxygenates and branched compounds are classified as the side-products and linear hydrocarbons, namely *n*-paraffins and *α*-olefins, as the main products of the FTS process (Claeys & Van Steen, 2004).

The formation of the FTS products is generally assumed to occur through reaction sequences which involve the formation of monomers, *i.e.* chemisorbed CH_2 surface species, and their subsequent reactions (Claeys & Van Steen, 2004). It is believed that CH_2 surface species once formed can either directly react with surface hydrogen species to form methane which desorbs from the surface or it can react with another CH_2 surface specie to form absorbed alkyl species. The absorbed alkyl species can undergo one of these three reaction paths, *i.e.* alkyl species can either further react with surface hydrogen species to form ethane or directly desorb as ethylene or link up with other CH_2 surface species to form long chain surface species, as illustrated in Figure 2. 1. The first two paths, which involve the desorption of surface species after or without hydrogenation are referred to as chain termination actions and the latter path which involve the growth of the carbon chain is known as the chain growth or propagation (Claeys & Van Steen, 2004).

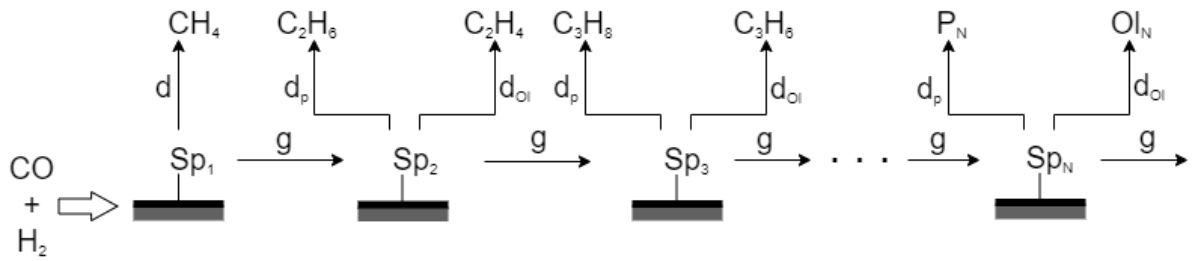

Figure 2. 1: Schematic of the mechanism for the formation of FTS products (olefins and paraffins). Adapted from (Claeys & Van Steen, 2004).

The likelihood for the occurrence of the chain growth, known as the chain growth probability (α-value), is intensively used in FTS as a key indicator of the products distribution. The α-

value is generally defined as the ratio of the rate of carbon chain propagation (R_p) to the sum of the former rate with the rate of carbon chain termination (R_t) as presented in $Eq.1$:

$$\alpha = \frac{R_p}{R_p + R_t} \qquad Eq.1$$

The mathematical equation depicting the chain growth probability proposed by Flory (1936), was further developed by Herington (1946) and Anderson et al. (1951). The resulting mathematical equation, known as the Anderson-Schulz-Flory (ASF) equation $(Eq.2)$, allows the direct calculation of the α-value from the ASF distribution plot which is the straight-line plot of $log\left(\frac{W_n}{n}\right)$ versus n as presented in $Eq.3$.

$$\frac{W_n}{n} = \frac{(1-\alpha)^2}{\alpha} \times \alpha^n \qquad Eq.2$$

$$log\left(\frac{W_n}{n}\right) = n\, log\alpha + log\left(\frac{1-\alpha}{\alpha}\right) \qquad Eq.3$$

Where W_n is the mass fraction of products and n is the number of carbon atoms.

The ideal distribution of the main products of the FTS process can be calculated/modelled using $Eq.1$ and schematised by the Anderson-Schulz-Flory (ASF) plot, shown in Figure 2. 2. However, deviations between the experimental data and the ASF plot have been extensively reported in literature. These deviations are traced back to the higher than calculated methane production, the high reactivity of ethylene, the high occurrence of secondary reactions and the curvature of the ASF distribution at high carbon numbers (Schulz & Claeys, 1999a).

The underestimation of the methane production/selectivity by the chain growth probability can be attributed to the fact that the methane formation does not involve CH_2 surface species insertion which is described by the chain growth probability but rather the formation of the CH_2 surface species (Dry, 2004b). It has also been suggested that the formation of the additional methane not predicted by the ASF model could occur on different sites which do not enhance chain growth (Schulz et al., 1994).

Furthermore, the relatively low content of C_2 in the overall FTS products is explained by the high intrinsic ethylene reactivity which results in a high rate of ethylene incorporation into the growing chains, rapid readsorption of ethylene and ethylene hydrogenation to ethane (Iglesia et al., 1993), (Schulz & Claeys, 1999b), (Van Der Laan & Beenackers, 1999). On the other hand, the curvature of the ASF distribution plot at high carbon number which yields another straight line with a lower slope, *i.e.* a higher α-value, is attributed to the preferential re-incorporation of long chain alkenes. Due to the high molecular weight of long chain alkenes,

the residence time of the long chain alkenes on and near the catalyst surface increase which enhances their involvement in secondary reactions and their incorporation in growing chains (Dry, 2004b), (Claeys & Van Steen, 2004). The high occurrence of secondary reactions of long chain alkenes has been attributed to the physisorption limitations by Kuipers et al. (1996) while Iglesia (1997) and Schulz & Claeys (1999a) attributed it to the diffusional and solubility effects, respectively.

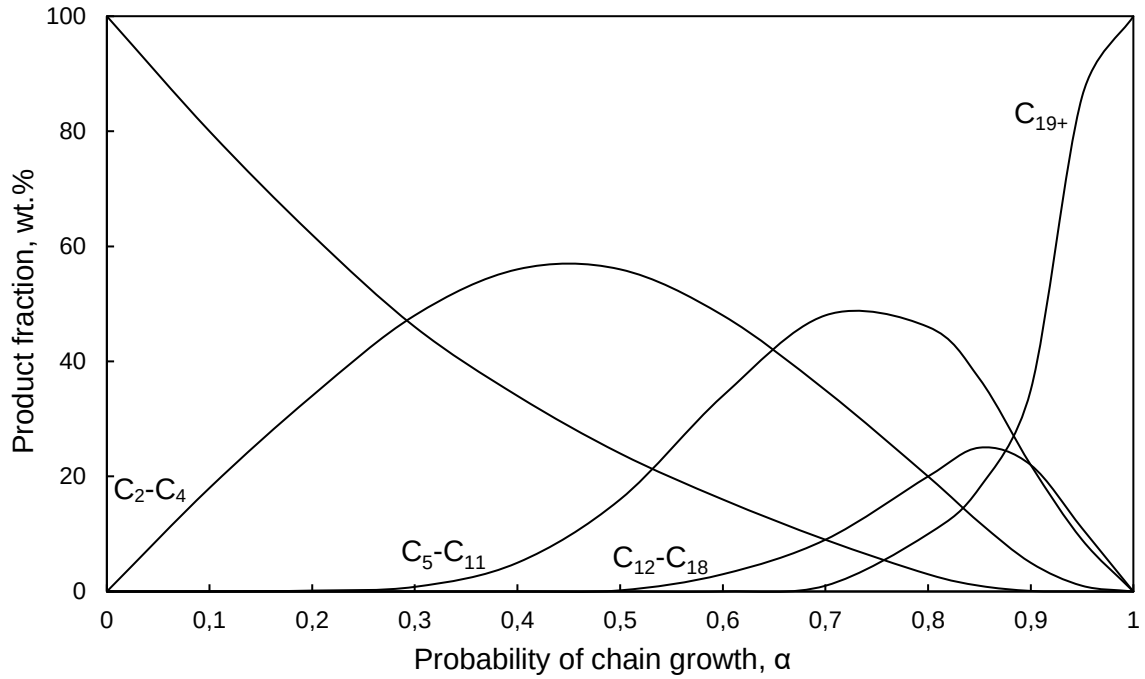

Figure 2. 2: Linear hydrocarbons (n-Paraffins and n-Olefins) distribution as a function of the chain growth probability, α-value. Adapted from (Dry, 2004b).

The α-value was found to be strongly dependent on the type of catalysts, *e.g.* Co- vs Fe-based catalysts, and the FTS operating conditions, *i.e.* temperature and H_2/CO ratio. An inverse relationship between the FTS operating conditions and the α-value was reported in literature. During LTFT (220-240˚C) and HTFT (300-350˚C) processes, the typical ranges of the α-value for Co- or Fe-based catalysts were found to be between 0.92-0.95 and 0.65-0.70 respectively. The significant decrease of the α-value at elevated temperature is attributed to the increase in the chain termination rate which favours the formation of short chain hydrocarbons and lowers the probability for the chain growth (Ma et al., 1999). Regarding the H_2/CO ratio, it has been reported that the α-value decreases as the H_2/CO ratio increases due to the excess of hydrogen present on the catalyst surface which enhances the hydrogenation of the surface species and limit their growth (Donnelly & Satterfield, 1989).

2.1.3. Factors influencing the performance of the Fischer-Tropsch synthesis

The composition and selectivity of the FTS products were found to be strongly dependent on various reaction variables, namely the catalyst composition, the reactor type and the reaction conditions, *e.g.* temperature, pressure, gas hourly space velocity and syngas composition (Van Der Laan & Beenackers, 1999), (Claeys & Van Steen, 2004). Over the past decades, various studies over Fe, Co and Ru based catalysts, dealing with the effects of the reaction variables on the FTS products spectrum, provided several observations and insights summarized in Table 2. 3.

Table 2. 3: The influence of the FTS reaction variables on the FTS performance indicators. Adapted from (Van Der Laan & Beenackers, 1999).

Parameter	Catalytic activity	Methane selectivity	Olefins selectivity	Alcohols selectivity	Chain growth probability
Temperature	↑	↑	*	↓	↓
Pressure	↑	↓	*	↑	↑
Space velocity	↓	↓	↑	↑	*
Syngas composition	*	↑	↓	↓	↓
Alkali-content in Fe-based catalysts	↑	↓	↑	↑	↑

The increase, decrease and undefined relationship between the increase of FTS reaction variables and the FTS performance indicators are represented by the ↑, ↓ and * symbols, respectively.

The following section provides a brief overview regarding the effects of the reaction conditions, *i.e.* reaction temperature, syngas composition and space velocity. The effects of the composition of Fe-based catalysts on the FTS products spectrum and selectivity are detailed in Section 2.3.

Reaction temperature

Studies revealed that the reaction temperature affects both the catalytic activity and FTS product distribution. The increase in the reaction temperature was found to enhance the formation of short-chain hydrogenated compounds and reduce the oxygenates selectivity independently of the type of catalyst used (Dry & Steynberg, 2004). Donnelly & Satterfield (1989), Dry (2004b) and Todic et al. (2016) agreed that the increase in reaction temperature strongly inhibits the chain growth while enhancing the chain termination step. During their study over a commercial precipitated iron catalyst (100 Fe/5 Cu/4.2 K/ 25 SiO_2 on mass basis), Todic et al. (2016) observed a decrease in the α-value followed by an increase in the short

chain hydrocarbons content, mainly methane and C_2-C_4, and a decrease in C_{5+} hydrocarbons selectivity as the reaction temperature increased from 220˚C to 270˚C. Additionally, a decline in the olefins to paraffins ratio was observed as the reaction temperature increased. This was attributed to the increase in the hydrogenation activity at high temperature which highly favours the formation of *n*-paraffins (Yang et al., 2003). Claeys & Van Steen (2004) also reported that an increase in reaction temperature enhances the occurrence of secondary reactions, *i.e.* hydrogenation, isomerization and incorporation, during which the olefins are converted into other FTS products. However, over a similar Fe-based catalyst (100 Fe/5 Cu/4.2 K/ 25 SiO_2 on mass basis), Bukur et al. (1997) observed that the olefins selectivity was essentially independent of the reaction temperature over the range of 235˚C to 265˚C. Interestingly, an increase in the olefins selectivity with increasing reaction temperature over a commercial Ruhrchemie catalyst, *i.e.* supported Fe-catalyst (Fe/Cu/K/SiO_2), and a K promoted iron oxide catalyst were also reported in literature by Donnelly & Satterfield (1989) and Dictor & Bell (1986) respectively. It was concluded that generally increased temperatures primarily lead to preferred olefins desorption and therefore higher olefins contents, however, this can be counteracted by preferred secondary hydrogenation of olefins at high temperatures (Claeys & Van Steen, 2004). Regarding the oxygenates formation, Van Der Laan & Beenackers (1999), Dry (2004b) and Todic et al. (2016) observed that the increase in reaction temperature impacts the oxygenates content by decreasing the alcohols selectivity and enhancing the formation of iso-alcohols and ketones. From these observations, Dry (2004b) suggested that the increase in reaction temperature favours secondary reactions during which alcohols are converted into other compounds such as iso-alcohols and ketones.

Syngas composition

Regarding the effects of the syngas composition on the FTS catalytic performance, Dry (1996) argued that the FTS products spectrum is affected by the syngas composition as the presence of carbon monoxide and hydrogen on the active sites directly impacts the chain growth and the chain termination. Therefore, the use of a syngas with a high H_2/CO ratio, *i.e.* a syngas rich in hydrogen, leads to the formation of shorter compounds as the chain termination by hydrogenation is enhanced. On the other hand, longer compounds are formed when a syngas with a low H_2/CO ratio, *i.e.* syngas poor in hydrogen, is used. Additionally, Donnelly & Satterfield (1989) observed a drop in the olefin to paraffin ratio, from 6 to 1, as the H_2/CO ratio was increased from 0.3 to 4. This observation was explained by the large availability of hydrogen-surface species at high H_2/CO ratio which favoured primary formation of paraffins upon desorption of surface alkyl species and increased secondary hydrogenation of olefins to form paraffins.

Gas hourly space velocity, GHSV

The effect of syngas space velocity on the FTS selectivity was investigated over various Fe-based catalysts. Dictor & Bell (1986) observed a slight increase in the olefins content as the space velocity was increased during the FTS over a Fe-based catalyst, *i.e.* potassium-free Fe_2O_3 powders. Similar observations were reported by Bukur et al. (1990) and Kuipers et al. (1996). Furthermore, Van Der Laan & Beenackers (1999) suggested that the decrease in the residence time of the reagents on the active sites at high space velocity limits the occurrence of secondary reactions and enhances the formation of primary FTS products, namely olefins and alcohols.

2.1.4. Proposed mechanisms of the Fischer-Tropsch synthesis

Intensive research had been performed to provide clear understandings of the FTS product formation by attempting to describe the FTS reaction pathways. In most studies, it has been concluded that the FTS reactions occur via a network of surface polymerization reactions. However, several pathways had been proposed with different steps, but all agree on the three main product formation steps, which are:

(i) the generation of the chain initiator,
(ii) the chain growth or propagation via sequential addition of a monomer and
(iii) the chain termination or desorption.

The debate about the exact mechanism of the FTS reactions is still ongoing due to the complexity of the FTS product spectrum. Nonetheless, among the numerous FTS pathways proposed, the alkyl, alkenyl, enol and the CO-insertion mechanisms, shown in Figure 2. 3, are the most relevant, popular and widely accepted FTS pathways. Each of these popular FTS pathways are discussed briefly in the following section.

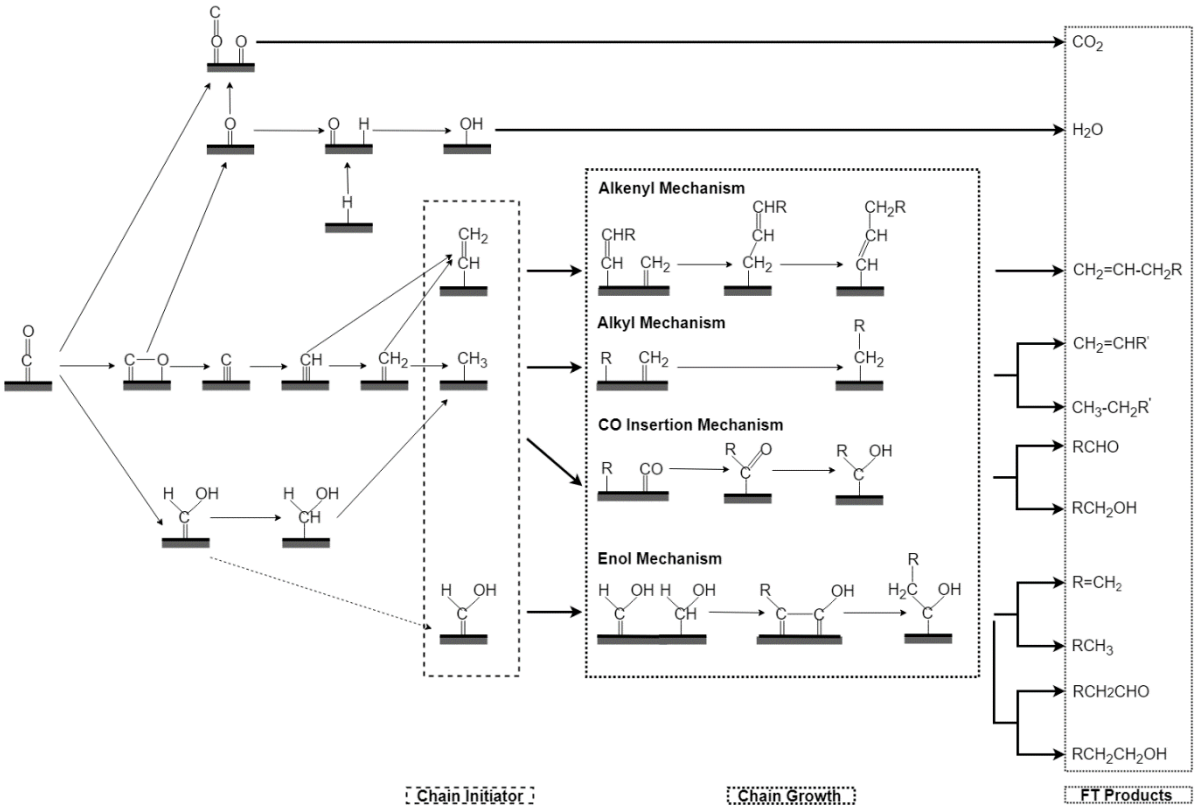

Figure 2. 3: Schematic representation of the four most popular FTS mechanisms. Adapted from (Mabaso, 2005).

The Alkyl mechanism

The alkyl mechanism is generally the most accepted pathway among the above-mentioned. In the alkyl pathway, the chain initiator is suggested to start with the dissociative chemisorption of H_2 and CO which leads to the formation of surface hydrogen, carbon and oxygen species (Claeys & Van Steen, 2004). The surface oxygen is then removed by reacting with surface hydrogen to form water and the surface carbon reacts with surface hydrogens to yield CH, CH_2 and CH_3 surface species. Furthermore, it is assumed that the chain growth occurs through the consecutive addition of monomers, *i.e.* CH_2 surface species, into the chain initiators, *i.e.* CH_3 surface species (Erley et al., 1983). The chain termination leading to the formation of α-olefins and *n*-paraffins takes place via the β-hydrogen elimination or the hydrogen addition respectively (Pichler & Schulz, 1970). The limitation of the alkyl mechanism lays on its inability to explain the formation of oxygenates.

The Alkenyl mechanism

The alkenyl mechanism proposed by Maitlis et al. (1999) suggests a mechanism for the formation of olefins during the FTS process over heterogenous catalysts. However, the formation mechanism of other FTS products, mainly primary paraffins and oxygenates, cannot

be explained through the alkenyl mechanism. In the alkenyl mechanism, the generation of the chain initiator follows similar steps as the one of the alkyl mechanism but leads to the formation of vinyl surface species ($CH=CH_2$) which are considered as the chain initiators in the alkenyl mechanism. The chain propagation occurs through the incorporation of CH_2 surface species into the chain initiators yielding surface allyl species. The chain termination is marked by the formation of α-olefins which occurs through the addition of hydrogen to the allyl species (Maitlis et al., 1999).

The Enol mechanism

According to the enol mechanism proposed by Anderson et al. (1952), the enol surface species (CHO) are the chain initiators and monomers. The formation of the enol surface species occurs through the surface polymerisation reaction between the chemisorbed CO species and the adsorbed hydrogen. The chain growth is marked by the addition of several enol surface species followed by the elimination of water which leads to the formation of enolic species. The chain termination then occurs through the desorption of enolic species yielding oxygenates and α-olefins. The enol mechanism suggests that the formation of paraffins occurs *via* the hydrogenation of olefins in a secondary reaction step (Claeys & Van Steen, 2004).

The CO insertion mechanism

The CO insertion mechanism, proposed by Pichler & Schulz (1970), identifies the methyl surface species and the chemisorbed CO species as the chain initiators and the monomers respectively. The chain growth is therefore enhanced by the addition of the chemisorbed CO species into the methyl surface species which allows the formation of acyl surface species. The hydrogenation of the acyl species is generally followed by water removal which leads to the formation of alkyl species. The chain termination of the CO insertion mechanism is similar to the one of the alkyl mechanism. The formation of α-olefins and n-paraffins occurs via the elimination of the β-hydrogen and the addition of hydrogen respectively. The chain termination can also lead to the formation of oxygenates if the desorbed surface species contained oxygen (Claeys & Van Steen, 2004).

2.2. Nitrogen Fischer-Tropsch synthesis

The nitrogen-containing compounds (NCCs) are considered as key chemicals and economically valuable as they are used as feedstock in various industries, namely the pharmaceutical, cosmetic and agricultural industries. Amines and nitriles are the two major classes of NCCs, where the former is defined as organic compounds containing a basic nitrogen atom with a lone pair and the latter is defined as organic compounds containing the cyano (-CN) group. Both aliphatic amines and nitriles are considered as important organic intermediates to produce agrochemicals, plastics, pesticides and pharmaceutics (Sango et al., 2015).

Due to the economic importance of the NCCs, researches have been dedicated to discovering new and more efficient reaction paths for their production. It was found that the amines can be synthesised through either the catalytic hydrogenation of nitriles or the catalytic reaction between ammonia with either olefins, alcohols or carbonyl compounds (Roose et al., 2000). Pollak et al. (2012) reported that the synthesis of nitriles can occur through either the ammoxidation of hydrocarbons or the catalytic reaction of acids with ammonia. The use of common FTS products, namely alcohols, aldehydes, acids, and potentially olefins and other hydrocarbons, as the feedstock for the formation of NCCs inspired several researches to investigate the direct formation of NCCs via the co-feeding of ammonia (NH_3) with the syngas under normal FTS conditions. The researches led to the creation of several patents for the production of amines (Alfred, 1950), (Walter, 1958), (Brown & Maselli, 1973), (Gredig et al., 1997) and nitriles (Olive & Olive, 1979), (Auvil & Penquite, 1981).

Over the past decades, increasing interests have been attributed to the co-feeding of (NH_3) into the FTS process, *i.e.* nitrogen FTS (NFTS), and research has been performed to provide a clear understanding of the impacts of NH_3 addition and to evaluate the feasibility and profitability of this process. Promising results were reported from these recent researches as the formation of different NCCs classes, *i.e.* nitriles, amines, amides, formamides and acetamides, was observed during the NH_3 co-feeding with a total NCCs selectivity between 5-36 C% (Sango, 2013), (Sango et al., 2015), (Henkel, 2013), (De Vries, 2017), (Rawoot, 2017). The following section provides a brief overview of the most recent research performed on the NFTS and highlights the main observations and the key findings of these researches.

2.2.1. Overview of recent studies on the nitrogen Fischer-Tropsch synthesis

Claeys et al. (2013) patented a process which permits the production of one or more linear nitriles, amides and formamides from the catalytic hydrogenation of CO and/or CO_2 in the presence of a nitrogen-containing compound, *i.e.* NH_3 or NO_x. The research was performed over an unsupported iron catalyst promoted with K (100 g Fe: 2 g K) in a slurry reactor at

250˚C, a synthesis gas pressure of 5 bar and a fixed synthesis gas space velocity of 75 ml/min with a H_2/CO molar ratio of 2:1. The investigation focused on the effects that the NH_3 concentration on the selectivity of NCCs. To enhance the formation of the desired NCCs, Claeys et al. (2013) recommended that the catalyst be selected from a supported cobalt, iron, ruthenium or rhodium or an unsupported iron catalyst modified with an alkali promoter (K), a reduction promoter (Cu) and a structural promoter (Al_2O_3, SiO_3).

Further work on the NFTS over an unsupported iron catalyst promoted with K (100 g Fe: 1.5 g K) in a slurry reactor at low temperature, *i.e.* below 250˚C, low pressure, *i.e.* 5 bar, with a H_2/CO ratio of 2:1 was conducted by Sango et al. (2013) (2015). Sango et al. (2013) (2015) investigated the effects of NH_3 content in the feed gas by varying the NH_3 content from 0 to 35 vol% to identify and quantify the synthesised NCCs, to study the effect of NH_3 partial pressure on the NCCs formation and selectivity as well as on the FTS performance and lastly to propose a mechanism explaining the formation of NCCs from the NFTS. Upon the co-feeding of NH_3, the formation of nitriles, amides, formamides, amines and a white solid identified to be ammonium carbonate observed without significant impact on the catalytic activity. Furthermore, the content of both nitriles and amines was found to be positively affected by the increase in the NH_3 content while the disappearance of oxygenates was observed. From the results obtained, Sango et al. (2013) (2015) suggested that the NCCs could be formed via secondary reactions, namely the amination of oxygenates and/or their precursors, the hydrogenation of nitriles to amines and the dehydrogenation of amines to nitriles. Additionally, primary reaction routes, such as the insertion of NH_2 or CN species into the alkyl species leading to the formation of amines and nitriles respectively, was also proposed by Sango et al. (2013) (2015). Regarding the ammonium carbonate, it was hypothesised that it might be formed from the reaction between CO_2 and NH_3 in presence of water (Sango, 2013) (Sango et al., 2015).

Henkel (2013) investigated the impact of NH_3 on the FTS performance and determined the feasible process conditions for the formation of NCCs during the NFTS over a bulk cobalt (Co) catalyst and potassium promoted iron (Fe) catalysts. The studies were conducted in a fixed bed reactor over a temperature range of 250˚C-300˚C at a pressure of 4 bar. A H_2/CO molar ratio of 1:1 was used over the Co-based catalyst. Over the Fe-based catalysts, the H_2/CO molar ratio was varied between 1:1, 2:1 and 4:1. During the NFTS process, a feed gas with a NH_3 partial pressure of 0.2 bar was introduced to the reactor. Various analytical techniques, namely online GC-TCD, GC-MS, GC-FID as well as an offline 2D-GC-TOF, were used to analyse the products streams from both normal FTS and the NFTS. Over the unpromoted Fe and bulk Co catalysts, the addition of NH_3 resulted in an increase in the formation of olefins, CO_2, and long chain products (high α-value) while a drop in the catalytic activity was observed.

Interestingly, minimal changes on the catalytic performance were observed during the co-feeding of NH_3 over the potassium promoted Fe-based catalyst. However, a significant decline in the oxygenates selectivity followed by the formation of NCCs such as amines, amides and nitriles was observed as results of the presence of NH_3 during the FTS over the potassium promoted Fe-based catalyst while no NCCs were formed over the unpromoted Fe catalyst. From these observations, Henkel (2013) agreed with the NCCs formation mechanisms proposed by Sango (2013). Furthermore, Henkel (2013) argued that the use of low reaction temperature and high H_2/CO ratio enhances the formation of alcohols and amines under normal FTS and NFTS conditions respectively.

Further investigations on the mechanism of NCCs formation during the NFTS were carried out by De Vries (2017). In this study, both theoretical and experimental techniques were used to provide valuable inputs on the understanding of the NFTS. The theoretical study performed used a spin-polarized periodic density functional theory (DFT) which provided some insights on the initial stage of the pathway on a model Fe (100) surface. It was found that the presence of NH_3 and NH_2 species on the Fe (100) surface enhances the CO dissociation while the opposite was observed in the presence of NH and N species. In the presence of all four species, *i.e.* NH_3, NH_2, NH and N, the CO dissociation was found to be limited as it becomes more endothermic. Furthermore, to test the hypothesis that some primary oxygenates produced during FTS reactions are converted into NCCs via a secondary reaction, (Claeys et al., 2013), (Sango, 2013), De Vries (2017) performed some experimental runs over an unsupported iron catalyst promoted with K (100 g Fe: 2 g K) in a slurry reactor at 250˚C, 5 bar, a H_2/CO ratio of 2:1 with 0-1 vol% NH_3. Negligible changes in the catalytic activity were observed upon addition of ammonia which was attributed to the low NH_3 concentration used. The use of online two-dimensional gas chromatography (2D-GC-TOF/FID) during the study allowed for accurate identification and quantification of the NCCs produced, *i.e.* nitriles, amides, primary, secondary and tertiary amines. As expected, a decline in oxygenates selectivity was also observed and the co-feeding of 1-octanol clearly indicated the correlation between the decline of oxygenates and the formation of NCCs. To check the stability of the NCCs formed during the synthesis, De Vries (2017) further co-fed nonanitrile and observed its readily conversion to secondary and tertiary amines.

Rawoot (2017) further investigated the hypothesis which stipulates that NCCs are produced via oxygenates and/or their precursors by performing the NFTS over an alumina-supported iron-rhodium catalyst (5.2 wt% Fe and 6.3 wt% Rh) known to yield a high oxygenates selectivity. To reach this objective, the effects of temperature and space velocity on the selectivity of NCCs and on the catalytic performance of the Fe-Rh catalyst were investigated. A fixed bed U-tube reactor was used to perform the experimental runs over a temperature and

space velocity ranges of 180˚C-360˚C and 10 ml/min.g_{cat} -100 ml/min.g_{cat} respectively. During the experimental runs, a combination of online GC-TCD, offline GC-FID and online two-dimensional gas chromatography (2D-GC-TOF/FID) was used for the product analysis and a NH_3 content of 5 vol% was used during the NFTS runs. Upon NH_3 addition, Rawoot (2017) observed a decline in the catalytic activity and the formation of nitriles, amides, amines, formamides and a white solid believed to be ammonium carbonate.

Additionally, Rawoot (2017) reported that the presence of NH_3 with increasing temperature and space velocity affects the product distribution as an increase in methane and olefin content was observed while a decline in the oxygenate content followed by the formation of NCCs. It was then assumed that the presence of NH_3 with increased temperature favours the desorption of olefins while limiting their readsorption. The increase of methane and olefin content as well as the drop in the α-value was also attributed to the competitive adsorption between NH_3, CO and H_2 species which limits the chain growth and the hydrogenation activity (Rawoot, 2017). Regarding the NCCs, it was found that the NCCs selectivity increased with decreasing space velocity which supports the hypothesis that the NCCs might be formed from the secondary reactions of oxygenates.

Further discussions of the results and observations reported in the studies above are presented in Section 6: Results and discussions.

2.2.2. Proposed mechanisms of nitrogen Fischer-Tropsch synthesis

During the studies on the nitrogen Fischer-Tropsch synthesis (NFTS) presented above, a strong correlation between the formation of NCCs and the significant decline or the disappearance of oxygenates was generally observed. Based on these observations, it has been assumed that the final stage of the mechanism for the formation of NCCs may involve reactions between oxygenated surface species and/or their precursors and NH_3 surface species.

Few mechanisms for the formation of NCCs via the NFTS have been proposed. However, debates about the extent to which the formation of NCCs occurs through the suppression of intermediates for primary oxygenates or the consumption of the primary oxygenates formed via secondary reactions are still ongoing.

The mechanism proposed by Sango et al. (2013) (2015) postulated that primary aliphatic amines, amides and nitriles are formed from the reaction between NH_x surface species, *i.e.* NH_2, N, and the oxygenated surface species during the final elementary step, as shown in Figure 2. 4.

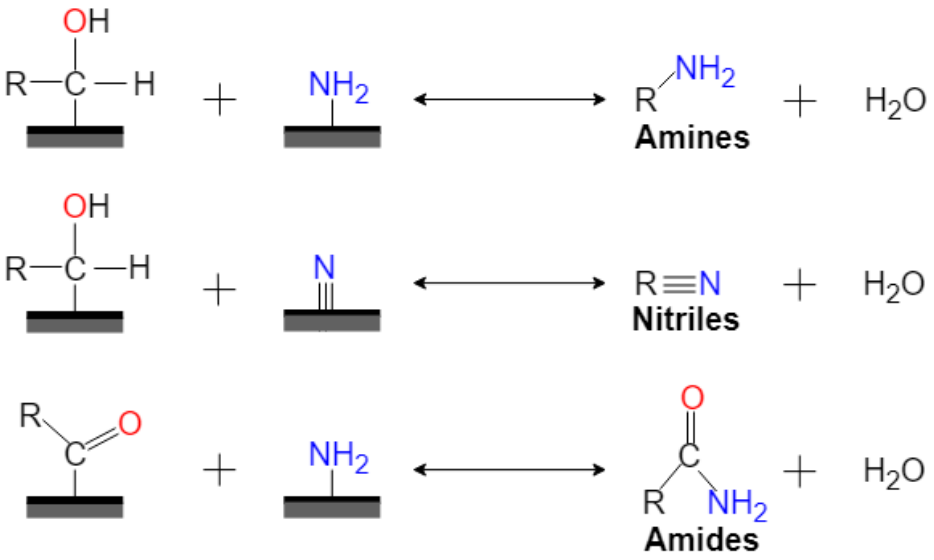

Figure 2. 4: Mechanism of nitrogen-containing compounds formation from the NFTS proposed by Sango et al. (2013) (2015).

The results obtained during the studies performed by Henkel (2013), regarding oxygenates selectivity during the FTS with and without ammonia, confirmed the strong relationship between the disappearance of oxygenates and the formation of NCCs during the NFTS. Based on the olefins content during the NFTS, Henkel (2013) concluded that the NCCs formation does not result from the secondary reactions of olefins. Furthermore, Henkel (2013) agreed with the NCCs formation mechanisms proposed by Sango et al. (2013) (2015), shown in Figure 2. 4, and suggested that amination reactions, presented on Figure 2. 5, may occur during the NFTS.

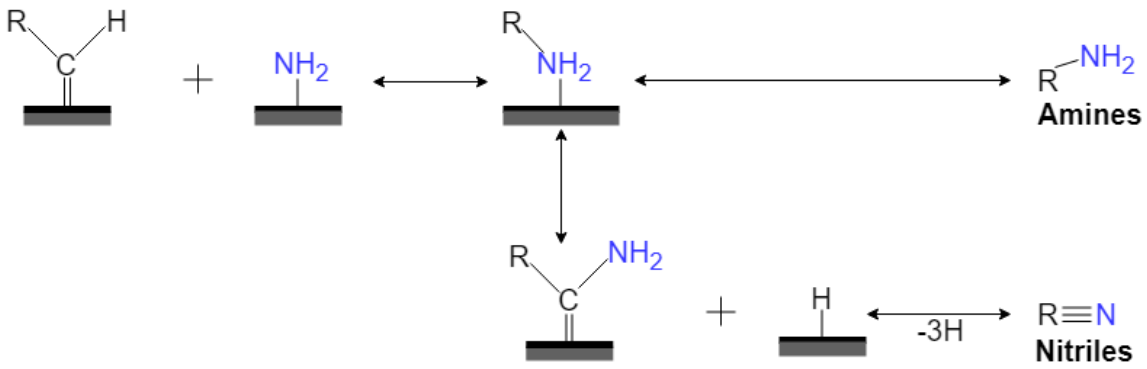

Figure 2. 5: Mechanism of nitrogen-containing compounds formation based on the amination reactions. Adapted from Henkel (2013).

Due to the gap in knowledge on the exact mechanisms of the NFTS, it has not yet been proven that the oxygenates and/or their precursors are the precursors of the NCCs. However, based on the results reported in literature, it can be hypothesised that the catalysts with high

selectivity to oxygenates under FTS conditions will also have a high selectivity to NCCs under NFTS conditions (Sango, 2013), (Sango et al., 2015).

2.3. Oxygenates synthesis via Fischer-Tropsch process

2.3.1. Overview on production of oxygenates via Fischer-Tropsch synthesis

The term “oxygenates” typically refers to oxygen-containing compounds such as alcohols, esters, acids, aldehydes and ketones. They are used as fuels additives and petrochemical feedstock for various industrial processes.

The synthesis of oxygenates from the catalytic hydrogenation of CO was discovered by Fischer & Tropsch (1926) as they reported the formation of the synthol mixture, *i.e.* a mixture mainly composed of n-alcohols and n-aldehydes and to a small extent esters, carboxylic acids, and ketones. Since the invention of the FTS process, studies have been dedicated to the optimization of the FTS process for the selective production of oxygenates (Surisetty et al., 2011). These studies led to the development of new processes such as the mixed alcohols synthesis, higher alcohols synthesis and methanol synthesis which aim to produce clean fuels and petrochemical feedstock from coal, natural gas and biomass (Fang et al., 2009).

Oxygenates production from the FTS process was found to be strongly dependent on the reaction temperature and the type of catalyst used. Noble metal-based catalysts such as Rhodium (Rh), Rhenium (Re) and Ruthenium (Ru) supported on various oxides, as well as non-noble metal-based catalysts such as MoS_2-, Cu-, Co- and Fe-based catalysts, have been identified as suitable catalysts for the high selectivity of oxygenates (Fang et al., 2009), (Schaller et al., 2018).

Despite the high oxygenates selectivity obtained over the noble-metals catalysts, these catalysts are not used industrially due to their limited availability and high price. Therefore, the non-noble metal-based catalysts have been widely investigated over the past decades to optimize the oxygenates production. It was found that, among the non-noble metal-based catalysts, Fe-based catalysts can be considered as promising catalysts for a feasible production of oxygenates via the FTS due to its availability, low cost and high catalytic activity. It was further reported that the catalyst preparation method, the type of support and loading as well as the addition of promoter(s) have significant impacts on the selectivity of oxygenates during the FTS (Schaller et al., 2018).

The following sections provide a review of FTS Fe-based catalysts reported to yield a relatively high oxygenates selectivity, *i.e.* between 30% to 65%, see Table 2. 4, and the mechanisms postulated for the oxygenates formation.

2.3.2. Iron-based catalysts for oxygenates formation

The nature, composition and type, of the iron (Fe)-based catalyst used during the FTS was found to have a direct impact on the oxygenate formation. The use of commercial Fe-based catalysts, *i.e.* the precipitated and fused Fe FTS catalysts, leads to the oxygenate formation making up to 6-12 wt% of the FTS products (Claeys & Van Steen, 2004).

Research has been performed on the bulk iron and iron-copper (Fe-Cu) based catalysts for the higher alcohols synthesis from the hydrogenation of CO due to their strong capacity to promote long chain hydrocarbons formation, higher water-gas shift activity and lower costs (Ding et al., 2012a). The effect of promoter(s) addition, reaction temperature and pressure on the catalytic performance of Fe-Cu based catalysts were investigated in several studies.

In the study by Lin et al. (2008), the effect of the addition of zinc oxide (ZnO) and manganese (Mn) promoters on the catalytic performance of Fe-Cu based catalysts were investigated. The investigation was completed over a temperature range of 220˚C to 280˚C at 40 bar, 6000 h^{-1} and a H_2/CO molar ratio of 2:1. It was found that ZnO can be considered as an electronic/chemical promoter which inhibits the sintering of Fe oxide phases and increases the catalyst surface area and the stability of the active phases through the formation of $ZnFe_2O_4$ phase. Mn was defined as a structural promoter which enhances the synergistic effect between copper and iron. Regarding the catalytic performance, compared to the unpromoted Fe-based catalyst, an increase in the CO conversion from 28.6% to 50.26%, followed by a slight decrease in the content of long chain alcohols from 80.7 wt% to 78.1 wt%, were observed over the Zn promoted Fe-Cu based catalyst. The authors suggested that the increase in the catalytic activity may be due to the formation of the stable $ZnFe_2O_4$ phase. Over the Mn promoted Fe-Cu based catalyst, an increase in the overall alcohol selectivity, from 12.3 C% to 22.9 C% compared to the unpromoted Fe-based catalyst, was reported and attributed to the synergistic interactions between Fe and Cu which are enhanced by the presence of Mn. It was then concluded that the synergistic effect of Zn and Mn promoters enhances the catalytic activity and reduces the methane selectivity and the formation of long chain alcohols and hydrocarbons.

Ding et al. (2012a) studied the influence of Fe promotion on the catalytic performance of a co-precipitated Cu-Mn-ZnO catalyst at 260˚C, 40 bar, 6000 h^{-1} and a H_2/CO molar ratio of 2:1. The experimental results pointed out that the addition of Fe improves the catalytic activity, enhances the formation of hydrocarbons and shifts the alcohols selectivity towards long chain alcohols. With increasing Fe concentration, a significant increase in hydrocarbons selectivity followed by a decrease in the alcohol selectivity were reported. From the characterization of both calcined Fe promoted Cu-Mn-ZnO catalyst and the unpromoted Cu-Mn-ZnO catalyst, it

was found that the presence of Fe promoted the dispersion of copper and iron carbides species which increases the availability of active phases for both higher alcohols and hydrocarbons synthesis.

The effect of manganese (Mn) as a promoter on a co-precipitated Fe-Cu-ZnO catalyst for the production of higher alcohols was further investigated by Ding et al. (2013). The results of the synthesis runs, performed at 260˚C, 40 bar, 6000 h^{-1} and a H_2/CO molar ratio of 2:1, showed that the use of a Mn promoted Fe-based catalyst (Fe-Mn-ZnO) leads to the production of olefins-rich mixture due to the interactions between the Fe and Mn species which significantly enhances the olefins selectivity. Due to the high methanol selectivity of Cu species, an alcohols rich mixture was obtained when the process was performed over a Mn promoted Cu-based catalyst (Cu-Mn-ZnO). The improvement of the performance of the Mn promoted Fe-Cu based catalyst was therefore attributed to the synergistic interactions between the Fe and Cu species. Thus, the optimum Mn to Cu ratio was found to be 0.5 as the increase of this ratio to 2 caused a significant decrease in the amount of methanol and a slight increase of the amount of C_2^+ alcohols.

The study on the effect of potassium (K) promoter on a co-precipitated Fe-Cu-Mn-ZnO catalyst conducted by Ding et al. (2015), at 260˚C, 40 bar, 6000 h^{-1} and a H_2/CO molar ratio of 2:1, indicated that the catalyst activity increased gradually with an increase in K content, reached a maximum at 0.5% K content before decreasing as more K was added. The initial increase in the catalyst activity, from 21.4% to 27.3%, was attributed to the fact that K reinforces the Fe-Cu interactions and enhances the CO chemisorption while limiting the H_2 chemisorption. Contrary to this, a gradual decrease in the alcohol selectivity, from 57 C% to 42.4 C%, followed by a monotone increase in the selectivity of long chain hydrocarbons was observed as the K loading was increased from 0 to 1.5 wt%. It was also reported that the C_2^+OH/C_1OH ratio increased with increasing K content and reached a maximum at 0.5% K content. These results are in agreement with the results obtained by Yang et al. (2004) and it was concluded that the alcohols formation is limited at very high K concentration because the K species may act as catalyst poisons by blocking the active sites of both Cu and Fe species (Ding et al., 2015).

The performance of various alkali metals promoted Fe-based catalysts for the production of higher alcohols were also investigated by Schaller et al. (2018). The study reported a gradual decrease in the CO conversion and an increase of the overall oxygenate selectivity as the potassium loading was changed from 0.1, 1 to 10 wt% at 200˚C, 20 bar, 0.045 ml/g_{cat}.s and a H_2/CO molar ratio of 2:1. It was also found that a K loading of 0.1 wt% provides the highest alcohol selectivity by predominantly increasing the content of C_5^+ alcohols. However, the highest overall oxygenate selectivity, 28 C%, was obtained at a K loading of 1.0 wt%. When the K promoted Fe-based catalysts were further promoted with sodium (Na), copper (Cu) or

aluminium (Al) *via* the incipient wetness impregnation, various impacts on the performance of the Fe-based catalysts were observed and pointed out that the addition of both K and Al improves the catalytic activity and enhances the oxygenate formation.

Additionally, the effect of reaction conditions and addition of promoter on the catalytic performance of supported Fe catalysts during the hydrogenation of CO has also been investigated extensively.

The effect of temperature and pressure on the alcohols formation from syngas on a γ-alumina supported Fe (Fe/Al_2O_3) catalyst was investigated by Pijolat & Perrichon (1985). The experiments were performed in a microreactor at operating temperatures and pressures between 200˚C to 250˚C and 0.8 to 20 bar, respectively. The study reported that the production of both alcohols and hydrocarbons increased as the pressure increased. At low temperature, 200˚C to 225˚C, a high selectivity of methanol was reported. However, as the reaction temperature increased to 250˚C, a significant decrease in the alcohol selectivity accompanied by an increase in the hydrocarbon selectivity were observed. The correlation between the relative formation of hydrocarbons and higher alcohols with increasing reaction temperature allowed the researchers to postulate that hydrocarbons and alcohols may share common precursors. Additionally, an increase in the CO conversion was observed as both temperature and pressure increased (Pijolat & Perrichon, 1985).

The use of a silica-silica bimodal support for the synthesis of higher alcohols from the hydrogenation of CO has been investigated by Ding et al. (2012b). Prepared through the incipient-wetness impregnation of silica gel with silica sol, the silica-silica bimodal support is considered to be a suitable support for the formation of higher alcohols as it enhances the catalytic performance by providing both a rapid transportation of reagents and products through the large pores and a large supported metal area through the small pores (Ding et al., 2012b). Ding et al. (2017) further investigated the catalytic performance of K-promoted Cu-Fe supported on the silica-silica bimodal support for the synthesis of higher alcohols from syngas. The K-promoted Cu-Fe bimodal pore catalysts were synthesised *via* the incipient-wetness impregnation of a solution containing $Fe(NO_3)_3$, $Cu(NO_3)_2$ and KNO_3 on a silica bimodal support. The study, performed at 320˚C, 50 bar, 6000 h^{-1} and a H_2/CO molar ratio of 2:1, revealed that the addition of K into the Cu-Fe bimodal pore (Cu-Fe/Silica) catalyst impacts both the physical and chemical properties as well as the catalytic performance. Upon addition of K, an increase in both the Brunauer-Emmett-Teller (BET) catalyst surface area and the dispersion of the Cu and Fe species into the support pores was observed. Moreover, the reduction of the Fe and Cu species and the formation of active bimodal species were found to be enhanced by the presence of K. Regarding the catalytic performance, it was found that the interaction between the K and bimodal active species improves the catalytic activity and

favours the production of higher alcohols. In addition, a drop in the methanol selectivity followed by an increase in the $C_{2+}OH$ selectivity were observed with the increasing of the K content. However, it was also reported that the use of excess K, above 0.5 wt%., causes a decrease in the catalyst performance as it enhances the aggregation of bimodal active species and the restriction of the Fe and Cu species reduction.

From the studies presented above four catalysts, summarized in Table 2. 4, have been selected based on their relatively high catalytic performance during the FTS. These catalysts were then synthesised, characterized and tested under both FTS and NFTS conditions in this study to investigate the correlation between the formation of oxygenates and NCCs under FTS and NFTS conditions respectively.

Table 2. 4: Operating conditions and catalytic performance of the four selected catalysts.

	Reference			
	Ding et al. (2013)	Schaller et al. (2018)	Pijolat, M. & Perrichon, V. (1984)	Ding et al. (2017)
Catalyst	Fe,Mn-CuZnO	K,Al-Fe	Fe/Al_2O_3	K-CuFe/Silica
Temperature (˚C)	260	200	225	320
Pressure (bar)	40	20	18	50
H_2/CO molar ratio	2	2	2	2
GHSV (h^{-1}) (*$ml/g_{cat}.s$*)	6000	*0.045*	40000	6000
CO conversion (%)	**23**	**6.8**	**5.3**	**51**
Alcohol selectivity (C%)	**61**	**34**	**41**	**62**
Hydrocarbon selectivity (C%)	20	63	59	11
CO_2 selectivity (C%)	20	4.1	N/A	26

2.3.3. Proposed mechanisms for the synthesis of oxygenates during the Fischer-Tropsch synthesis

Due to the complexity of the FTS, few mechanisms for the formation of oxygenates have been proposed and they are still being debated. Among the mechanisms proposed, the CO-insertion mechanism, proposed by Pichler & Schulz (1970), is considered as the most plausible mechanism for the oxygenates formation during the FTS process. As already explained in Section 2.1.4, chemisorbed CO and surface methyl species are considered as monomers and chain initiators in the CO-insertion mechanism respectively. The insertion of the chemisorbed CO into a metal-alkyl bond results in the formation of surface acyl species which allows the growth of the carbon chain. The formation of either *n*-paraffins or *α*-olefins

were found to occur when the chain termination involves the addition of hydrogen or the β-hydrogen elimination respectively. However, if the chain termination involves oxygen surface species, it results in the formation oxygenates. Aldehydes and alcohols are formed from the addition of hydrogen to acyl species and RCHOH surface species respectively, shown as Path 1 on Figure 2. 6. Furthermore, the addition of a surface alkyl group to the acyl species leads to the formation of ketones (Claeys & Van Steen, 2004). According to Johnston & Joyner (1993), the surface acyl species could also be formed from the addition of an hydroxyl group into a surface alkylidene group, shown as Path 2 in Figure 2. 6. Therefore, Johnston & Joyner (1993) postulated that the formation of primary alcohols or aldehydes occurs when the chain termination of the acyl species involves a hydrogen addition or a β-hydrogen elimination respectively. Additionally, from the results and observations obtained upon the co-feeding of oxygenates during the FTS runs, the reabsorption and inter-conversion of oxygenates as well as the secondary reactions of oxygenates to the corresponding paraffins and olefins were observed by Cairns (2008).

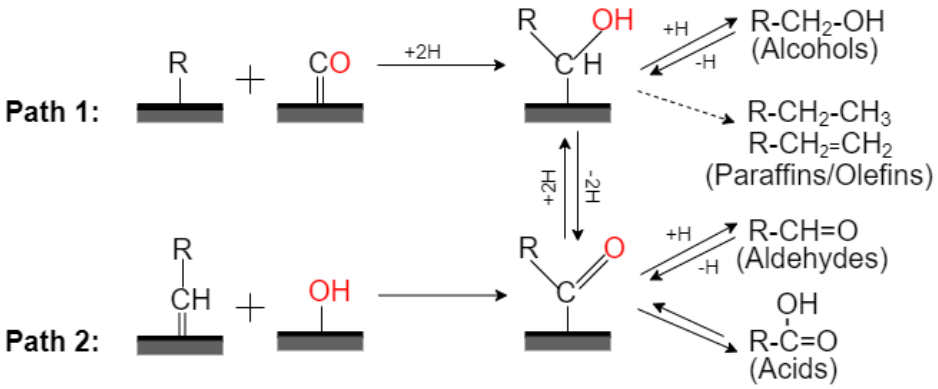

Figure 2. 6: Proposed mechanisms for the formation of oxygenates (primary alcohols, aldehydes and acids) during the FTS process. Adapted from (Claeys & Van Steen, 2004).

2.4. Fischer-Tropsch synthesis product analysis techniques

The identification and quantification of both major, *i.e.* paraffins and olefins, and minor, *i.e.* oxygenates, FTS products have been the subject of several investigations as the accurate characterisation of the minor FTS products might provide critical information on the mechanistic pathway of FTS product formation (Snel, 1986), (Patzlaff et al., 1999), (Schulz & Claeys, 1999b), (van der Westhuizen et al., 2008).

Over the past decades, one-dimensional gas chromatography (1D-GC) has been extensively used for the analysis of FTS products. Recently, an increasing interest has been dedicated to two-dimensional gas chromatography (2D-GC) which is a powerful and versatile analytical

instrument for the analysis of complex samples. The following sections aim to provide an overview of one- and two-dimensional gas-chromatography techniques.

2.4.1. One-dimensional gas-chromatography

During the one-dimensional gas chromatography (1D-GC) analysis, a volume of the gaseous sample is injected into a capillary column packed with a stationary phase of which the material and therefore its polarity can be chosen, *e.g.* 100% dimethyl polysiloxane (non-polar), (50%-phenyl)-methylpolysiloxane and polyethylene glycol (highly polar) (Rahman et al., 2015). To move the sample through the column, a carrier gas also known as a mobile phase is used (Grobler, 2008). Helium, hydrogen, nitrogen or argon are the most commonly used carrier gases for the GC analysis. The separation of the different components of the sample is generally based on one of the two chemical properties which are the volatility and the polarity of the components. The choice of the stationary phase present in the capillary column is the determining factor for which chemical property is used, *i.e.* volatility or polarity. As the sample moves through the column, the sample components interact differently with the stationary phases and adsorb onto the column based on their molecular properties (Grobler, 2008). The different sample components elute from the column at different time, known as the retention time, thus providing separation of the components. The components are analysed as they elute from the column using a suitable detector such as a flame ionization detector (FID) or a mass spectrometer (MS) for identification and quantification purposes (Snel, 1986), (Patzlaff et al., 1999), (Schulz & Claeys, 1999b).

The 1D-GC has been intensively used as the analytical technique for the characterisation of the FTS products due to the high peak capacities, *i.e.* the maximum theoretical number of components that can be successfully separated at a given set of analytical conditions with the modern capillary columns (Shen & Lee, 1998). However, due to the complexity of the FTS products, the 1D-GC analysis fails to provide a complete and accurate analysis of the FTS products spectrum, specifically for minor products. The misidentification of minor FTS products, *i.e.* oxygenates and aromatic compounds, and the incorrect quantification of major FTS products due to the co-elution of major and minor FTS products were found to be the main limitations of the 1D GC for the FTS product analysis (da Silva Maciel et al., 2017).

2.4.2. Two-dimensional gas-chromatography

The comprehensive two-dimensional gas chromatography (2D-GC) was first introduced in the analytical world in 1991 as a solution for the analysis of complex samples due to its ability to identify and quantify trace products accurately (Liu & Phillips, 1991). 2D-GC has been used for the characterization of the FTS products and was found to be suitable for the identification

and quantification of oxygenates and other minor FTS products such as cyclic olefins over the carbon number range of C_{10} to C_{30} (van der Westhuizen et al., 2011).

The 2D-GC technique relies on two basic principles which are the orthogonal separation of the sample and the use of a modulator. The 2D-GC is comprised of two columns connected by the modulator as illustrated on Figure 2. 7.

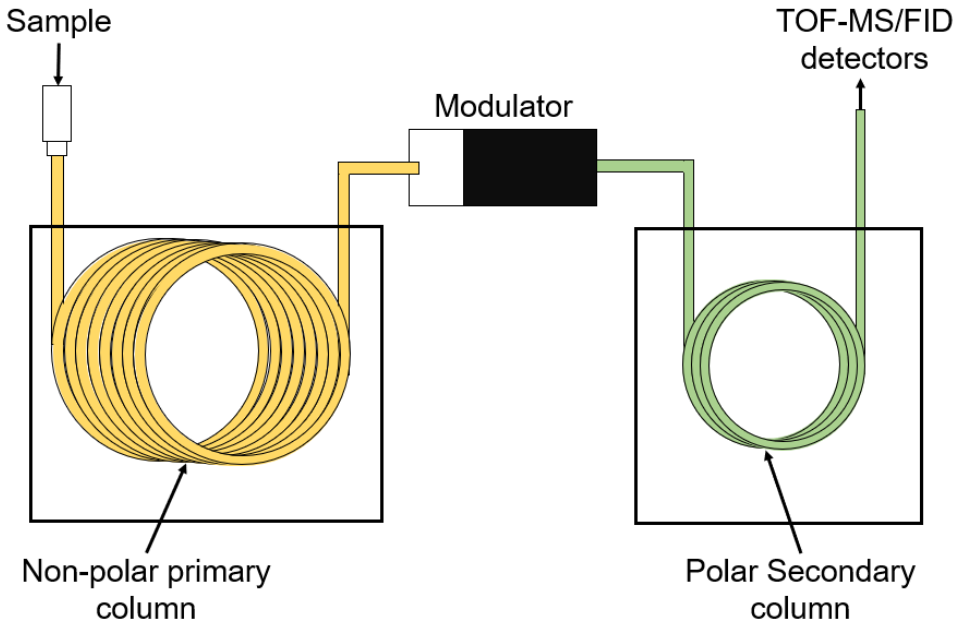

Figure 2. 7: Schematic of the general configuration of the two-dimensional gas-chromatography (2D-GC). Adapted from (Dallüge et al., 2003).

During the 2D-GC analysis, the sample is injected into the primary column where the different components are separated typically based on their volatility, *i.e.* their boiling point, which leads to the formation of various chromatographic bands. The chromatographic bands elude the primary column and get trapped inside the modulator where they are focused into narrow band and then remobilised into the secondary column for further separation based on their polarity, *i.e.* their interaction with the polar stationary phase.

The choice of the type of columns is of paramount importance as the stationary phase of these columns must be of different nature to ensure that the sample undergoes fundamentally different separation mechanisms in each column to create orthogonal separation conditions. If the column in the first dimension has a non-polar stationary phase, the column in the secondary dimension should be polar and vice versa (Dallüge et al., 2003). This separation mechanism results in the separation of the components based on carbon number, nature of carbon chain, *i.e.* linear vs branched, and functional group, *e.g.* paraffins, olefins, alcohols acids, etc. This is achieved by using liquid nitrogen or CO_2 modulators with cold and hot jets

for trapping the analytes into narrow bands and remobilised them into the secondary column (Phillips et al., 1999), (Edwards et al., 2011).

Considered as the “heart” of the 2D-GC system, the modulator plays a critical role on the overall performance of the system. Located between the two columns, the modulator regulates the concentration and the sampling for the chromatographic bands eluting from the primary column into the secondary column (Grobler, 2008), (Grobler et al., 2009). During the 2D-GC analysis, small adjacent chromatographic bands eluting from the primary column are continually trapped inside the modulator while the sample is undergoing the first-dimension separation. These chromatographic bands are then refocused either in time or space and then injected as narrow pulses into the secondary column from the modulator (Grobler, 2008); (Grobler et al., 2009).

During the investigation of the selectivity of Fe-based LTFT products, Grobler et al. (2008) (2009) compared the performance of both one-dimensional (1D) and two-dimensional (2D) GC-FID analyses. In addition to the major FTS products characterized by the 1D-GC-FID, the 2D-GC-FID allowed the identification and quantification of the minor FTS products, *i.e.* linear acids, ketones, aldehydes, secondary alcohols as well as branched- paraffins, olefins, alcohols and acids. With the increase in the complexity of the products obtained during the co-feeding of ammonia and the inadequacy of the conventional 1D-GC for the characterization of nitrogen-containing products, 2D-GC has been successfully used for this challenging analysis in few recent studies (Henkel, 2013), (De Vries, 2017), (Rawoot, 2017).

In order to obtain a complete and accurate identification and quantification of the products obtained during the normal FTS and NFTS runs, an online GC-TCD and 2D-GC equipped with a Time-Of-Flight MS and FID as well as an offline GC-FID were used during this study.

Chapter 3: Project description

3.1. Project objectives

Based on the information and the results obtained from previous studies, summarized in Chapter 2: Literature review, the objectives of this project have been defined as follows:

- Synthesise and characterize four catalysts selected based on their high oxygenates yield
- Test the selected catalysts under normal FTS conditions to determine the catalytic activity and oxygenate selectivity
- Test the selected catalysts under NFTS conditions to determine the influence of ammonia on the performance of the four selected catalysts
- Test the selected catalysts under NFTS conditions to determine the selectivity towards nitrogen-containing compounds (NCCs)

3.2. Hypothesis

From the information gathered in the Introduction and Literature Review sections, the following hypothesis has been postulated:

“The use of a catalyst, yielding a high percentage of oxygenates during the Fischer-Tropsch synthesis (FTS), will allow the selective production of nitrogen-containing compounds (NCCs) during the nitrogen Fischer-Tropsch synthesis (NFTS) as it is speculated that the oxygenates and/or their precursors are the precursors for nitrogen-containing compounds.”

3.3. Key questions

Based on the project objectives and the hypothesis, the following key questions have been formulated:

- How does the co-feeding of NH_3 affect the catalytic activity of the four selected catalysts?
- How does the co-feeding of NH_3 affect the FTS products formation over each of the four selected catalysts?
- Does the use of a catalyst yielding a high oxygenates content during the FTS lead to the selective production of NCCs during the NFTS?

Chapter 4: Experimental methodology

The experimental system of the project was comprised of five key building blocks which are the catalysts synthesis, catalysts characterization, FTS and NFTS run tests and product analysis. The following sections provide detailed information regarding each of these key building blocks.

4.1. Catalyst synthesis

The study started with the syntheses of the four selected catalysts, namely Cu-ZnO promoted with Fe and Mn (Fe,Mn-CuZnO), Fe-based catalyst promoted with K and Al (K,Al-Fe), Fe supported on alumina catalyst (10 wt%. Fe/Al_2O_3) and K promoted Cu-Fe supported on bimodal silica-silica catalyst (K-CuFe/M). The following section outlines the procedures, chemicals and techniques used during the synthesis of each catalyst.

Fe,Mn-CuZnO catalyst

The Fe and Mn promoted CuZnO catalyst was prepared using the co-precipitation technique prescribed by Ding et al. (2013). The amount of each hydrated nitrate salt; *i.e.* 6.01 g of $Fe(NO_3)_3.9H_2O$ (≥98%, Sigma-Aldrich Inc.), 24.17 g of $Cu(NO_3)_3.3H_2O$ (99-104%, Sigma-Aldrich Inc.), 12.56 g of $Mn(NO_3)_2.4H_2O$ (99.99%, Sigma-Aldrich Inc.) and 29.76 g of $Zn(NO_3)_2.6H_2O$ (99%, Sigma-Aldrich Inc.); required to reach the desired Fe:Cu:Mn:Zn molar composition of 0.15:1:0.5:1; were dissolved in 50 ml of warmed deionised water. The resulting nitrate solutions were mixed in a 200 ml beaker, then heated up to 80˚C and continually mixed using a heating plate stirrer. To enhance the precipitation, a 4M Na_2CO_3 solution, made by dissolving 42 g of Na_2CO_3 into 1 l of water, was added to reach and maintain a pH value of 8±0.1. Furthermore, the solution was continually stirred over an aging period of two hours at 80˚C. After aging, the precipitate was filtered using a vacuum filter and washed with deionized water until the pH of the filtrate reached 7. The washed precipitate was then dried in an oven (Memmert UNB400) at 120˚C overnight, crushed and sieved to particle sizes of d = 45-100 µm. The catalyst was further calcined in air at 450˚C for 3h in a calcination oven (Labofurn, manufactured by Kiln contracts (PTY) LTD Cape Town), with a ramping rate of 3˚C/min.

K,Al-Fe catalyst

A precipitation method was used to synthesise the iron precursor which was further promoted with potassium (K) and aluminium (Al) *via* the incipient-wetness impregnation method (Schaller et al., 2018). The iron precursor was prepared by dissolving 40 g of $Fe(NO_3)_3.9H_2O$, (≥98%, Sigma-Aldrich Inc.) in 100 ml boiling deionised water. The iron nitrate solution was heated to 90˚C and continually stirred using a heating plate stirrer. For the precipitation of the

iron metals, an ammonia solution (25 vol% in water, Sigma-Aldrich Inc.) was added to the stirred iron nitrate solution until a pH of 9 was reached. The pH of the solution was then maintained to 9 over a period of 20 mins by adding ammonia solution dropwise. The suspension was left for an aging period of 30 mins under stirring and cooling conditions. After aging, the precipitate was filtered and washed with deionised water through a vacuum filter. The iron precipitate was dried overnight at 120˚C in an oven (Memmert UNB400), crushed and sieved to particle sizes of d = 45-100 µm. Furthermore, the amount of aluminium and potassium nitrate salts, *i.e.* 0.29 g of $Al(NO_3)_3.9H_2O$ (≥98.5%, Sigma-Aldrich Inc.) and 0.01 g of KNO_3 (99.999%, Sigma-Aldrich Inc.), required to reach the desired Fe:K:Al mass ratio of 100:0.1:1, were dissolved into a small volume of distillate water and added dropwise onto the iron oxide powder which was mixed until homogeneity was reached. The powder was further dried overnight at 120˚C in an oven (Memmert UNB400) and then calcined at 500˚C for 4h in air with a ramping rate of 1˚C/min in a calcination oven (Labofurn, manufactured by Kiln contracts (PTY) LTD Cape Town).

10 wt% Fe/Al_2O_3 catalyst

The synthesis of the 10 wt% Fe/Al_2O_3 catalyst was done using the wet impregnation method prescribed by Pijolat & Perrichon (1985). During the synthesis, 9.0 g of the alumina support, aluminium oxide (Puralox SCCA-5/200, Sasol Germany), was mixed with 30 ml deionised water and then sonicated for 30 mins to enhance the mixing. In order to reach the 10 wt% loading of Fe on alumina, 7.23 g of $Fe(NO_3)_3.9H_2O$ (≥98%, Sigma-Aldrich Inc.), was dissolved in 30 ml distillate water and further sonicated for 10 mins to ensure complete dissolution of the salt. The iron nitrate solution was added dropwise to the alumina solution and the resulting solution was sonicated for 30 mins to ensure a perfect dispersion. After mixing, a rotary evaporator (Büchi Rotavapour R-205) was used to remove the water content. The water bath of the rotary evaporator was set at 70˚C with a rotation speed at 85 rpm and the pressure was decreased from 760 mbar to 100 mbar with a rate of 5 mbar/s. The resulting solids were further dried overnight at 120˚C in an oven (Memmert UNB400), sieved to particle sizes of d = 45-100 µm and then calcined in air for 4h at 450˚C with a ramping rate of 1˚C/min in a calcination oven (Labofurn, manufactured by Kiln contracts (PTY) LTD Cape Town).

K-CuFe/Silica catalyst

The silica-silica bimodal pore support was synthesised using an incipient-wetness impregnation method prescribed by Ding et al. (2012b). Silica gel, high-purity (Davisil Grade 646), 35-60 mesh, pore size 150 Å, and Silica sol, LUDOX HS-40 colloidal silica, 40 wt% suspension in H_2O with a density of 1.3 g/ml were used for the synthesis of the bimodal pore support. To obtain a bimodal pore support with a silica sol loading of 20 wt% on silica gel, 3.85

ml of Silica sol diluted in 7.4 ml of deionised water was impregnated into 8.0 g of Silica gel by incipient-wetness method under ultrasonic conditions at 80˚C. After impregnation, the silica support was dried overnight at 120˚C in an oven (Memmert UNB400). The dried support was further calcined in air at 600˚C for 2h with a ramping rate of 3˚C/min. The K promoted CuFe bimodal supported catalyst was then synthesized through the incipient-wetness impregnation of the silica bimodal support with a nitrate solution containing Fe, Cu and K in the desired mass ratio, *i.e.* Fe:Cu:K = 0.3:0.2:0.05:1 (Ding et al., 2017). The nitrate solution was obtained by dissolving the amount of nitrate salts, *i.e.* 3.26 g of $Fe(NO_3)_3.9H_2O$ (≥98%, Sigma-Aldrich Inc.), 1.14 g of $Cu(NO_3)_3.3H_2O$ (99-104%, Sigma-Aldrich Inc.) and 0.04 g of KNO_3 (99.999%, Sigma-Aldrich Inc.), required to reach the desired mass ratio into 1.5 ml of warm distillate water. The catalyst precursors were then dried in air at 120˚C for 12 h, sieved to particle sizes of d = 45-100 μm and further calcined in air at 450˚C for 3h with a temperature ramping rate of 3˚C/min.

4.2. Catalysts characterisation techniques

In this project, several analytical techniques were used to determine the physical and chemical properties of the calcined and spent catalysts. The calcined catalysts were analysed by means of powder X-ray diffraction (PXRD) and in-situ PXRD to determine their phase composition and to investigate their reduction behaviour respectively. In addition, the elemental composition of the catalysts was determined through ICP-OES analysis. The Brunauer–Emmett–Teller (BET) analysis and the N_2 isotherms were used to obtain the BET-surface area, pore volume and average pore diameter.

4.2.1. X-Ray diffraction, XRD

X-Ray diffraction (XRD, Bruker D8 Advance Laboratory X-ray diffractometer) was used to analyse the crystalline phases and determine the average crystallite size of the calcined and spent catalysts. XRD, equipped with a cobalt source (Co-Kα radiation, λ = 1.78897 Å) and position sensitive detector (LynxEye E 1D mode), was operated at 35 kV and 40 mA. The scan range was set to 20˚< 2θ < 120˚ with a scanning step size of 0.012˚ and a scan rate of 1˚/min. The diffraction patterns obtained for all calcined and spent catalysts were compared with those of the standard compounds reported in the International Centre for Diffraction Data PDF-2 database to identify the phases present in each catalyst. However, due to the limited sensitivity of the XRD, the phases of the compounds with a mass percent less than 2% were not detected during the analysis.

The average crystallite size, d_C, was calculated from the XRD scans using the Debye-Scherrer equation:

$$d_C = \frac{K \times \lambda}{\beta \times cos\theta} \qquad Eq.3$$

Where K is the shape factor (0.9), λ is the wavelength of the X-ray, β is the line broadening at half the maximum intensity (FWHM) in radians and θ is the diffraction angle in degrees.

4.2.2. In-situ X-Ray diffraction, In-situ XRD

The investigation of the reduction behaviour of the catalysts as well as the identification and quantification of the phases present after reduction were done using a UCT-developed XRD cell (Claeys & Fischer, 2013). The XRD cell was mounted to a laboratory X-ray diffractometer (Bruker D8 Advance) equipped with a molybdenum source ($\lambda_{K\alpha1}$ = 0.7093 Å) and position sensitive detector (Bruker Vantec) which was operated in parallel beam mode at 50 kV and 35 mA. The in-situ XRD analysis was performed over a scan range of 15˚< 2θ < 30˚ with a scanning step size of 0.019˚ and a scan rate of 1 scan per 5 mins. A time per step of 0.2 sec and the scan time of 4 mins 2 sec with a delay time of 54 sec between scans were chosen to minimise the effects of phase changes during scan.

Prior to the in-situ XRD analysis, 10-20 mg of the catalyst was loaded into the XRD capillary (borosilicate with 1.0 mm outside diameter, 75 mm length and 0.02 mm wall thickness). Glass wool was added on both sides of the capillary to maintain the catalyst bed in the isothermal zone of the reactor cell. During the in-situ XRD analysis, a hydrogen flowrate between 1 to 2 ml/min, controlled by a Brooks MFCs, was used. Additionally, a K-type thermocouple and a Grefran 800P were used to read and control the capillary temperature which was increased from 50˚C to 300˚C during the analysis of Fe,Mn-CuZnO and K-CuFe/Silica catalysts and from 50˚C to 400˚C during the analysis of K,Al-Fe and 10 wt% Fe/Al_2O_3 catalysts. A temperature ramping rate of 1˚C/min was used during heating and cooling.

4.2.3. Inductively coupled plasma-optical emission spectrometry, ICP-OES

A Varian 730 Series spectroscope was used to conduct the inductively coupled plasma optical emission spectrometry (ICP-OES) measurements to determine the concentration of the metals present in the calcined catalysts. The instrument was equipped with a radial torch configuration and an internal standard, *i.e.* scandium, which enables the instrument to detect and quantify small traces of metals.

Prior to the ICP-OES analysis, the catalyst samples were prepared via acid digestion with the aqua regia solution, *i.e.* a mixture of hydrochloric acid and nitric acid in a HNO_3:HCl ratio of 1:3. A quantity of 30 mg of each catalyst was dissolved in 20 ml of the aqua regia inside a

250 ml Erlenmeyer flash and then slowly heated up using a heating plate. Enough time was given to permit the complete digestion of the catalysts and to reduce the volume of the resulting solution, from 20 ml to approximatively 10 ml. The resulting solutions were then transferred to 100 ml volumetric flasks and diluted to 100 ml with purified water. For the metal concentration to fit in the standard range, 1 ml of each diluted solution was further diluted with 2 wt%. HNO_3 solution to 50 ml and 100 ml respectively.

4.2.4. Brunauer-Emmett-Teller method, BET

The BET surface area, pore volume and average pore diameter of the calcined catalysts were determined by N_2 adsorption/desorption according to the BET method at liquid nitrogen temperature using a TriStar II 3020 instrument (Micromeritics). Prior to the BET analysis, the catalyst samples were degassed under vacuum via a VacPre061, where the temperature of the samples was increased from 30˚C to 60˚C, held for 30 mins, then to 90˚C, held for 1 hour, thereafter to 120˚C, held overnight. The samples were then cooled down by decreasing the temperature in the same intervals.

4.3. Catalyst testing

The following section provides detailed information about the experimental set-up and procedures used to perform both FTS and NFTS runs.

4.3.1. Experimental set-up

The test unit consists mainly of a fixed-bed reactor, several valves, pressure controllers and mass flow controllers, as presented in the schematic on Figure 4. 1. The feed gases, CO, H_2, Ar and NH_3/H_2 (10 vol% NH_3), were supplied by Air Liquide and fed into the system via mass flow controllers, F-1 – F-4 (Brooks 5850S from Brooks Instruments, The Netherlands). The mass flow controllers were calibrated prior to the synthesis runs using the bubble flow meter method. Argon was co-fed in the system to be used as an internal standard for the online gas analysis which was done through an online micro gas-chromatograph equipped with thermal conductivity detector, GC-TCD.

The three-way valves 3WV-1 and 3WV-2 were used to change the direction of the feed gases from bypass stream to reactors. In this study, all synthesis runs were performed in a fixed bed reactor. Furthermore, hot and cold traps (T-1 and T-2) located after the fixed bed reactor, with a set temperature of 160˚C and 10˚C respectively, were used to collect liquid hydrocarbons formed during the synthesis runs. All lines after the reactor were heated and maintained to 180˚C to avoid the condensation of the products inside the lines.

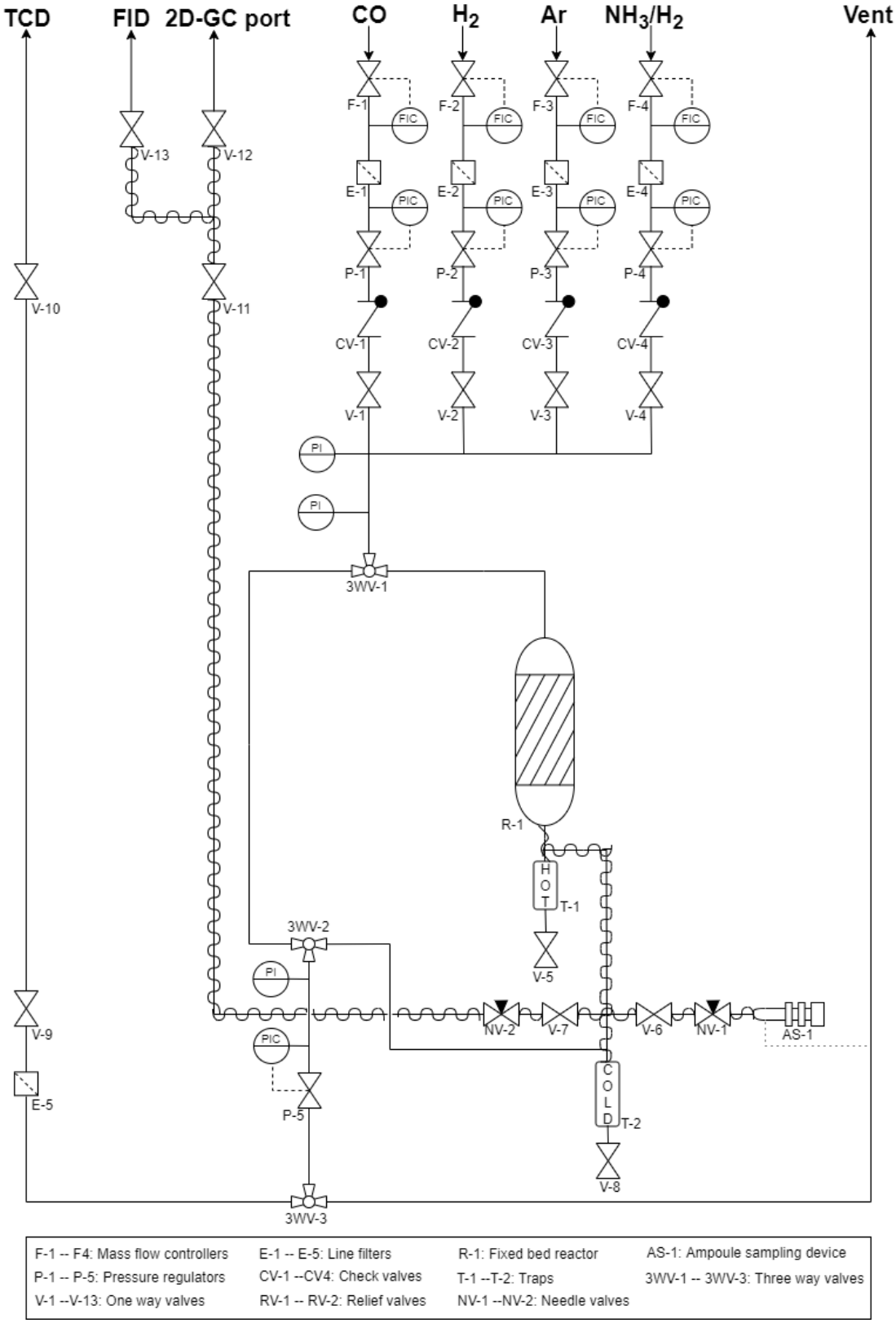

Figure 4. 1: Schematic of the experimental set-up of the test unit used for both FTS and NFTS runs.

4.3.2. Reactor loading

All synthesis runs were carried out inside a fixed bed reactor made of stainless steel with an external and internal diameter of 12.7 mm and 10.3 mm respectively and a length of 50 cm approximately and equipped with a central thermocouple, as illustrated in Figure 4. 2.

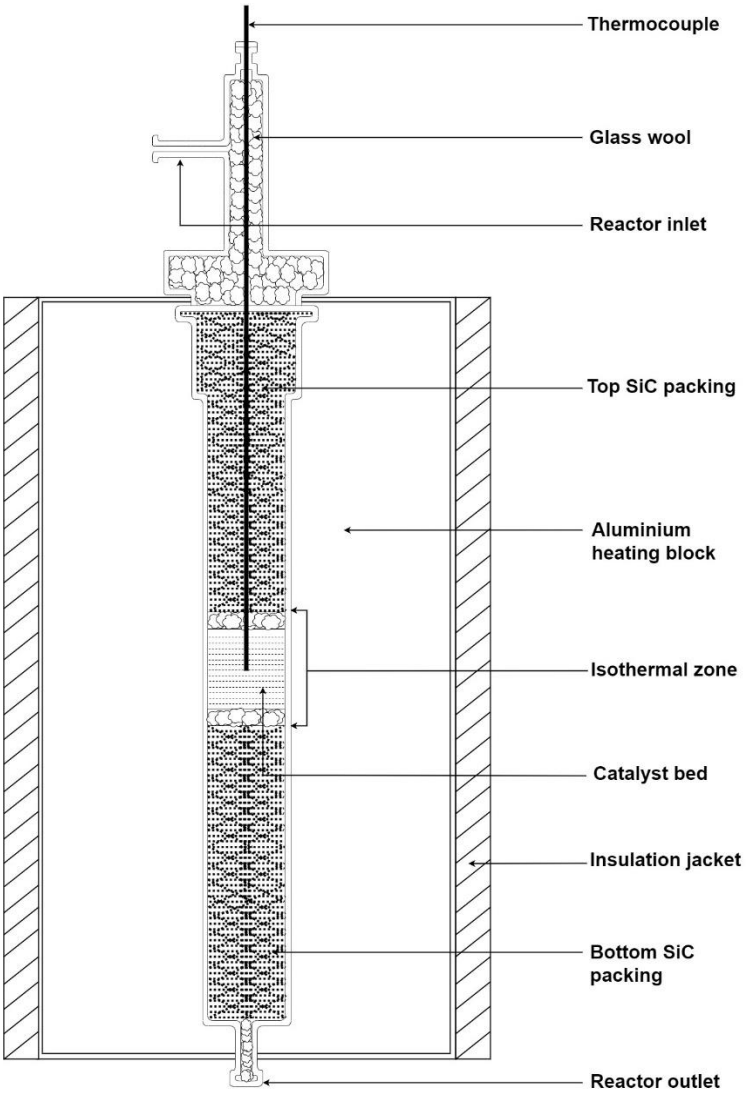

Figure 4. 2: Configuration of a fixed bed reactor (drawing not to scale).

During the loading of the reactor, silicon carbide (Aldrich, 600-900 µm) was first packed from the reactor head to the tip of the central thermocouple which marked the start of the reactor isothermal zone, ± 2˚C and 3 cm. Glass wool was then added before and after the loading of the catalyst and more silicon carbide (Aldrich, 600-900 µm) was added. Glass wool was also used to plug the reactor outlet. During the loading, the reactor was constantly tampered to ensure the tightening of the reactor packing which prevents the catalyst bed, *i.e.* 1.5-2 cm, from moving during the synthesis runs. Silicon carbide packed before the catalyst bed, *i.e.* the top SiC packing, ensured the heating and the homogenous mixing of the feed gas.

On the other hand, the bottom SiC packing stabilized the catalyst bed and provided an inert environment which reduces the occurrence of further reactions and interactions between the products.

In this study, all catalysts, with a catalyst loading of 0.50 g (45-100 µm), were diluted in fine silicon carbide (Aldrich, 215-300 µm) at a catalyst to silicon carbide mass ratio of 1:3 to reduce the amount of heat released per catalyst bed volume during the exothermic Fischer-Tropsch reactions as silicon carbide has a high thermal conductivity. The particle size ranges of both diluent and catalysts were chosen to ensure that $\frac{ID_{Reactor}}{d_p} > 10$, (Ertl et al., 1997) to allow an ideal plug flow behaviour with negligible wall effects and minimum pressure drop across the catalyst bed, *i.e.* pressure drop less than 0.1 bar, during the runs. Moreover, the catalyst particle sizes were less than 300 µm to avoid hampering effects which are caused by intra-particle diffusion of the reactants (Claeys & Schulz, 2004).

The packed reactor was then placed inside a temperature controlled electric furnace, a brass block housing, which contains heating cartridges and thermocouples that control and monitor the reactor temperature. During the synthesis runs, an insulating jacket was fastened around the brass block housing to reduce the exchange of heat between the furnace and its surrounding.

4.3.3. Synthesis runs procedure

Prior to starting the synthesis runs, a pressure test was conducted using argon at room temperature at 20 bar (absolute) for 1 hour to detect any possible leaks present in the reactor system. After a successful pressure test, the reactor system was de-pressurized to atmospheric pressure to perform the in-situ activation of the catalysts by reduction in pure hydrogen under the conditions presented in Table 4. 1.

Table 4. 1: Conditions used to perform the in-situ activation, i.e. reduction, of the catalysts.

Catalyst	Fe,Mn-CuZnO K-CuFe/Silica	10wt% Fe/Al_2O_3 K,Al-Fe
Activation gas	Hydrogen	Hydrogen
Space velocity	50 ml/min	50 ml/min
Pressure	Atmospheric	Atmospheric
Temperature	At 1˚C/min to 300˚C, 4h isothermal At 1˚C/min to 180˚C, 5h isothermal	At 1˚C/min to 400˚C, 10h isothermal

After the in-situ reduction of the catalyst, the synthesis reactions were performed in three stages. The first stage was an unmodified FTS reaction, *i.e.* FTS-Before, which was performed for 24 hours to ensure achieving the steady state of the reaction. The second stage was the co-feeding of NH_3, *i.e.* nitrogen FTS (NFTS), which was conducted by introducing 5 vol% NH_3 into the reaction feed gas for a period of 6 hours investigating the effects of NH_3 co-feeding on the catalytic performance, *i.e.* the catalytic activity and products selectivity. And during the third stage, *i.e.* FTS-After, the NH_3 co-feeding was stopped and the system was further monitored under normal FTS conditions over a minimum period of 6 hours, when possible, to investigate the impact of NH_3 on the catalytic activity and stability.

All synthesis reactions were carried out at 240˚C, with a total pressure of 20 bar, a space velocity of 6000 h^{-1}, a H_2/CO ratio of 2 and 10 vol% of the total flowrate being the reference gas, argon.

4.3.4. Sampling procedure

The reactor outlet stream, made of organic and inorganic products as well as unreacted reagents, was continuously analysed through an online gas chromatograph equipped with thermal conductivity detection (GC-TCD) during the three reaction stages. Additionally, ampoules samples for the offline gas chromatography equipped with a flame ionisation detector (GC-FID) were taken after 24 hours under normal FTS conditions (FTS-Before) (Schulz & Gokcebay, 1984), every hour during the 6 hours of co-feeding NH_3 (NFTS) and after 6 hours after removal of NH_3 (FT-After). An online two-dimensional gas-chromatograph equipped with time of flight-MS and FID (2D-GC TOF-MS/FID) analysis was con-currently performed with the ampoules sampling. The combination of the products analyses obtained from the offline GC-FID, *i.e.* characterization of short chain hydrocarbons, and the online 2D-GC, *i.e.* characterization of minor products such as nitrogen containing compounds and oxygenates, allowed to obtain accurate and detailed characterization of the products.

The ampoule sampling used for the GC-FID, illustrated in Figure 4. 3, consists of the collection of gas samples into evacuated glass ampoules.

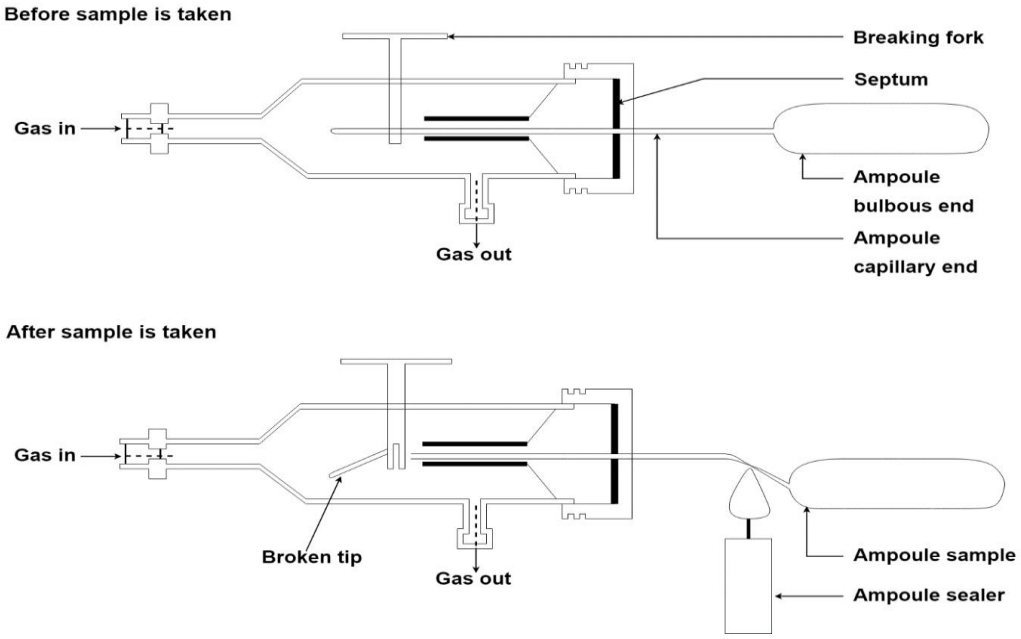

Figure 4. 3: Ampoule sampling device and procedure.

The glass ampoules were made of a capillary end and a bulbous end. During the sampling, the capillary end of an evacuated ampoule was inserted inside the gas-sampling device. The breakage of the capillary end inside the gas-sampling device with the breaking fork allowed some of the reactor outlet gas to be sucked into the ampoule which was then sealed with a butane flame. The ampoule samples contained all the products present in gaseous or vapour phase at the reaction temperature (Schulz & Gokcebay, 1984).

4.4. Product analysis methods

The following section summarizes the parameters and operating conditions for the different instruments used for the product characterization.

4.4.1. Inorganic compound analysis

The online analysis of the reactor outlet stream was performed using a Varian Micro Gas Chromatograph, CP-4900, equipped with three channels and thermal conductivity detectors (TCD) to monitor the concentrations of carbon monoxide (CO), carbon dioxide (CO_2), methane (CH_4), hydrogen (H_2) and argon (Ar).

For the quantification of the GC-TCD results, the molar flowrate of each reactant and product before and during the synthesis reaction was calculated using the following formula ($Eq.4$):

$$\dot{n}_i = \frac{A_i}{A_{Ar}} \times \dot{n}_{Ar} \times f_{TCD,i} \qquad Eq.4$$

Where, $\dot{n}_i$ and $\dot{n}_{Ar}$ are the molar flowrates of compound i and argon respectively; A_i and A_{Ar} are the peak area on the chromatogram of compound i and argon respectively; $f_{TCD,i}$ is the TCD response factor for compound i relative to argon.

Prior to the reactions, a calibration of the GC-TCD was performed using a mixed gas of known composition to determine the TCD response factor for each compound i relative to argon, $f_{TCD,i}$, using the following formula ($Eq.5$):

$$f_{TCD,i} = \frac{C_{Ar}}{C_i} \times \frac{A_i}{A_{Ar}} \qquad Eq.5$$

Where, C_i and C_{Ar} are the concentration of compound i and argon respectively in the mixed gas; A_i and A_{Ar} are the peak area on the chromatogram of compound i and Argon respectively.

A summary of the concentration of the mixed gas used during the GC-TCD calibration and the TCD response factors obtained are presented in Appendix A.1. The operating conditions of the Micro GC-TCD used in this study are shown in Table 4. 2.

Table 4. 2: Operating conditions and settings for the online Micro GC-TCD analysis.

Parameter	Channel 1	Channel 2	Channel 3
Gas analysed	Ar, CH_4, CO	CO_2	H_2
Carrier gas	H_2	H_2	Ar
Column description	20 m MS5	10m PPQ	10m MS5
Column temperature [˚C]	80	50	80
Injection temperature [˚C]	100	100	100
Injection pressure [bar]	1.50	0.80	1.50
Injection time [ms]	300	80	350
Backflush time [s]	180	-	180
Sampling time [s]	35	35	35
Run time [s]	300	300	300

The conversion of CO based on GC-TCD analysis, *i.e.* $X_{CO,TCD}$, was then calculated using the molar flowrate of CO entering the reactor and the molar flowrate of CO leaving the reactor as presented on the following formula ($Eq.6$):

$$X_{CO,TCD} = \frac{\dot{n}_{CO,in} - \dot{n}_{CO,out}}{\dot{n}_{CO,in}} \qquad Eq.6$$

Where, $\dot{n}_{CO,in}$ and $\dot{n}_{CO,out}$ are the molar flowrates of CO entering and leaving the reactor respectively.

4.4.2. Organic compounds analysis

Gas chromatography-Flame ionisation detector, GC-FID

The analysis of the ampoule samples collected during the synthesis reactions were performed offline *via* a Varian GC, CP-3900, equipped with a capillary column and a flame ionisation detector (FID) to determine the concentration of the volatile organic products. The content of the ampoule samples was injected into the GC-FID split injector using a syringe. The operating conditions of the GC-FID used in this study are summarised in Table 4. 3.

The FID responses obtained for each organic compound differ in intensity as they are strongly dependent on the total number of carbon atoms and the number of carbon atoms bonded to an oxygen atom present in the organic compound. Therefore, theoretical FID response factors are calculated using the increment method proposed by Kaiser (1969) which accounts for the variation in FID response strength. According to the increment method, carbon atoms only bonded to hydrogen or other carbon atoms have an increment of 1; carbon atoms with a single bond to an oxygen atom have an increment of 0.55 and carbon atoms with a double bond to an oxygen atom have an increment of 0. Based on these rules, the FID response factor of each FT organic product, $f_{FID,i}$, can be calculated using the following equation ($Eq.7$):

$$f_{FID,i} = \frac{N_{C,i}}{N_{C(C-C)} + 0.55 \times N_{C(C-O)} + 0 \times N_{C(C=O)}} \qquad Eq.7$$

Where, $N_{C,i}$ is the total number of carbon atoms present in compound i, $N_{C(C-C)}$ is the number of carbon atoms only bonded to hydrogen or other carbon atoms, $N_{C(C-O)}$ is the number of carbon atoms with a single bond to an oxygen atom and $N_{C(C=O)}$ is the number of carbon atoms with a double bond to an oxygen atom.

The response factors for nitrogen-containing compounds (NCCs), used in this study and summarised in Appendix A.2, were reported by Sango (2013). Sango (2013) observed that the response factor of all nitriles is equivalent to that of hydrocarbons of the same chain length, while the response of the amine group is zero and the factor needs to be adjusted accordingly.

Table 4. 3: Operating conditions and settings for the offline GC-FID analysis.

Parameter	Channel 1
Gas analysed	Organic products
Carrier gas	H_2
Coolant	CO_2
Carrier gas flowrate [ml/min]	30
Air flowrate [ml/min]	300
N_2 make-up flow [ml/min]	25
Column	Fused silica capillary column, stationary phase: CP-Sil 5CB, inner diameter: 0.15 mm, length: 25 m, film thickness: 2.00 µm
Column head pressure [bar]	0.12
Injection temperature [˚C]	200
Split ratio	12-15:1*
Temperature progamme	-55˚C, 1.5 min isothermal 5˚C/min to 0˚C, 0 min isothermal 5˚C/min to 100˚C, 0 min isothermal 10˚C/min to 280˚C, 2.36 min isothermal 20˚C/min to 150˚C, 999 min isothermal
Total analysis time [min]	35

* Split ratio was varied with CO conversion

After the GC-FID analysis, the identification of the different compounds on the FID chromatogram, as shown in Figure 4. 4, was done *via* comparison with chromatograms obtained in previous studies performed in the research group during which the same FID method was used.

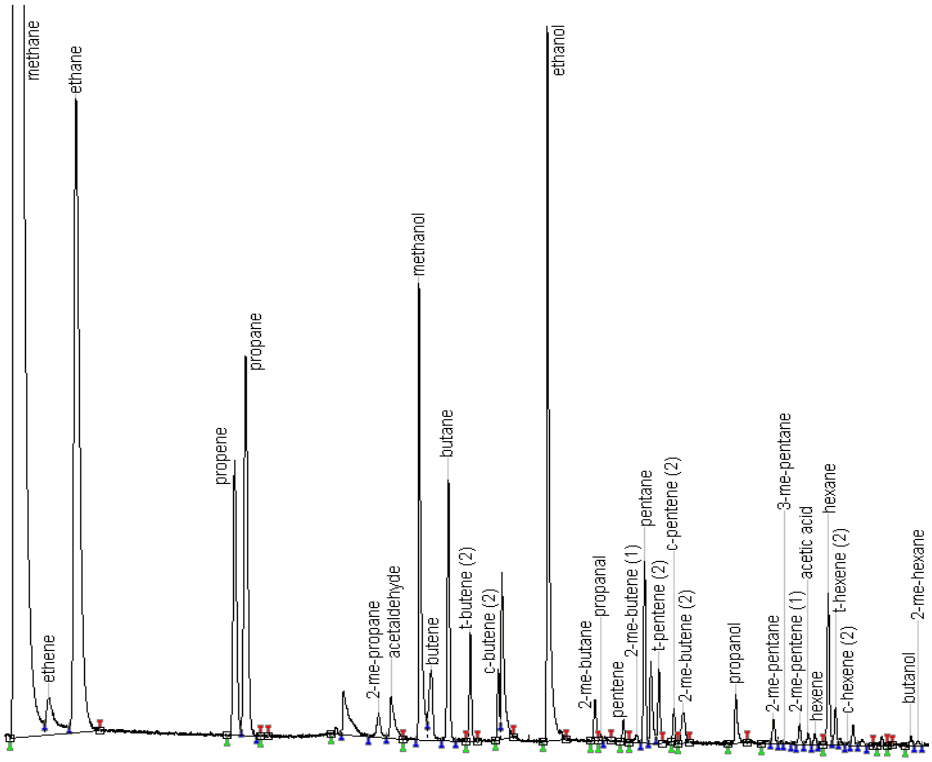

Figure 4. 4: Typical FID chromatogram showing the location of the major hydrocarbon peaks (C_1-C_6 fraction). Adapted from (Rawoot, 2017).

In this study, methane, the molar flow rate of which is known from TCD analyses, was used as the internal standard of the GC-FID analysis. The molar flowrate of each compound, $\dot{n}_i$, was then calculated using the following formula ($Eq.8$):

$$\dot{n}_i = \frac{N_{CH_4}}{N_i} \times \frac{f_{FID,i}}{f_{FID,CH_4}} \times \frac{A_i}{A_{CH_4}} \times \dot{n}_{CH_4} \qquad Eq.8$$

The molar flowrate on carbon basis of each compound, $\dot{n}_{iC}$, was also calculated using the following formula ($Eq.9$):

$$\dot{n}_{iC} = N_{CH_4} \times \frac{f_{FID,i}}{f_{FID,CH_4}} \times \frac{A_i}{A_{CH_4}} \times \dot{n}_{CH_4} \qquad Eq.9$$

Where, $\dot{n}_{CH_4}$ is the molar flowrates of CH_4; A_i and $A_{CH_4}$are the peak area of compound i and CH_4 respectively; $f_{FID,i}$ and f_{FID,CH_4} are the FID response factors of compound i and CH_4 respectively; N_i and N_{CH_4} are the total number of carbon atoms present in compound i and CH_4 respectively.

The selectivity on a carbon based, S_{iC}, for compound i was then calculated using the following formula ($Eq.10$):

$$S_{iC} = \frac{\dot{n}_{iC}}{\dot{n}_{CO,in} - \dot{n}_{CO,out}} \qquad Eq.10$$

Where, $\dot{n}_{iC}$ is the carbon-based flowrate of compound i, $\dot{n}_{CO,in}$ and $\dot{n}_{CO,out}$ are the molar flowrates of CO entering and leaving the reactor.

Furthermore, the weighted selectivity, S_i, for each organic product, *i.e.* paraffins, olefins, oxygenates and NCCs, was calculated as the fraction of the overall selectivity towards the organic products as shown in ($Eq.11$):

$$S_i = \frac{S_{iC}}{\sum S_{iC}} \qquad Eq.11$$

Two-dimensional gas chromatography, 2D-GC (TOF/MS & FID)

The (un)modified FTS organic product spectrum was analysed by 1D-GC and 2D-GC, where the former was mainly used for analysis of C_1 to C_{10} products and the latter was exclusively used the analysis of longer chain hydrocarbons (C_{11} to C_{15}) and NCCs (all chain lengths). Pentanol was used as the 'tie' component which allowed to connect the data obtained from the two GC analyses.

In this study, a LECO-Pegasus 4D system equipped with a time of flight mass spectrometer (TOF-MS) and a flame ionization detector (FID), was used. The TOF-MS and FID detectors were utilised for the identification and quantification of the FTS and NFTS products respectively. However, both detectors could not be used simultaneously and analyses on each detector required different operating conditions. When the TOF-MS was in use, the FID was shut off at the transfer line port in order to maintain its low pressure. The general parameters and operating conditions used for the 2D-GC analysis through TOF-MS and FID detectors are summarized in Table 4. 4.

The results for a typical analysis of a gas phase sample obtained during the FTS (at 240˚C, 20 bar, 6000 h^{-1}, a H_2/CO ratio of 2.0 after 24 hours) and NFTS runs (at 240˚C, 20 bar, 6000 h^{-1}, a H_2/CO ratio of 2.0, 5 vol% NH_3 after 1 hour) over Fe,Mn-CuZnO catalyst are shown in Figure 4. 5.

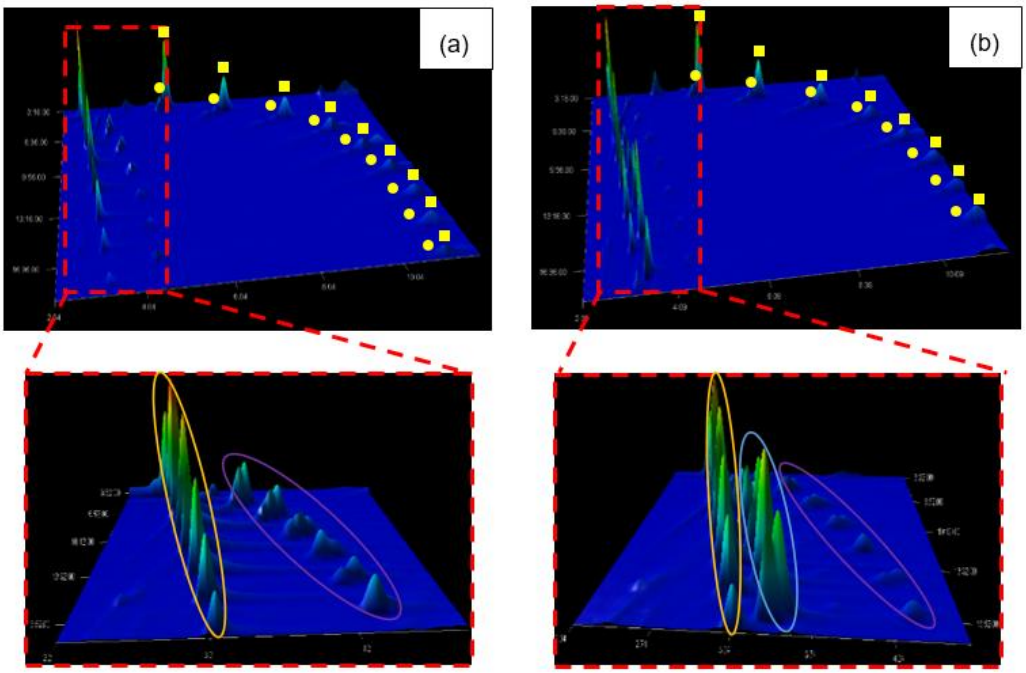

Figure 4. 5: 3D plot of the 2D-GC analysis results obtained (a) FTS run (at 240˚C, 20 bar, 6000 h^{-1}, H_2/CO ratio of 2.0 after 24 hours) and (b) NFTS run (at 240˚C, 20 bar, 6000 h^{-1}, H_2/CO ratio of 2.0, 5 vol% NH_3 after 1 hour) over the Fe,Mn-CuZnO catalyst. [Alcohols: orange circle, Aldehydes: pink circle, Nitriles: blue circle, Olefins: yellow circles and Paraffins: yellow squares]

Table 4. 4: Operating conditions and settings for the two-dimensional gas chromatography analysis.

Parameter	Information/Values	
Carrier gas	He	
	Settings and conditions of the injector	
Injection method	Online	
Mode (Split ratio)	Split (5-20:1)*	
Injection temperature	280˚C	
	Columns specifications	
Primary column	Varian capillary column, stationary phase: CP-Wax 52 CB, length: 30 m, inner diameter: 250 µm, film thickness: 0.25 µm	
Secondary column	Fused silica capillary column, stationary phase: RTX-5, length: 1.39 m, inner diameter: 180 µm, film thickness: 0.2 µm	
	Setting and conditions used during the GC×GC analysis	
Detector	Time of flight mass spectrometer (TOF-MS)	Flame ionization detector (FID)
Total flowrate	1.1 ml/min	2.1 ml/min
Detector temperature	225˚C	280˚C
Modulator offset	+35˚C	+35˚C
Modulation period	8 seconds	12 seconds
Hot pulse	2 seconds	3 seconds
Cold pulse	2 seconds	3 seconds
Primary oven	60˚C, 1 min isothermal	60˚C, 1 min isothermal
	5 ˚C/min to 240˚C, 5 mins isothermal	5 ˚C/min to 240˚C, 5 mins isothermal
Secondary oven	95˚C, 1 min isothermal	135˚C, 1 min isothermal
	5 ˚C/min to 275˚C, 5 mins isothermal	5 ˚C/min to 315˚C, 5 mins isothermal
Total analysis time	42 mins	42 mins

* Split ratio was varied with CO conversion

Chapter 5: Catalyst characterisation results and discussion

5.1. X-ray Diffraction, phase identification and crystallite size

X-ray diffraction analysis of the four selected catalysts was performed to determine the crystalline phases present and the average crystallite sizes of the active phase. The following section summarises the results obtained.

Fe,Mn-CuZnO catalyst

The comparison of the diffraction patterns of the calcined Fe,Mn-CuZnO catalyst, shown in Figure 5. 1, with the standard patterns of tenorite (CuO: PDF-00-001-1117), zincite (ZnO: PDF-00-001-1136) and maghemite (γ-Fe_2O_3: PDF-00-004-0755) confirmed the presence of these three oxides in the catalyst. The broadness of the peaks can be attributed to the overlapping of the peaks corresponding to the three different oxide phases and/or the presence of small crystallites. Ding et al. (2013) reported similar diffraction pattern and no manganese-based phases were detected. This could be due to the low loading of manganese or that the manganese-based phase was present in an amorphous state, thus undetectable by XRD analysis.

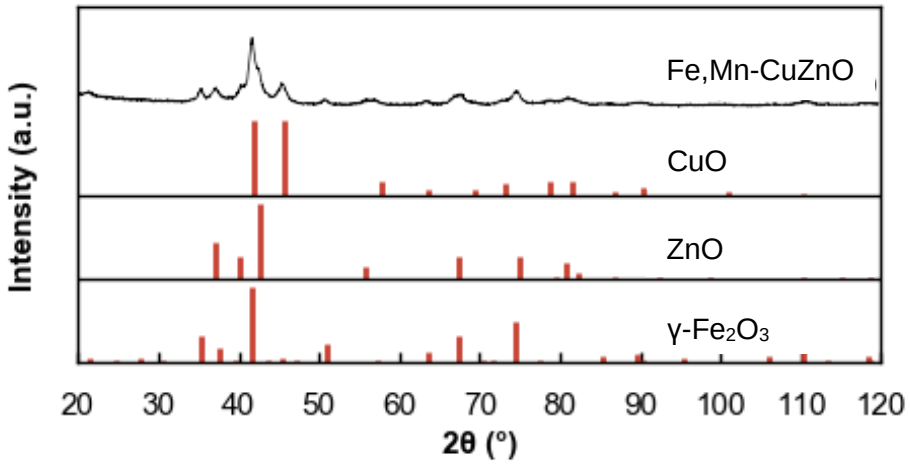

Figure 5. 1: XRD patterns obtained for the calcined Fe,Mn-CuZnO catalyst sample and the reference patterns of CuO, ZnO and γ-Fe_2O_3.

K,Al-Fe catalyst

The XRD patterns of the calcined K,Al-Fe catalyst, shown in Figure 5. 2, were similar to the ones of the calcined iron oxide precursor which matched the reference patterns of hematite (α-Fe_2O_3: PDF-01-087-1165). The potassium and aluminium phases were not identified through this analysis due to the small loading used, *i.e.* 0.10 wt% K and 1.00 wt% Al or they are present in an amorphous phase.

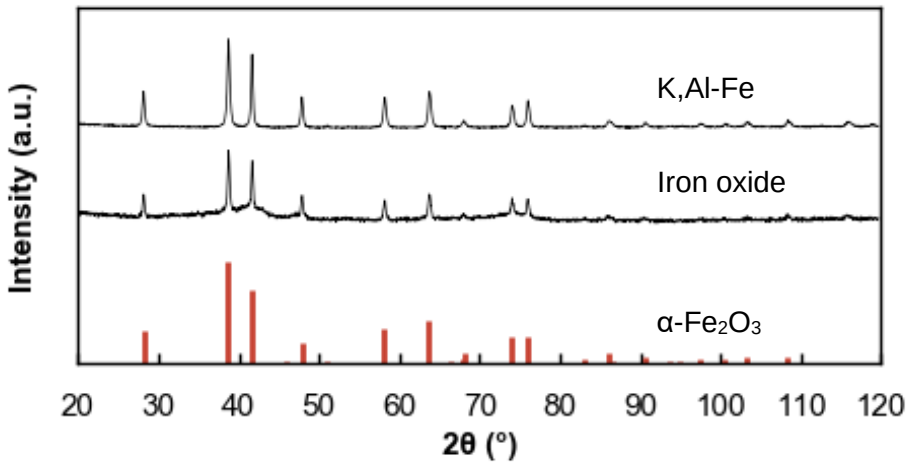

Figure 5. 2: XRD patterns obtained for the calcined K,Al-Fe catalyst, calcined iron oxide precursor samples and the reference pattern of α-Fe_2O_3.

10 wt% Fe/Al_2O_3 catalyst

The comparison of the XRD patterns of the 10 wt% Fe/Al_2O_3, shown in Figure 5. 3, with the alumina support shows the presence of additional peaks which matched the reference patterns of hematite (α-Fe_2O_3: PDF-01-087-1165). None of the composite oxides such as $FeAlO_3$ or $FeAl_2O_4$ were present in the calcined Fe/Al_2O_3 catalyst as none of the XRD peaks matched the reference patterns of these composite oxides.

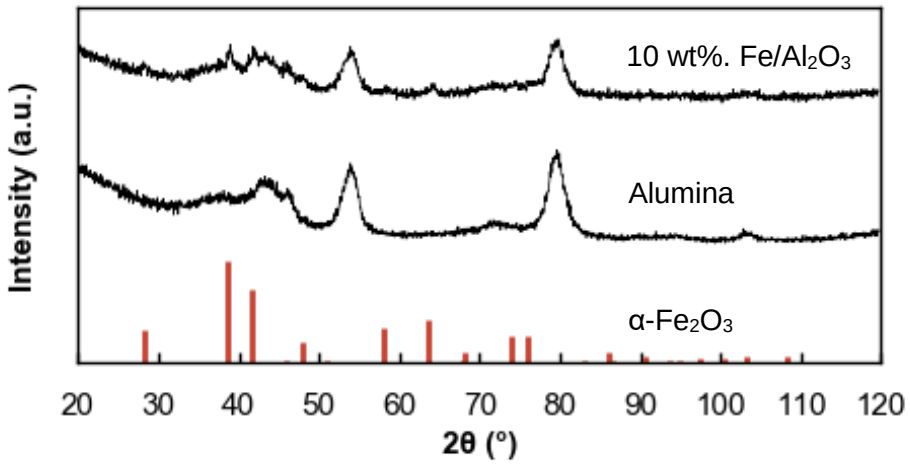

Figure 5. 3: XRD patterns obtained for the calcined 10 wt% Fe/Al_2O_3 catalyst, alumina support samples and the reference pattern of α-Fe_2O_3.

K-CuFe/Silica catalyst

The XRD results of the calcined K-CuFe/Silica catalyst, shown in Figure 5. 4, pointed out that hematite (α-Fe_2O_3: PDF-01-087-1165) and tenorite (CuO: PDF-01-073-6023) are the main phases present in the calcined K-CuFe/Silica catalyst. The broadness of the peaks can be

accredited to the overlapping for the different phase peaks and/or the presence of small crystallites. These results are similar to that reported by Ding et al. (2017).

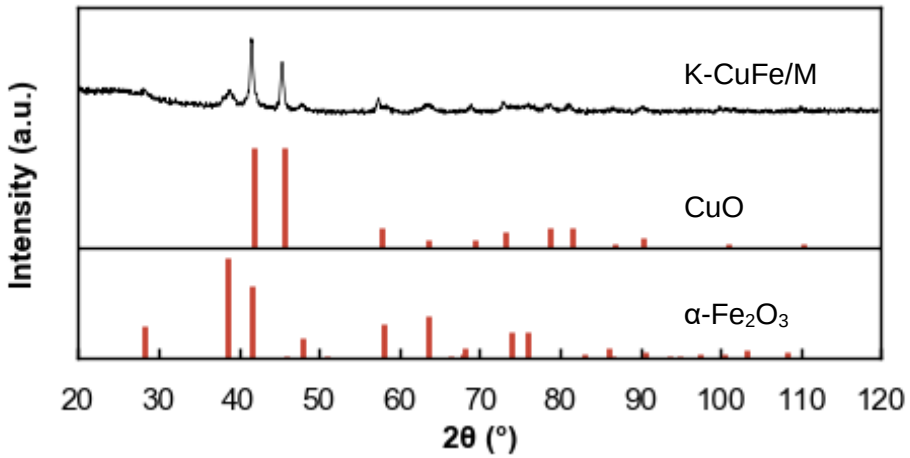

Figure 5. 4: XRD patterns obtained for the calcined K-CuFe/Silica catalyst sample and the reference pattern of CuO and α-Fe_2O_3.

XRD analysis, crystallite sizes

The average sizes of the detected crystalline phases in the four selected catalysts were determined using the Debye-Scherrer equation, see Section 4.2.1. The major peak of each phase identified in each calcined catalyst was used for the measurement of the crystallite size, summarised in Table 5. 1.

Table 5. 1: Summary of phases and the average sizes of the detected crystalline phases in the four selected catalysts obtained through XRD.

Catalyst	Summary of phases identified using PXRD	Calculated crystallite size obtained from PXRD (nm)
Fe,Mn-CuZnO	ZnO	11.9
	CuO	12.0
	γ-Fe_2O_3	18.4
K,Al-Fe	α-Fe_2O_3	38.6
10 wt% Fe/Al_2O_3	α-Fe_2O_3	-*
	γ-Al_2O_3	-*
K-CuFe/Silica	α-Fe_2O_3	32.5
	CuO	37.3

*Due to the amorphous nature of the calcined 10 wt%. Fe/Al_2O_3 catalyst, it was impossible to calculate the crystallite size of the phases present.

5.2. In-situ X-ray diffraction, reduction behaviour

The reduction behaviour and pathway of the selected catalysts were investigated through the in house developed in-situ XRD cell, under hydrogen environment. The in-situ XRD experimental protocol mimicked that of the catalyst activation (reduction) prior to the FTS synthesis, to determine the phases present in the activated catalyst.

Fe,Mn-CuZnO catalyst

As shown in Figure 5. 5, the onset reduction of Fe,Mn-CuZnO catalyst to the metallic Cu, and the iron manganese phase ($(FeO)_{0.3}(MnO)_{0.7}$) occurred at around 150˚C. The low onset reduction temperature could be attributed to the presence of Cu which is classified as a reduction promoter, due to its high hydrogen dissociation ability which facilitates the hydrogen spill-over mechanism (Li et al., 2002). The complete reduction of the copper oxide (CuO) to metallic copper (Cu) and the formation of an iron manganese oxide ($(FeO)_{0.3}(MnO)_{0.7}$) phase occurred as the temperature reached 150˚C and 185˚C, respectively. Further increase of the temperature to 300˚C followed by 4 hours holding time did not cause further transformation of the phases. Similar results were obtained by Ding et al. (2013) during the temperature reduction programme (H_2-TPR) analysis performed over CuZnO catalysts promoted with iron and manganese. The reduction of Fe_2O_3 to Fe_3O_4 and CuO to Cu were found to occur over the temperature range of 160˚C-300˚C, however the formation of the iron manganese oxide phase was not reported. As expected, the ZnO phase did not undergo any transformation during the reduction, as the peaks corresponding to that phase remained unchanged during the reduction.

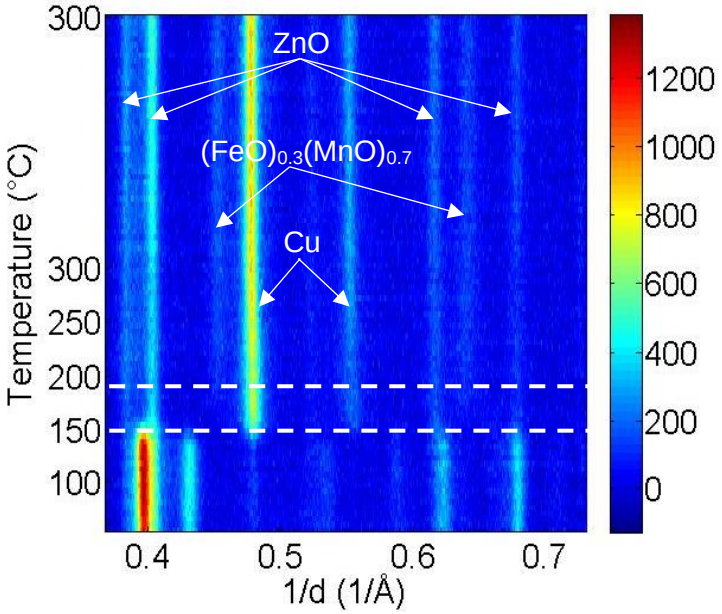

Figure 5. 5: On top view of XRD patterns obtained during the in-situ reduction of the calcined Fe,Mn-CuZnO catalyst sample. Reduction temperature = 300˚C, total of 97 scans.

K,Al-Fe catalyst

The complete reduction of the K,Al-Fe catalyst to the metallic Fe phase occurred via two steps, as shown in Figure 5. 6. The first reduction step which corresponds to the reduction of the hematite (Fe_2O_3) to the magnetite (Fe_3O_4) phase started around 275˚C. The magnetite phase stayed stable up to 400˚C, after which the magnetite phase started reducing to the metallic iron (Fe) phase. The reduction of Fe_2O_3 to Fe_3O_4 and Fe_3O_4 to Fe in a pure Fe_2O_3 was found to occur around 215˚C-280˚C and 605˚C respectively (Lohitharn & Goodwin, 2008). The occurrence of the reduction of Fe_3O_4 to Fe at a relatively low temperature, *i.e.* 400˚C, obtained in this study may be due to the presence of the potassium and aluminium.

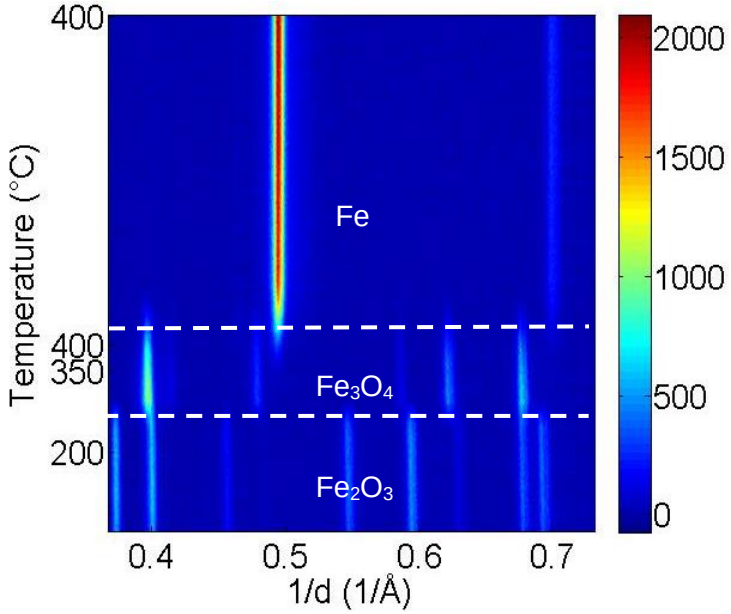

Figure 5. 6: On top view of XRD patterns obtained during the in-situ reduction of the calcined K,Al-Fe catalyst sample. Reduction temperature = 400˚C, total of 157 scans.

10 wt% Fe/Al_2O_3 catalyst

As expected, the γ-alumina phase did not undergo any transformation during the reduction, as the peaks corresponding to that phase stayed unchanged during the reduction of the 10 wt% Fe/Al_2O_3 catalyst, as shown in Figure 5. 7. The reduction of the hematite (Fe_2O_3) phase to the magnetite (Fe_3O_4) phase occurred gradually around 340˚C while further reduction of the magnetite phase to the metallic iron (Fe) phase occurred at 390˚C. Further increase of the reduction temperature to 400˚C and the 10 hours holding time did not cause any phase change. Over a 3.3 wt% Fe supported on γ-alumina, Mosallanejad et al. (2018) reported similar results as a two-stage reduction of the iron oxides, from Fe_2O_3 to Fe_3O_4 and from Fe_3O_4 to Fe at 275˚C and 370˚C respectively, was observed.

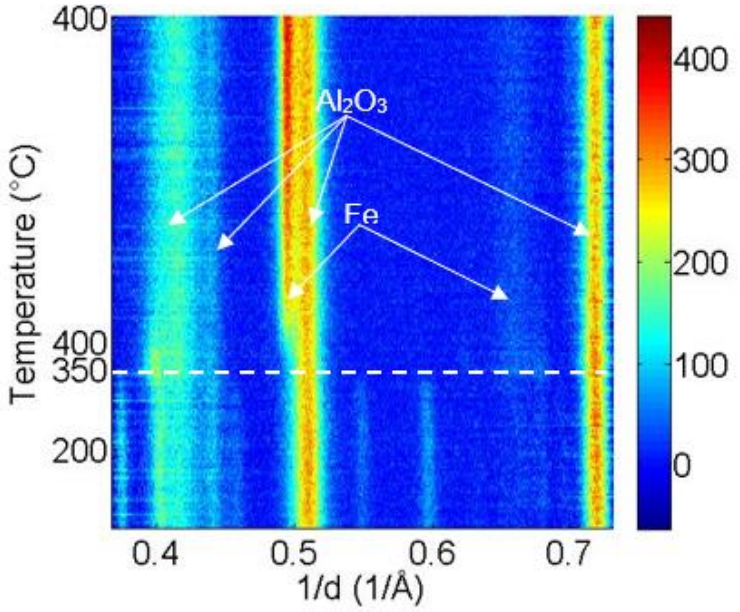

Figure 5. 7: On top view of XRD patterns obtained during the in-situ reduction of the calcined 10 wt% Fe/Al_2O_3 catalyst sample. Reduction temperature = 400˚C, total of 157 scans.

K-CuFe/Silica catalyst

The complete reduction of the copper oxide (CuO) to metallic copper (Cu) and the transformation of the hematite (F_2O_3) phase to the magnetite (Fe_3O_4) phase occurred around 165˚C, as shown in Figure 5. 8. Upon further increase of the reduction temperature to 300˚C and 4 hours holding time, a gradual reduction of the Fe_3O_4 phase to the metallic iron (Fe) phase was observed. The late reduction of the magnetite phase into the metallic phase can be attributed to the interaction between the iron oxide particles and the silica support (Mosallanejad et al., 2018). The increase in the reduction and/or the increase of the holding time may result in the complete reduction of the Fe_3O_4 phase into the Fe phase.

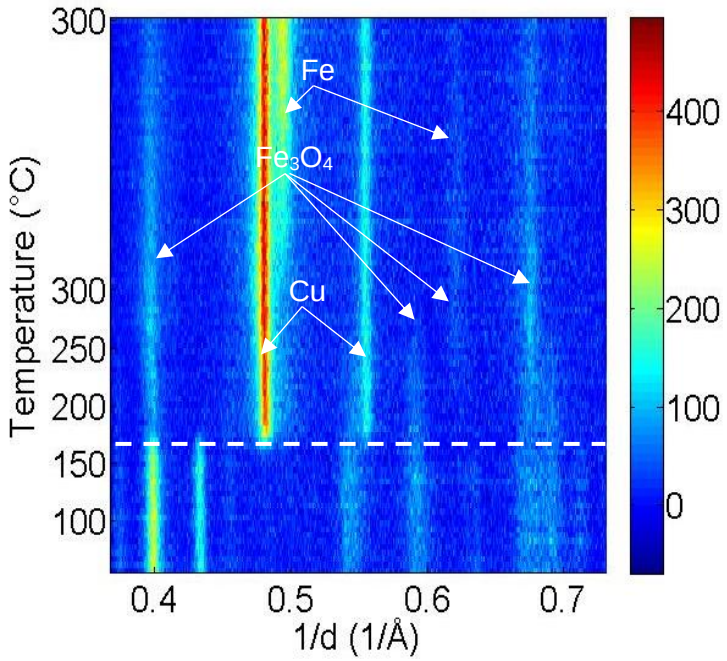

Figure 5. 8: On top view of XRD patterns obtained during the in-situ reduction of the calcined K-CuFe/Silica catalyst sample. Reduction temperature = 400˚C, total of 157 scans.

5.3. Inductively coupled plasma – optical emission spectroscopy results

ICP-OES analysis was performed to determine the composition of the four selected catalysts. From the ICP-OES results, summarised in Table 5. 2, it can be seen that the actual compositions of all four prepared catalysts were close to the theoretical, *i.e.* expected, compositions.

Table 5. 2: Theoretical and actual composition of the calcined catalysts as determined by ICP-OES.

Calcined catalyst	Theoretical composition	Actual composition
Fe,Mn-CuZnO	Fe:Cu:Mn:Zn=0.15:1.0:0.5:1.0 (Molar ratio)	Fe:Cu:Mn:Zn=0.16:1.0:0.34:1.0 (Molar ratio)
K,Al-Fe	0.10 wt% K 1.0 wt% Al	0.09 wt% K 1.0 wt% Al
10 wt% Fe/Al_2O_3	10.0 wt% Fe	9.88 wt% Fe
K-CuFe/Silica	Fe:Cu:K:Silica=0.3:0.2:0.01:1.0 (Mass ratio)	Fe:Cu:K:Silica=0.3:0.2:0.011:1.0 (Mass ratio)

5.4. Brunauer-Emmett-Teller (BET) surface area measurement results

The BET surface area, pore volume and average pore diameter of the calcined catalysts were calculated from the N_2 adsorption-desorption isotherms, *i.e.* the BET measurement technique. The results obtained are summarized in Table 5. 3. The supported catalysts, *i.e.* 10 wt% Fe/Al_2O_3 and K-CuFe/Silica, had the largest BET surface area, 168 m^2/g and 136 m^2/g respectively. On the other hand, the calcined Fe,Mn-CuZnO catalyst had the smallest pore volume, 0.182 cm^3/g, and the K,Al-Fe catalyst was found to have the largest average pore diameter, 29.3 nm. All four catalysts contained mesopores as their average pore size was found to be greater than 2 nm and smaller than 50 nm.

Table 5. 3: BET surface area, pore volume and average pore diameter determined via the N_2 adsorption-desorption measurements.

Catalyst	BET Surface area [m^2/g]	Pore volume [cm^3/g]	Average pore diameter [nm]
Fe,Mn-CuZnO	36.3	0.182	21.2
K,Al-Fe	28.1	0.206	29.3
10 wt% Fe/Al_2O_3	168	0.409	7.8
K-CuFe/Silica	136	0.462	11.8

Chapter 6: Effects of ammonia co-feeding on the catalytic performance of the selected catalysts results and discussion

It has been reported in literature that the co-feeding of NH_3 during the FTS affects both the catalytic activity (Sango, 2013), (Henkel, 2013), (De Vries, 2017) and the FTS products formation highlighted by an increase in the olefinic content (Rausch et al., 2016) and a decrease in the oxygenates formation followed by the formation of nitrogen-containing compounds (NCCs) (Alfred, 1950), (Brown & Maselli, 1973), (Claeys et al., 2013), (Sango, 2013), (Henkel, 2013), (De Vries, 2017). From the correlation between the disappearance of oxygenates and the formation of NCCs, it has been hypothesised that oxygenates and/or their precursors are the precursors of NCCs during the NFTS. However, due to the complexity of the FTS mechanisms, this hypothesis needed to be further investigated.

In the attempt to investigate the correlation between the presence of oxygenates during FTS and the formation of NCCs during the NFTS, a series of FTS runs were performed over four selected catalysts, *i.e.* Fe,Mn-CuZnO; K,Al-Fe; 10 wt% Fe/Al_2O_3 and K-CuFe/Silica. The following chapter presents the results obtained from these investigations.

6.1. Overall catalytic performance

Figure 6. 1 to Figure 6. 4 present a summary of the catalytic performance (of the Fe,Mn-CuZnO, K,Al-Fe, 10 wt% Fe/Al_2O_3 and K-CuFe/Silica) obtained during the three reaction stages, *i.e.* before (24 hours under FTS conditions, FTS-Before), during (6 hours under NFTS conditions, NFTS) and after (6 hours after returning under FTS conditions, FTS-After) the co-feeding of ammonia (NH_3). Over the K,Al-Fe and K-CuFe/Silica catalysts, the analysis of the FTS products after the removal of NH_3 from the feed gas (FTS-After) was unsuccessful due to the occurrence of a pressure build-up within the system which prevented the online analysis of the reactor outlet stream.

A close inspection of the results obtained pointed out that the NH_3 co-feeding affects the catalytic activity and products formation of each of the four selected catalysts at different extent. Over the Fe,Mn-CuZnO, K,Al-Fe and K-CuFe/Silica catalysts, the presence of NH_3 caused a catalytic deactivation while a minimal change in the catalytic activity of the 10 wt% Fe/Al_2O_3 catalyst was observed. However, over all four catalysts, a significant drop in the CO_2 selectivity was observed as a result of NH_3 co-feeding. Regarding the products formation, the co-feeding of NH_3 enhanced the formation of methane, olefins and NCCs while limiting the oxygenates formation during the FTS over all four selected catalysts. Further discussions of these results are provided in the following subsections in order to identify the effects of the presence of NH_3 on the overall catalytic performance of the four selected catalysts.

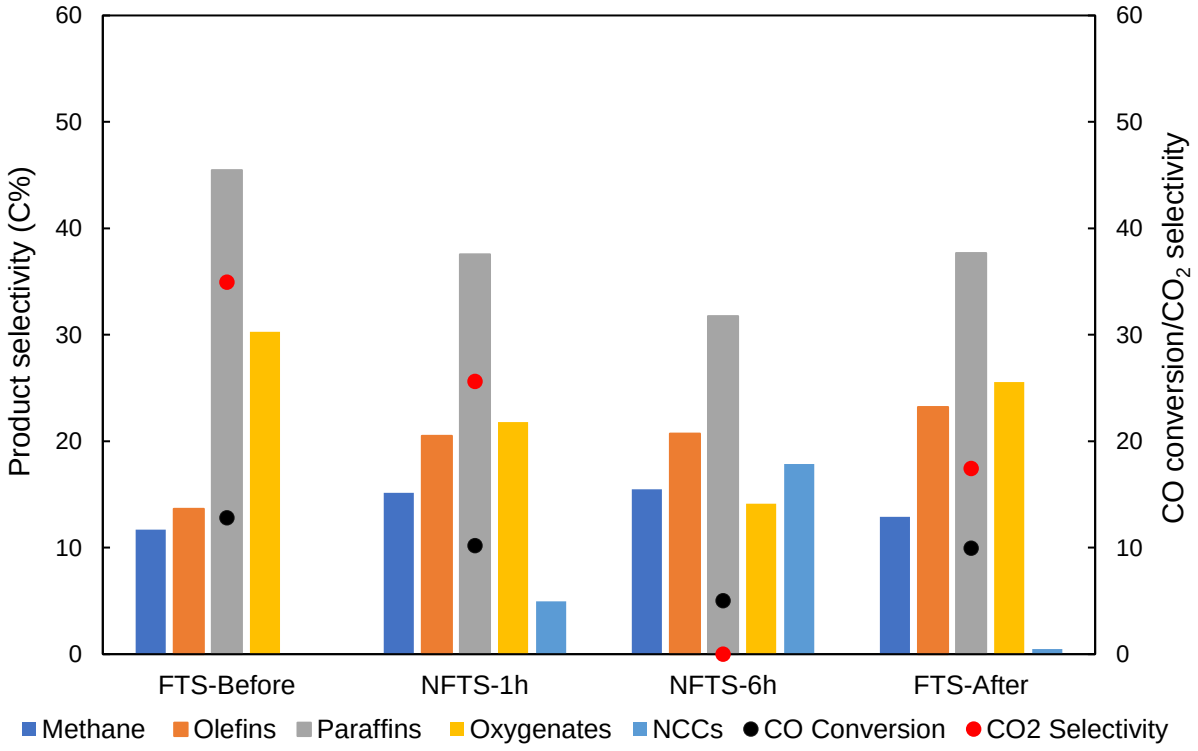

Figure 6. 1: Overall catalytic performance obtained during the reaction stages over the Fe,Mn-CuZnO catalyst (Reaction conditions: T = 240˚C, P = 20 bar, GHSV = 6000 h^{-1}, H_2/CO = 2:1, 5% vol NH_3).

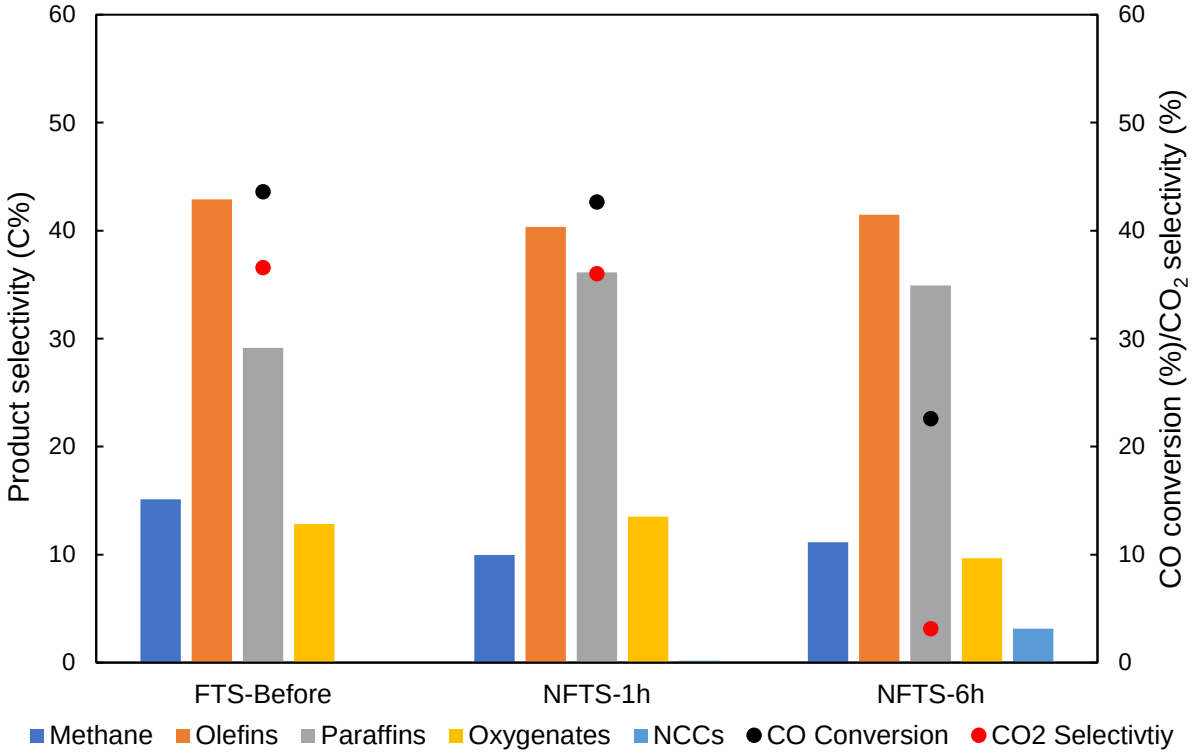

Figure 6. 2: Overall catalytic performance obtained a during the reaction stages over the K,Al-Fe catalyst (Reaction conditions: T = 240˚C, P = 20 bar, GHSV = 6000 h^{-1}, H_2/CO = 2:1, 5% vol NH_3).

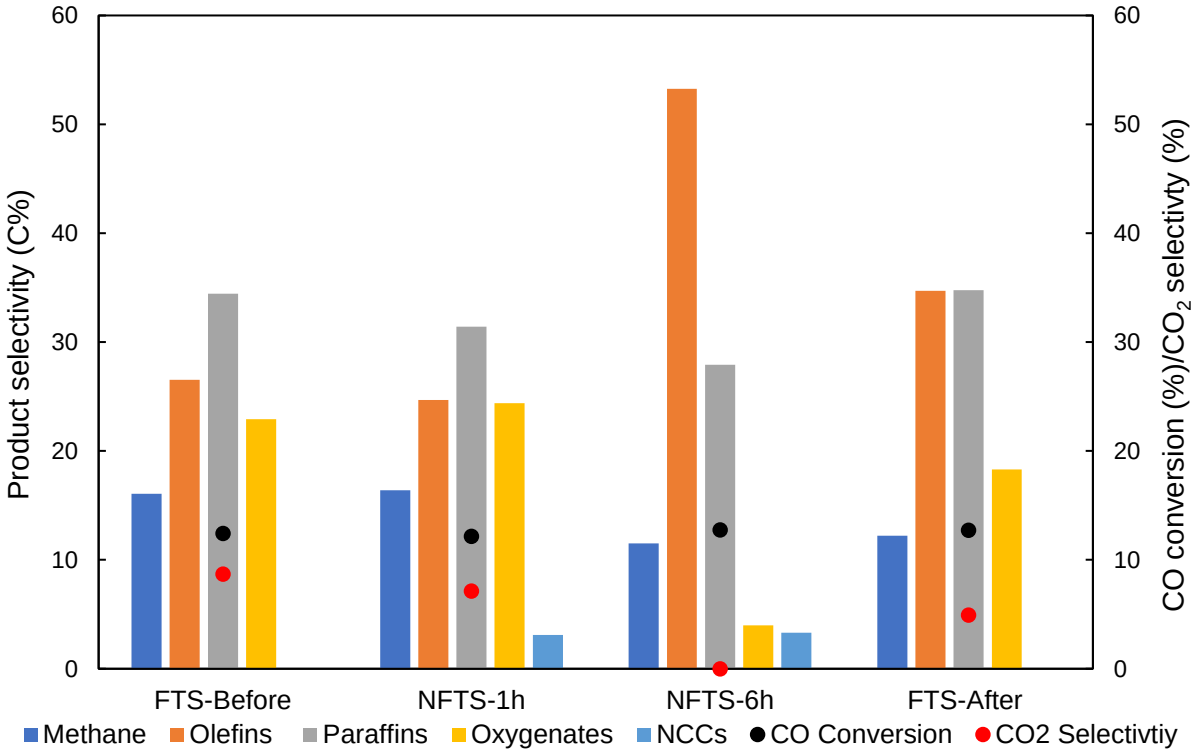

Figure 6. 3: Overall catalytic performance obtained during the reaction stages over the 10 wt% Fe/Al_2O_3 catalyst (Reaction conditions: T = 240˚C, P = 20 bar, GHSV = 6000 h^{-1}, H_2/CO = 2:1, 5% vol NH_3).

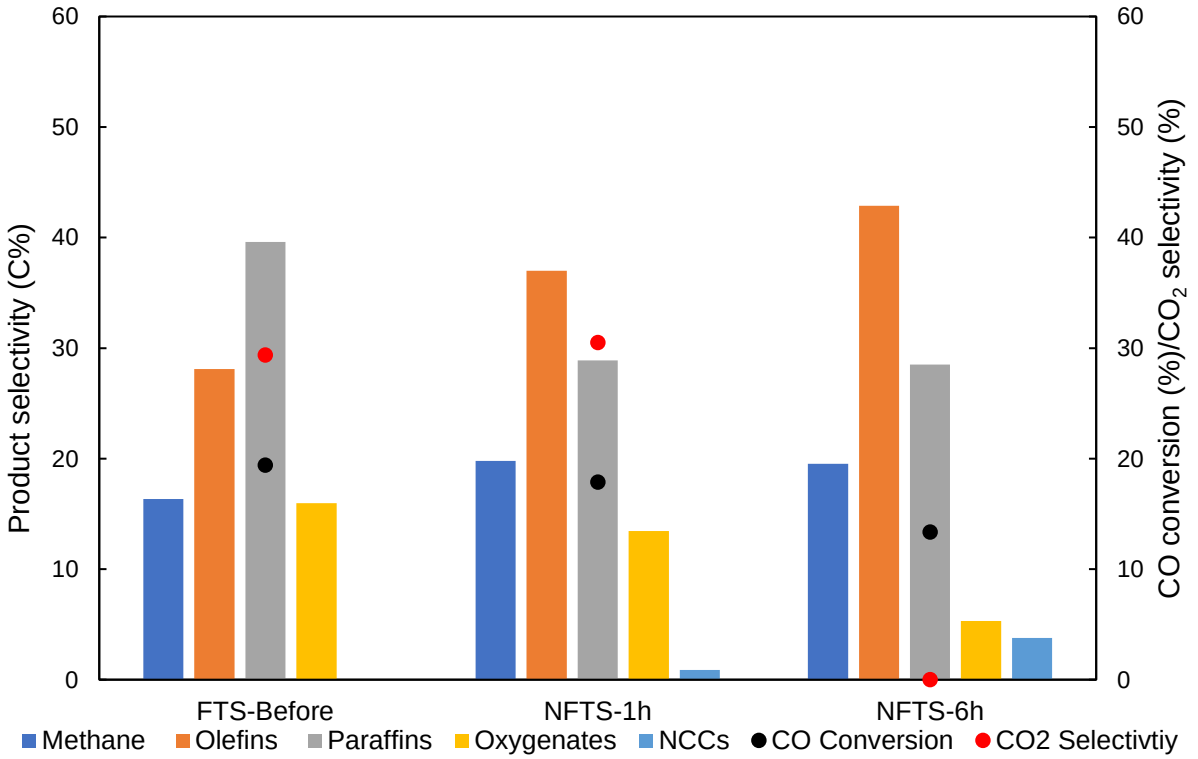

Figure 6. 4: Overall catalytic performance obtained during the reaction stages over the K-CuFe/Silica catalyst (Reaction conditions: T = 240˚C, P = 20 bar, GHSV = 6000 h^{-1}, H_2/CO = 2:1, 5% vol NH_3).

6.2. CO conversion

Recent investigations on the NH_3 co-feeding during the FTS over various Fe-based catalysts led to various observations and conclusions regarding the impacts of NH_3 on the catalytic activity. NH_3 has been considered as a poison for most FTS catalysts due to its strong chemisorption and blockage of the catalytic sites (Bartholomew, 2001). The impact of NH_3 over Co-based FTS catalysts has been intensively studied over the past decades compared to the impact of NH_3 on Fe-based catalysts. Over Co-based catalysts, NH_3 poisoning attributed to the competitive absorption was found to be less severe than sulphur poising (Van de Loosdrecht et al., 2013) (Leviness et al., 2001).

From the study conducted by Sango et al. (2013) (2015) over an unsupported Fe-based catalyst promoted with potassium, comparable catalytic activities were obtained during the normal FTS and NFTS when a low ammonia content, *i.e.* 0-2 vol%, was introduced into the feed gas. Further investigations performed by Henkel (2013) and De Vries (2017) over a similar catalyst during the NFTS with a NH_3 content of 2 vol% and 1 vol% respectively, led to similar observations as minimal changes in the catalytic activity were reported. Additionally, during the investigation of the effects of reaction temperature (210-330˚C) and space velocity (10-100ml/min.g_{cat}) during the co-feeding of 5 vol% NH_3 over an alumina-supported iron-rhodium catalyst (6.3 wt% Rh and 5.2 wt% Fe), Rawoot (2017) observed that the catalytic activity was hardly affected by the presence of NH_3.

However, upon co-feeding of a high NH_3 content, *i.e.* 5-20 vol%, Sango et al. (2013) (2015) observed a drop in the catalytic activity, which indicates the deactivation of the catalyst. Upon removal of NH_3 from the feed gas, a partial recovery of the catalytic activity was reported (Sango, 2013), (Sango et al., 2015). From these observations, Sango et al. (2013) (2015) argued that NH_3 species have a reversible poisonous effect on the catalyst sites.

In this study, the co-feeding of 5 vol% NH_3 during the FTS over each of the four selected catalysts resulted in various impacts on the catalytic activity over time as presented on Figure 6. 5 and summarized in Table 6. 1. From Figure 6. 5, it can be observed that a pseudo-steady state was obtained during the NFTS as, the CO conversion was found to be relatively constant after 3 hours on stream over the Fe,Mn-CuZnO, K,Al-Fe and K-CuFe/Silica catalysts. Over the 10 wt% Fe/Al_2O_3, the CO conversion was found to be relatively constant throughout the different reaction stages.

Table 6. 1: CO conversion (%) obtained during the reaction stages over the four selected catalysts.

Reaction stage	24 hours under FTS	1 hour under NFTS	6 hours under NFTS	After returning under FTS
Fe,Mn-CuZnO	12.8	10.2	5.00	10.0
K,Al-Fe	43.6	42.7	22.6	-
10 wt% Fe/Al_2O_3	12.4	12.2	12.8	12.7
K-CuFe/Silica	19.4	17.9	13.6	-

Reaction conditions: T = 240˚C, P = 20 bar, GHSV = 6000 h^{-1}, H_2/CO ratio = 2.0, 5 vol% NH_3

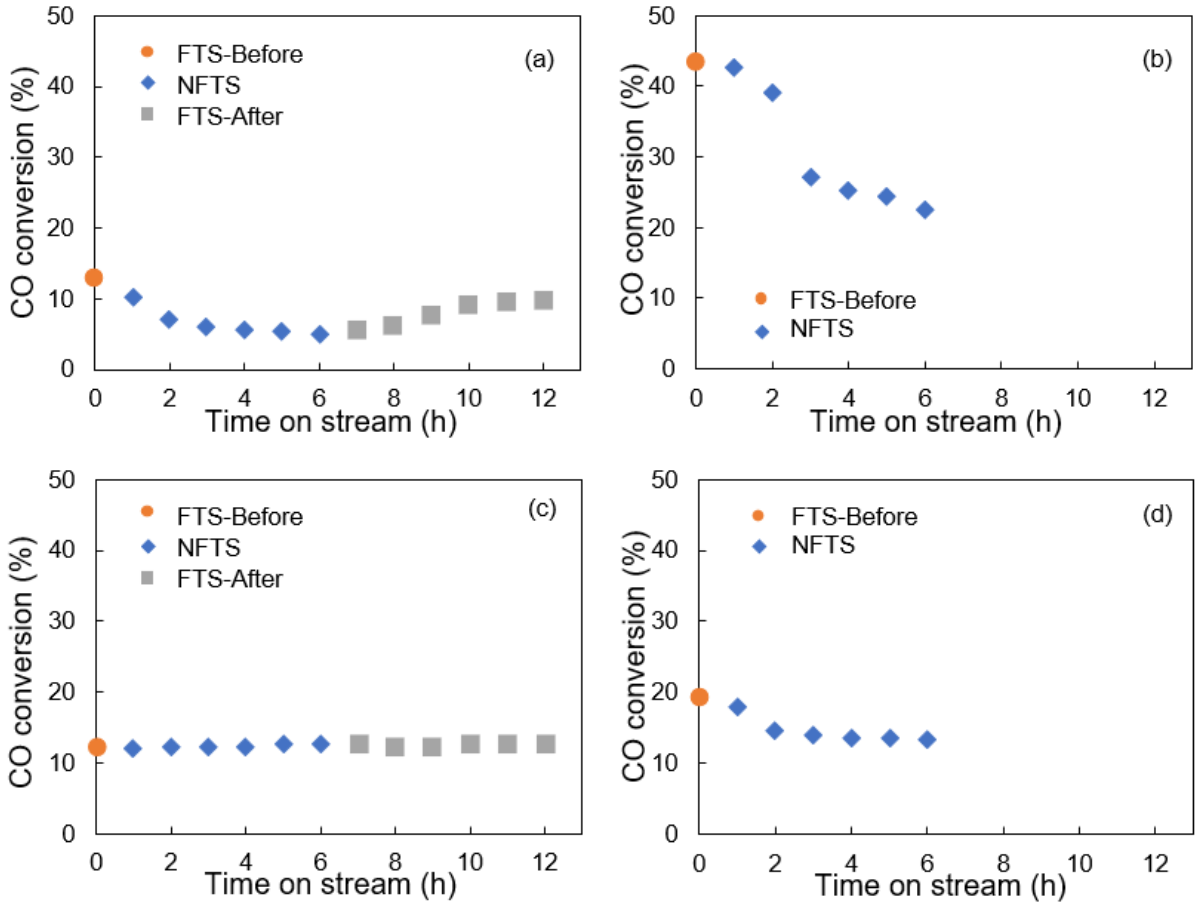

Figure 6. 5: CO conversion as function of time during the reaction stages over the Fe,Mn-CuZnO (a); K,Al-Fe (b); 10 wt% Fe/Al_2O_3 (c) and K-CuFe/Silica (d) catalysts (Reaction conditions: T = 240˚C, P = 20 bar, GHSV = 6000 h^{-1}, H_2/CO = 2:1, 5% vol NH_3).

Over the Fe,Mn-CuZnO and K,Al-Fe catalysts, the presence of NH_3 led to the significant loss in the catalytic activity, *i.e.* around 50% drop in the CO conversion as presented in Figure 6. 5(a) and Figure 6. 5(b), which pointed out the catalytic deactivation of both Fe,Mn-CuZnO and K,Al-Fe catalysts induced by the presence of NH_3. Similar results with a decrease in the catalytic activity of potassium promoted Fe catalysts were reported by Henkel (2013). Henkel (2013) argued that the catalyst deactivation could be mainly due to the presence of potassium

which has the ability to block the active sites of the catalysts (Claeys & Van Steen, 2008). However, in this present study, due to the low potassium loading used, *i.e.* 0.1 wt%, in the K,Al-Fe catalyst, the catalyst deactivation observed can be attributed the presence of NH_3 species onto the catalyst surface which inhibit the adsorption of CO species (Sango et al., 2015) .Additionally, upon the removal of NH_3 to the feed gas, a partial recovery of the catalytic activity of Fe,Mn-CuZnO was observed. This indicated that the presence of NH_3 led to a reversible deactivation of the Fe,Mn-CuZnO catalyst. The deactivation of a Fe-based catalyst was also reported by Sango et al. (2015) who argued that the drop in the catalytic activity upon the addition of 5-10 vol% NH_3 might due to the adsorption of NH_3 species onto the catalyst surface which compete for the active sites and limit the adsorption of CO species (Sango et al., 2015).

Over the 10 wt% Fe/Al_2O_3 catalyst, the presence of NH_3 did not significantly affect the catalytic activity as minimal changes in the CO conversion were observed before, during and after the co-feeding of NH_3, as shown in Figure 6. 5(c). This indicated that the presence of NH_3 does not induce the deactivation of the 10 wt% Fe/Al_2O_3 catalyst. Similar observations were reported by Ordomsky et al. (2016) who did not observed any deactivation of a 10 wt% Fe-based catalyst supported in alumina during the co-feeding of 2500 ppmv NH_3 or acetonitrile during the FTS.

Over the K-CuFe/Silica catalyst, the presence of NH_3 affected at a low extent the catalytic activity as a slight decrease in the CO conversion was observed, as shown in Figure 6. 5(d). The stability of the K-CuFe/Silica catalyst in the presence of NH_3 can be attributed to the use of the silica support which is known to enhance the activity and stability of Fe-based catalysts (Bukur & Sivaraj, 2002).

Due to the different features and compositions of each catalyst used in the study, the analysis and discussions were only focusing on the effect of ammonia on each catalyst and direct comparisons between the catalysts were not made.

Based on literature, a high CO conversion is expected over supported catalysts due to their high surface area (Dry, 2004a). However, in the present study, the K,Al-Fe catalyst, an unsupported catalyst with the lower surface area, *i.e.* 28.1 m^2/g, see Table 5. 3, allowed the highest CO conversion, *i.e.* 43.6%, see Table 6. 1, compared to the three other catalysts, *i.e.* Fe,Mn-CuZnO, 10 wt% Fe/Al_2O_3 and K,CuFe/Silica catalysts. The difference in the CO conversion obtained over the four selected catalysts can be attributed to both physical and chemical proprieties of the catalysts which were not investigated in-depth in the present study.

6.3. CO_2 formation

The formation of carbon dioxide (CO_2) during the FTS is believed to occur through the Water-Gas Shift (WGS) and the Boudouard reactions. Dry et al. (1970) reported that the presence of NH_3 into the syngas feed can result in the inhibition of the Boudouard reaction. Therefore, the formation of CO_2 during the NFTS can be assumed to occur mostly through the WGS reaction. The effect of NH_3 on the formation of CO_2 was then investigated in this study to assess the impact of NH_3 on the activity of the WGS reaction.

The CO_2 selectivities obtained during the different reaction stages presented in Figure 6. 6 and summarised in Table 6. 2, point out that the NH_3 co-feeding resulted in a significant impact in the CO_2 selectivity over all four selected catalysts.

Table 6. 2: CO_2 selectivity (%) obtained during the reaction stages over the four selected catalysts.

Reaction stage	24 hours under FTS	1 hour under NFTS	6 hours under NFTS	After returning under FTS
Fe,Mn-CuZnO	34.9	25.6	0.0	17.4
K,Al-Fe	36.6	36.0	3.1	-
10 wt% Fe/Al_2O_3	8.7	7.1	0.0	4.9
K-CuFe/Silica	29.4	30.1	0.0	-

Reaction conditions: T = 240˚C, P = 20 bar, GHSV = 6000 h^{-1}, H_2/CO ratio = 2.0, 5 vol% NH_3

The addition of NH_3 to the feed gas caused a drastic decline in the CO_2 selectivity which resulted in the disappearance of CO_2 over all four catalysts, as highlighted on Figure 6. 6. Upon the removal of NH_3 from the feed gas over the Fe,Mn-CuZnO and 10 wt% Fe/Al_2O_3 catalysts, the partial recovery of the CO_2 selectivity, *i.e.* 50% recovery, was observed. Although the catalytic activity of the Fe,Mn-CuZnO was largely recovered upon removal of NH_3 and a relatively constant catalytic activity was obtained over the 10 wt% Fe/Al_2O_3 during and after the NH_3 co-feeding, the CO_2 selectivity was found to lower after NFTS, as shown in Figure 6. 6(a) and Figure 6. 6(c). These results may suggest that the presence of NH_3 suppresses the CO_2 formation via the WGS reaction and that the NH_3 species selectively inhibit the metal sites responsible for the occurrence of WGS reaction.

However, the formation of a white solid was detected in the entrance of the cold trap during the NFTS over the Fe,Mn-CuZnO catalyst and a pressure build-up was observed during the NFTS over the Fe,Mn-CuZnO, K,Al-Fe and K-CuFe/Silica catalysts. It was therefore assumed that the pressure build-up might have been the result of the accumulation of the white solid within the catalyst bed and/or the reactor outlet streams.

The drop in the CO_2 selectivity observed as a result of the NH_3 co-feeding has also been reported in literature (Henkel, 2013), (Sango, 2013), (Sango et al., 2015), (De Vries, 2017).

According to Sango et al. (2013), (2015) the decline in the CO_2 selectivity might be due to the reaction occurring between the NH_3 species and the CO_2 formed in presence of water which leads to the formation of a white solid identified to be ammonium carbonate. However, the analysis of the spent catalysts via XRD, performed in this study, did not revealed the presence of ammonium carbonate.

Therefore, the drop in the CO_2 selectivity observed during the co-feeding of NH_3 could either be due to the inhibition of the WGS reaction activity by NH_3 species blocking the metal sites responsible for the WGS reaction and causing a partially irreversible impact on these metals sites and/or to the use of the CO_2 formed for the formation of the ammonium carbonate solid.

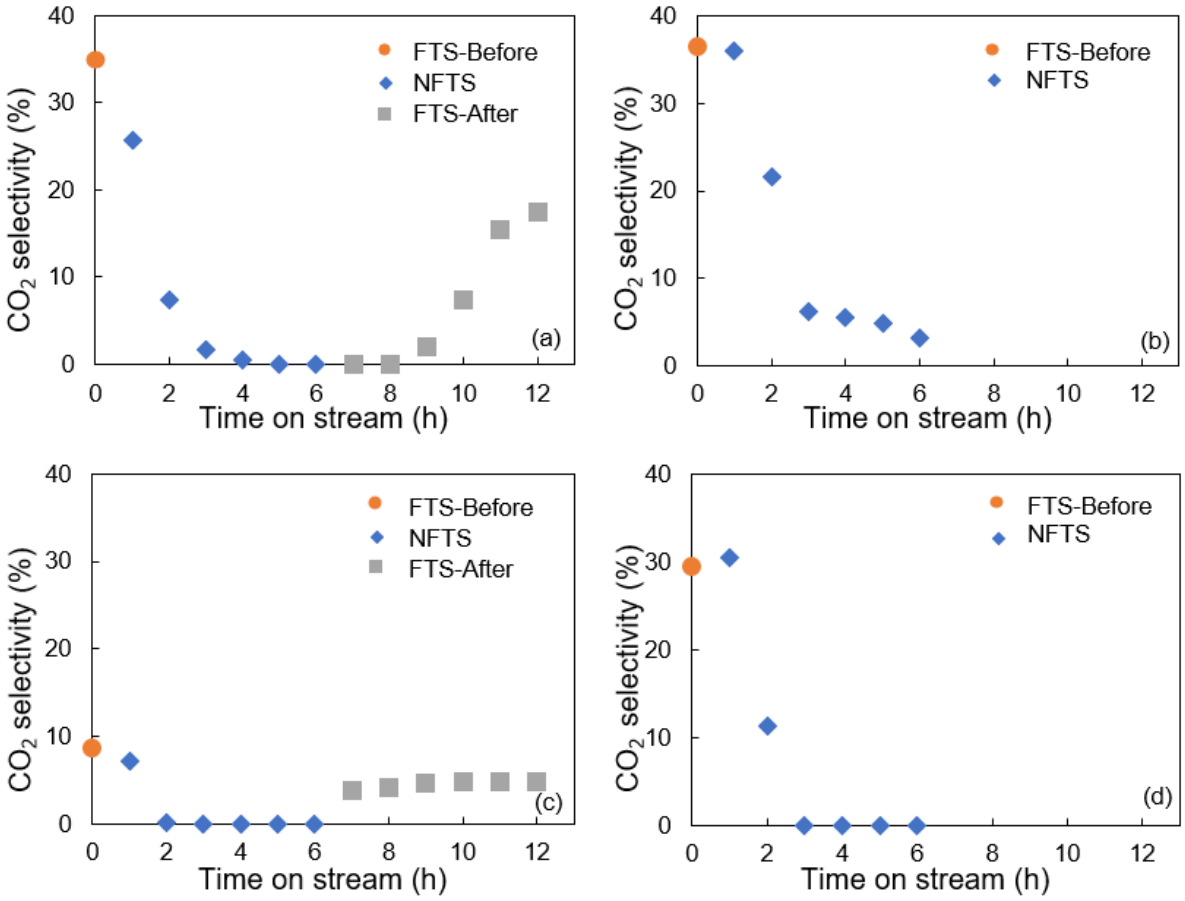

Figure 6. 6: CO_2 selectivity as function of time during the reaction stages over the Fe,Mn-CuZnO (a); K,Al-Fe (b); 10 wt% Fe/Al_2O_3 (c) and K-CuFe/Silica (d) catalysts (Reaction conditions: T = 240˚C, P = 20 bar, GHSV = 6000 h^{-1}, H_2/CO = 2:1, 5% vol NH_3).

6.4. CH_4 formation

Methane (CH_4) is the most thermodynamically stable and low economical-value product of the FTS (Claeys & Van Steen, 2004). According to the alkyl mechanism, the methane formation results from the complete hydrogenation and desorption of surface methyl species. Alternatively, the surface methyl species can participate in the chain growth as chain initiators

for the formation of long chain products (Erley et al., 1983). The effect of NH_3 on the formation of methane was then investigated in this study to assess the impact of NH_3 on the desorption of the surface methyl species.

The CH_4 selectivities obtained during the different reaction stages, presented on Figure 6. 7 and summarised in Table 6. 3, indicate that the NH_3 co-feeding had a different impact on the formation of CH_4 over each of all four selected catalysts.

Table 6. 3: CH_4 selectivity (C%) obtained during the reaction stages over the four selected catalysts.

Reaction stage	24 hours under FTS	1 hour under NFTS	6 hours under NFTS	After returning under FTS
Fe,Mn-CuZnO	11.7	15.2	15.5	12.9
K,Al-Fe	15.1	10.0	11.1	-
10 wt% Fe/Al_2O_3	16.1	16.4	11.5	12.2
K-CuFe/Silica	16.4	19.8	19.5	-

Reaction conditions: T = 240˚C, P = 20 bar, GHSV = 6000 h^{-1}, H_2/CO ratio = 2.0, 5 vol% NH_3

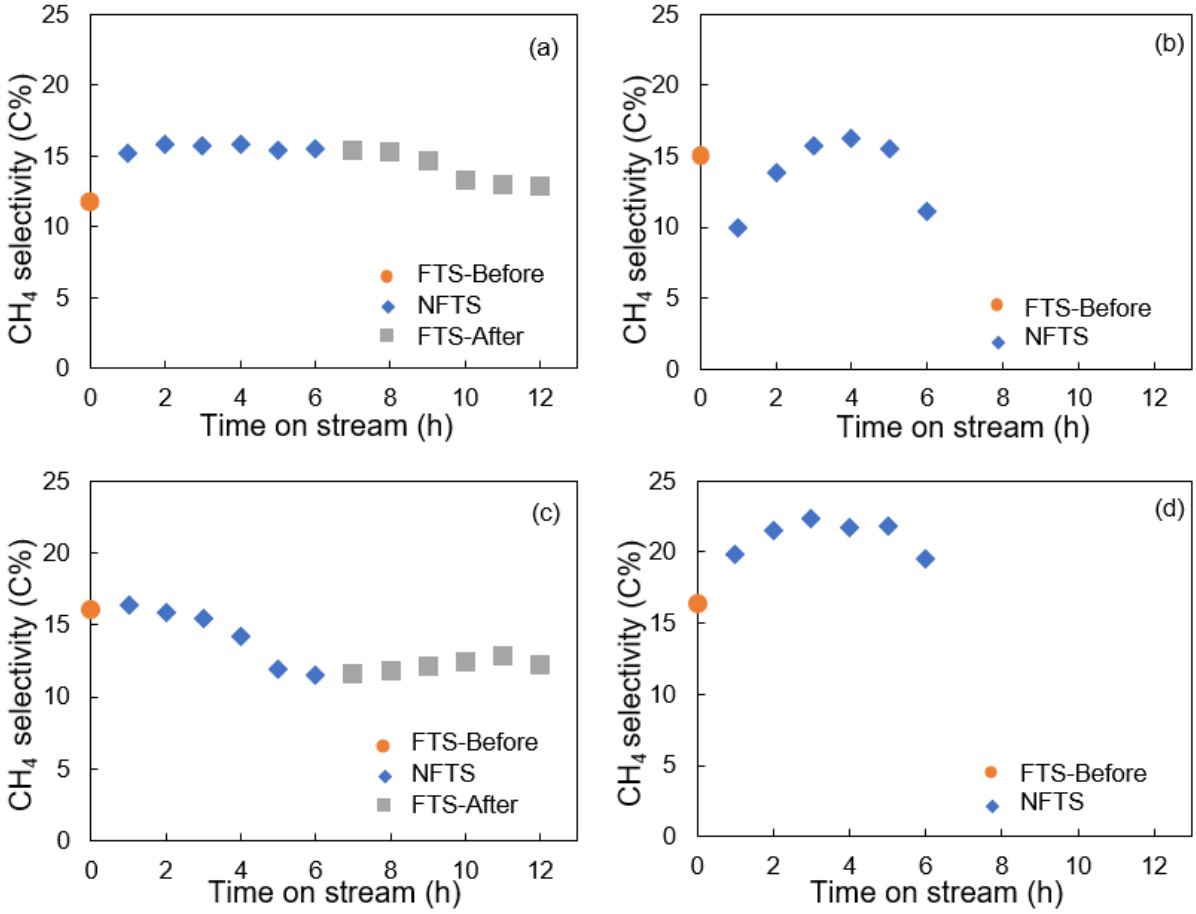

Figure 6. 7: CH_4 selectivity as function of time during the reaction stages over the Fe,Mn-CuZnO (a); K,Al-Fe (b); 10 wt% Fe/Al_2O_3 (c) and K-CuFe/Silica (d) catalysts (Reaction conditions: T = 240˚C, P = 20 bar, GHSV = 6000 h^{-1}, H_2/CO = 2:1, 5% vol NH_3).

Over the Fe,Mn-CuZnO and K-CuFe/Silica catalysts, the addition of NH_3 led to an increase in CH_4 selectivity and upon the removal of NH_3 from the feed gas, a decrease in the CH_4 selectivity was observed while the selectivity was slightly higher than the one obtained before the co-feeding of NH_3, which may be a result of the lower conversion after NH_3 removal. From the changes observed in the CH_4 selectivity upon co-feeding and removal of NH_3, shown in Figure 6. 7(a) and Figure 6. 7(d), it can be speculated that the presence of NH_X species onto the Fe,Mn-CuZnO and K-CuFe/Silica catalyst surfaces favours the desorption of surface methyl species to form methane by inhibiting or competing with the adsorption of CO species (Schulz et al., 1995). Similar trends were reported in the work of Sango et al. (2015) and De Vries (2017) where an increase in the CH_4 selectivity from 3.7 C% to 4.8 C% and 11.5 C wt% to 12.6 C wt% were observed as the NH_3 content was increased from 0 to 5 vol% and 0 to 1 vol% respectively.

Over the K,Al-Fe catalyst, a drop in the CH_4 selectivity was observed after 1-hour co-feeding NH_3 and over time, the selectivity increased slightly from 10.0 C% to 11.1 C%, as shown in Figure 6. 7(b). Similar observations were reported by Henkel (2013). Upon addition of 5 vol% CH_4 during the FTS over an unpromoted Fe-based catalyst, Henkel (2013) also observed a decline in the CH_4 selectivity while no change in the CH_4 selectivity was noticed over 2 and 5 wt% potassium promoted Fe-based catalysts. Based on these observations, Henkel (2013) argued that the presence of NH_X species over an unpromoted Fe-based catalyst surface may lead to the inhibition of the adsorption of H_2 species by lowing the hydrogen-metal binding strength which results in a drop of the CH_4 selectivity. The same conclusion regarding the effect of CH_4 on the CH_4 selectivity obtained over the K,Al-Fe catalyst can be reached in this study as a low loading of potassium, *i.e.* 0.1 wt%, was added to the catalyst.

Over the 10 wt% Fe/Al_2O_3 catalyst, the NH_3 co-feeding led to a decrease in the CH_4 selectivity and after removal of NH_3 from the syngas feed, the CH_4 selectivity increased slightly but remained much lower than the selectivity obtained before the co-feeding of NH_3. These observations highlighted in Figure 6. 7(c) point out that the presence of NH_3 leads to the irreversible inhibition of the formation of methane. This may be attributed either to the selective and irreversible poisoning of the methanation sites of the Fe-based catalyst supported on alumina by the NH_3 species (Ordomsky et al., 2016) or to the inhibition of the desorption of surface alkyl surface species followed by their incorporation in the chain growth (Sango, 2013), (Sango et al., 2015).

6.5. Chain growth probability, α-value

The chain growth probability (α-value) is defined as the probability of a surface specie to grow instead of desorbing (Claeys & Van Steen, 2004). The investigation of the effect of NH_3 co-

feeding on the α-value allowed to further assess the impact of NH_3 on the desorption and growth of the surface species. α-values were calculated from the linear regression of the ASF distribution plots of both hydrocarbons and oxygenates over the C_3-C_7 carbon number range. The hydrocarbons and oxygenates ASF distribution plots obtained before, during and after the co-feeding of 5 vol% NH_3 over the four selected catalysts are shown in Appendix A.3. and the α-values obtained are summarised in Table 6. 4.

Table 6. 4: α-values of hydrocarbons and oxygenates (C_3-C_7) obtained during the reaction stages over the four selected catalysts.

Reaction stage	24 hours under FTS	1 hour under NFTS	6 hours under NFTS	After returning under FTS
		α-values (Hydrocarbons)		
Fe,Mn-CuZnO	0.59	0.60	0.60	0.61
K,Al-Fe	0.58	0.66	0.62	-
10 wt% Fe/Al_2O_3	0.65	0.64	0.72	0.69
K-CuFe/Silica	0.59	0.60	0.62	-
		α-values (Oxygenates)		
Fe,Mn-CuZnO	0.50	0.60	0.46	0.48
K,Al-Fe	0.56	0.60	0.56	-
10 wt% Fe/Al_2O_3	0.57	0.58	0.41	0.62
K-CuFe/Silica	0.55	0.56	0.63	-

Reaction conditions: T = 240˚C, P = 20 bar, GHSV = 6000 h^{-1}, H_2/CO ratio = 2.0, 5 vol% NH_3

Over the Fe,Mn-CuZnO catalyst, similar hydrocarbons α-values were obtained during the three reaction stages while a decrease in the oxygenates α-values was observed. These results pointed out that the presence of NH_3 has a limited impact on the α-values of hydrocarbons as observed by De Vries (2017) and Rawoot (2017). Sango et al. (2013), (2015) only reported a decrease in the α-values when a high content of NH_3, *i.e.* 35 vol%, suggesting a competitive adsorption between NH_3 and CO species which enhances the desorption of the surface species while inhibiting the chain growth (Schulz et al., 1995). Furthermore, the drop in the oxygenates α-values can be attributed to the inhibition of the formation and/or growth of oxygenates caused by the presence of NH_3 species on the Fe,Mn-CuZnO catalyst surface (Sango, 2013), (Sango et al., 2015).

Over the K,Al-Fe based catalyst, an increase in the α-values was observed upon the co-feeding of NH_3. As observed with the CH_4 selectivity, the presence of NH_3, during the FTS over the K,Al-Fe catalyst, limits the formation of methane due to the inhibition of the adsorption of H_2 species which favours the incorporation of methyl species in the chain growth resulting

in the formation of long chain hydrocarbons (Henkel, 2013). Furthermore, the addition of NH_3 during the FTS over the K,Al-Fe catalyst led to minimal changes in the α-value of oxygenates as the same α-value, *i.e.* 0.56, was obtained before and after 6 hours co-feeding NH_3.

Over the 10 wt% Fe/Al_2O_3 catalyst, the addition of NH_3 led to an increase in the hydrocarbons α-values while a drop in the oxygenates α-values was observed. The α-values of both hydrocarbon and oxygenates obtained after removal of NH_3 (FTS-After) were much higher than the ones obtained under the normal FTS conditions (FTS-Before). These results point out that the presence of NH_3 during the FTS over the 10 wt% Fe/Al_2O_3 catalyst inhibits the formation of long chain hydrocarbons and oxygenates. This may be due to the competitive adsorption between the NH_3 species and CO species which limits the availability of CO species which then inhibits the chain growth (Rawoot, 2017).

Over the K-CuFe/Silica, a minimal change in the hydrocarbons α-values and an unexpected increase in the oxygenates were observed upon NH_3 co-feeding. Furthermore, from the hydrocarbons ASF distribution plots presented in Appendix A.3, a deviation from a straight line was noticed with increasing carbon number upon NH_3 co-feeding which indicated a drop in the α-values of long chain hydrocarbons (C_8-C_{11}), *i.e.* from 0.84 to 0.66. These results pointed out that the co-feeding of NH_3 over the K-CuFe/Silica catalyst inhibits the formation of long chain hydrocarbons while not affecting the formation of short chain hydrocarbons. This may be due to the presence of NH_3 species on the catalyst surface which blocks olefins readsorption and incorporation which then limits the occurrence of secondary olefins reactions leading to the formation of long chain hydrocarbons (Claeys & Van Steen, 2004). Additionally, from the minimal change in the hydrocarbons α-values and the increase in methane observed upon NH_3 co-feeding over the K-CuFe/Silica, it can be deduced that there is not a direct link between methane formation and the chain growth, *i.e.* the increase in methane would result in the decrease in the chain growth and vice versa. This may indicate that methane formation over the K-CuFe/Silica catalyst can happen on metal sites which are not capable of chain growth and these sites are affected differently (Schulz et al., 1994).

6.6. Olefins

Olefins (and paraffins) are considered as primary and valuable products of the FTS due to their use as feedstock materials in various industrial processes respectively (Schulz & Claeys, 1999b). After being produced through the elimination of the β-hydrogen from a surface alkyl chain, it is believed that olefins can be re-adsorbed and undergo secondary reactions such as hydrogenation to paraffins, double bond shift isomerization and incorporation into growing chains (Claeys & Van Steen, 2004).

In order to assess the effect of the NH_3 co-feeding on the olefin formation and the occurrence of olefins secondary reactions such as hydrogenation to paraffins and/or double bond isomerization, the molar content of olefins in linear hydrocarbons and the molar content of α-olefins in linear olefins were calculated before, during and after the co-feeding of 5 vol% NH_3 over all four selected catalysts and plotted as a function of carbon number, presented Figure 6. 8 to Figure 6. 11. The olefin content gives an indication of the degree of secondary hydrogenation that occurs in the absence of additional secondary reactions and the absence of incorporation into growing chains. Carbon number independent olefin contents are believed to be between 70-90 mol% with at least 95% of the olefins being primary olefins (α-olefins) (Schulz & Claeys, 1999b).

Over all four selected catalysts, the molar olefin content was lower at C_2, reached a maximum at C_3 and then decreased with increasing carbon number during all three stages, as shown in Figure 6. 8(a) to Figure 6. 11(a). These observations can be attributed to the higher reactivity of ethylene (Claeys & Van Steen, 2004) and the increasing residence times for long chain olefins which enhances their involvement in secondary reactions (Schulz & Claeys, 1999b). However, the effects of NH_3 on the overall olefin content were found to be different from one catalyst to the other.

Over the Fe,Mn-CuZnO catalyst, the co-feeding of NH_3 led to a significant increase in the molar olefin content across all carbon numbers, as illustrated in Figure 6. 8(a). Furthermore, an increase in the molar content of α-olefins in linear olefins was also noticed upon the co-feeding of NH_3, as shown in Figure 6. 8(b). After returning to normal FTS conditions (FTS-After), the olefin content, presented in Figure 6. 8(a), and the α-olefin content, presented in Figure 6. 8(b), dropped at higher carbon numbers but was still higher than the contents obtained before the co-feeding of NH_3. At low carbon numbers, very high α-olefin contents were obtained (~90 mol%) indicating almost primary selectivity.

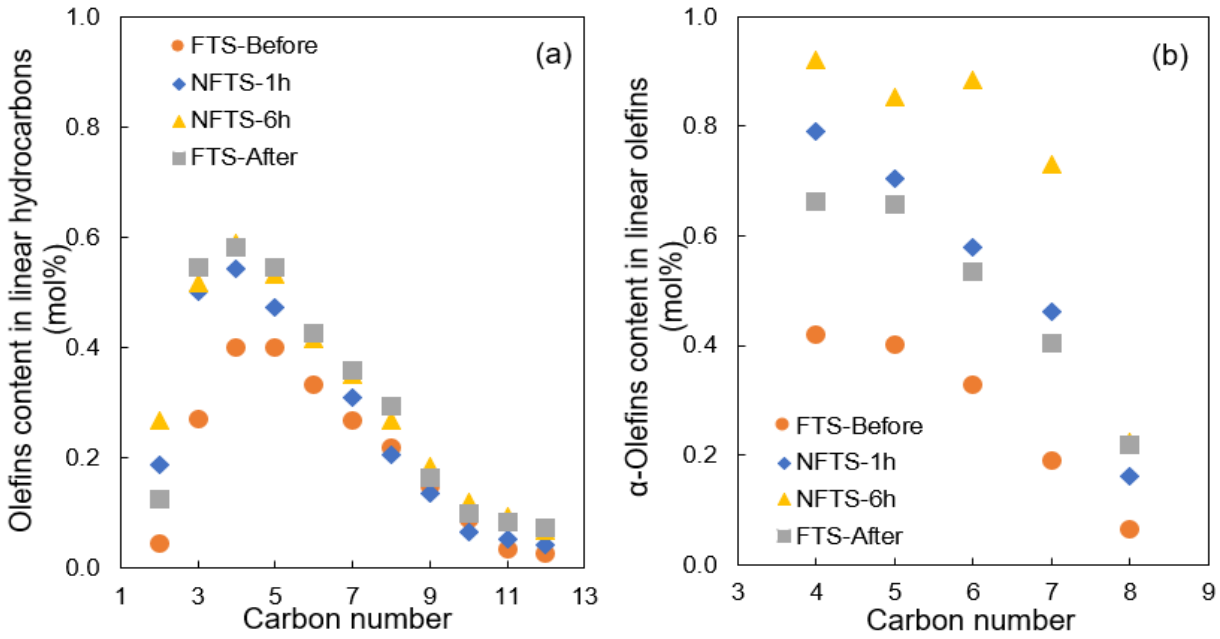

Figure 6. 8: Molar content of olefins in linear hydrocarbons (a) and molar content of α-olefins in linear olefins (b) as function of carbon number obtained during the reaction stages over the Fe,Mn-CuZnO catalyst (Reaction conditions: T = 240˚C, P = 20 bar, GHSV = 6000 h^{-1}, H_2/CO = 2:1, 5 vol% NH_3).

Over the K,Al-Fe based catalyst, the addition of NH_3 did not significantly affect the overall molar olefin content, shown in Figure 6. 9(a). At low carbon numbers, *i.e.* C_2-C_5, negligible changes in the molar olefin content were observed upon addition of NH_3 while a slight drop of this content was noticed at higher carbon numbers, *i.e.* C_6-C_{11}. Regarding the effect of the co-feeding of NH_3 on the molar α-olefin content, it can be observed from Figure 6. 9(b) that the presence of NH_3 caused a slight decrease in the molar α-olefin content. Additionally, very high α-olefin contents were obtained (~90 mol%) across all carbon numbers before and during the NH_3 co-feeding indicating almost primary selectivity.

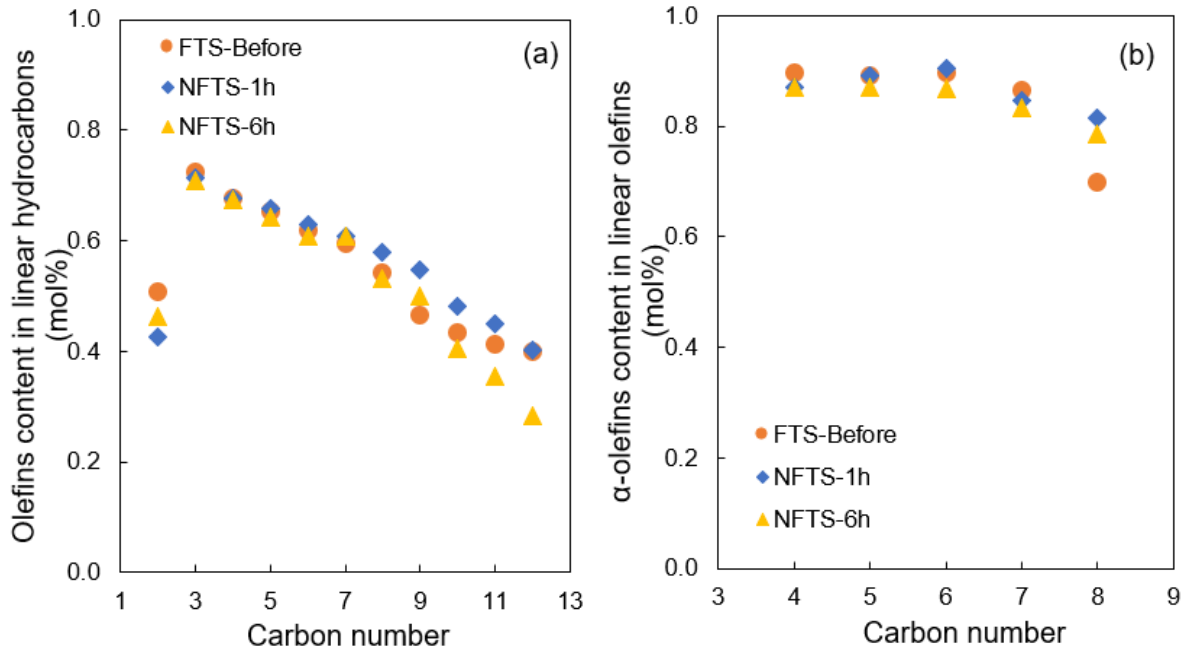

Figure 6. 9: Molar content of olefins in linear hydrocarbons (a) and molar content of α-olefins in linear olefins (b) as function of carbon number obtained during the reaction stages over the K,Al-Fe catalyst (Reaction conditions: T = 240˚C, P = 20 bar, GHSV = 6000 h^{-1}, H_2/CO = 2:1, 5 vol% NH_3).

Over the 10 wt% Fe/Al_2O_3 catalyst, a significant increase in the olefin contents was observed across all carbon number as a result of the NH_3 co-feeding, as shown in Figure 6. 10(a). At 6 hours of NH_3 co-feeding almost carbon number independent olefins level of 72 mol% were observed indicative of a very low extent of secondary hydrogenation. Upon removal of NH_3 from the feed gas, slightly higher olefin contents were obtained over the C_2-C_6 carbon number range compared to the olefin contents obtained before the co-feeding of NH_3 (FTS-Before). The significant and gradual increase in the olefin content in the C_7-C_{11} carbon number range is believed to be due to the products in these carbon number ranges not having achieved steady state after ammonia removal. Similar trends were also observed in the molar α-olefin contents in the linear olefin fractions, presented in Figure 6. 10(b). Additionally, a significant increase in the α-olefin contents was obtained (~90 mol%) across all carbon numbers during and after the NH_3 co-feeding (NFTS and FTS-After) indicating almost primary selectivity.

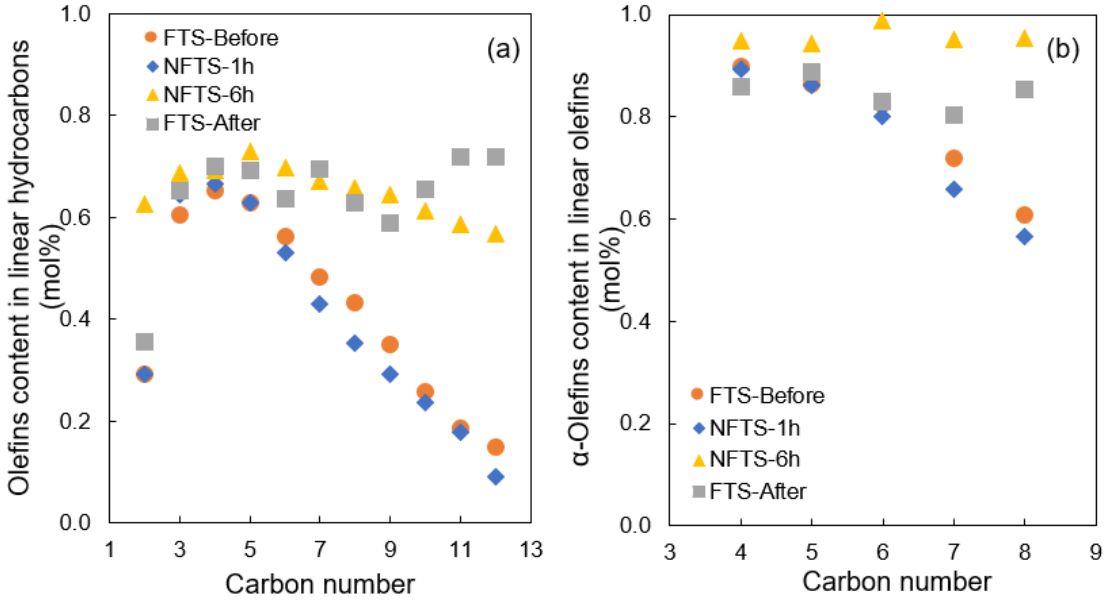

Figure 6. 10: Molar content of olefins in the linear hydrocarbons (a) and molar content of α-olefins in the linear olefins (b) as function of carbon number obtained during the reaction stages over the 10 wt% Fe/Al_2O_3 catalyst (Reaction conditions: T = 240˚C, P = 20 bar, GHSV = 6000 h^{-1}, H_2/CO = 2:1, 5 vol% NH_3).

Over the K-CuFe/Silica catalyst, upon addition of NH_3, an increase in the olefin contents was only observed at high carbon numbers, as shown in Figure 6. 11(a). Additionally, a significant increase in the α-olefin content to levels of primary selectivity (*i.e*. no double bond shift isomerisation) was obtained as a result of the co-feeding of NH_3, as shown in Figure 6. 11(b).

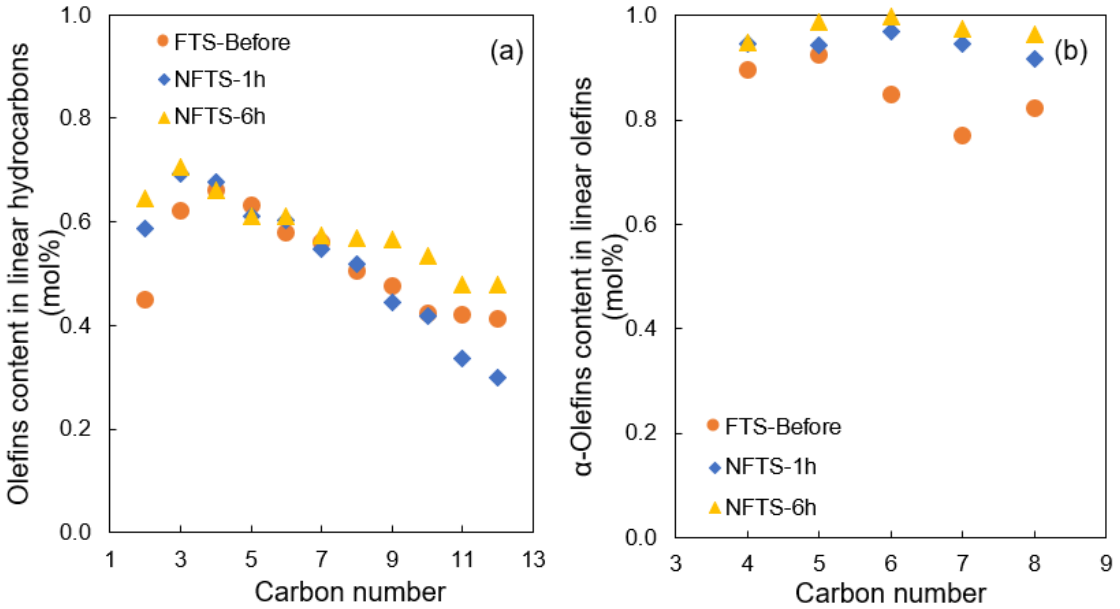

Figure 6. 11: Molar content of olefins in the linear hydrocarbons (a) and molar content of α-olefins in the linear olefins(b) as function of carbon number obtained during the reaction stages over the K-CuFe/Silica catalyst (Reaction conditions: T = 240˚C, P = 20 bar, GHSV = 6000 h^{-1}, H_2/CO = 2:1, 5 vol% NH_3).

The increase in both olefin and α-olefin contents observed during the co-feeding of NH_3 over the Fe,Mn-CuZnO, 10 wt% Fe/Al_2O_3 and K-CuFe/Silica catalysts may be attributed to the inhibition of the hydrogenation reaction due to the competitive adsorption of NH_3 and H_2 species which results in less H_2 species available on the catalyst surface (Sango, 2013), (Sango et al., 2015), (Rausch et al., 2016), (Rawoot, 2017). Alternatively, the adsorption of NH_3 species onto the catalyst surface might have enhanced the desorption of the alkyl surface species through the β-hydrogen elimination and limited the readsorption of α-olefins leading to a high α-olefins content and a low occurrence of secondary reactions, namely hydrogenation to paraffins, chain branching, incorporation into growing chains and/or double bond shift isomerization reactions (Sango, 2013), (Sango et al., 2015), (Rausch et al., 2016), (Rawoot, 2017). It can then be speculated that the adsorption of NH_3 species onto the Fe,Mn-CuZnO, 10 wt% Fe/Al_2O_3 and K-CuFe/Silica catalyst surfaces block certain metal surface sites responsible for H_2 adsorption and/or olefins readsorption resulting in the inhibition of the secondary reactions and the formation of hydrogenated compounds (Ordomsky et al., 2016).

The negligible changes observed in both olefin and α-olefin contents, during the NH_3 co-feeding over the K,Al-Fe catalyst, may be attributable to the presence of the potassium promoter as reported by Henkel (2013). During the investigation under both normal FTS and NFTS conditions, Henkel (2013) observed an significant increase in olefin and α-olefin contents over potassium-free Fe-based catalysts upon the NH_3 co-feeding while minimal changes in both olefin and α-olefin contents were observed potassium promoted Fe-based catalysts. From these results, Henkel (2013) then suggested that ammonia in the syngas may have similar promotional effects to that of potassium, *i.e.* affects the alkalinity of the Fe-based catalyst.

6.7. Oxygenates

In addition of the primary FTS products, *i.e.* paraffins and olefins, the formation of oxygenates, namely alcohols, aldehydes, acids and ketones, has also been observed during the FTS over various Fe-based catalysts (Pichler & Schulz, 1970), (Schulz et al., 1994) (Surisetty et al., 2011), (Schaller et al., 2018). Due to their industrial uses and their relatively low content compared to the other hydrocarbons, the oxygenates are classified as high-value minor FTS products (Claeys & Van Steen, 2004). However, over various catalyst systems, *i.e.* Fe-, Co-based catalysts, a significant drop in the oxygenates formation has been reported in literature as a result of the co-feeding of NH_3 during the FTS (Alfred, 1950), (Brown & Maselli, 1973), (Claeys et al., 2013), (Sango, 2013), (Henkel, 2013), (De Vries, 2017). The following subsection presents the overall selectivity and the distribution of oxygenates obtained during

the three reaction stages performed in this study to assess the impact of the NH_3 co-feeding on the oxygenates formation over the four selected catalysts.

The use of an offline GC-FID and an online 2D-GC equipped with a time-of-flight mass spectrometer (TOF-MS) and flame ionisation detector (FID) allowed to identity and quantify the different oxygenate classes produced during the present study.

The formation of alcohols, aldehydes and acids were detected under the normal FTS conditions (FTS-Before) over all four selected catalysts. Alcohols were found to be the dominant oxygenate class followed by aldehydes and acids, as presented in Figure 6. 12. The production of a small amount of ketones was only obtained over the Fe,Mn-CuZnO catalyst while the production of ketones was not detected over the three other catalysts.

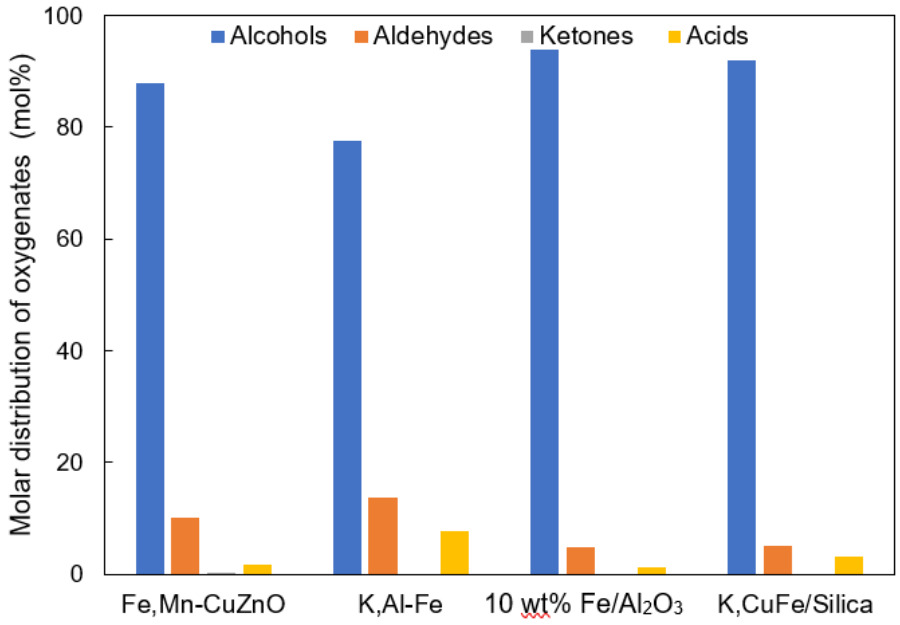

Figure 6. 12: Molar distribution of oxygenates obtained under the normal FTS conditions (FTS-Before) over the four selected catalysts (Reaction conditions: T = 240˚C, P = 20 bar, GHSV = 6000 h^{-1}, H_2/CO = 2:1, 5 vol% NH_3).

A close look at the oxygenate selectivity as a function of carbon number obtained before the NH_3 co-feeding (FTS-Before), summarized in Table 6. 5, points out that the $C_{2,\ Oxy}$ as the dominant carbon number obtained over the Fe,Mn-CuZnO, K,Al-Fe and K-CuFe/Silica catalysts while the $C_{1,\ Oxy}$ was found to have the highest selectivity over the 10 wt% Fe/Al_2O_3 catalyst. It is worth to emphasize that methanol was the only $C_{1,\ Oxy}$ detected during all reaction stages over all four selected catalysts. A high methanol selectivity was also reported by Pijolat & Perrichon (1985) during a FTS over a 10 wt% Fe/Al_2O_3. The low $C_{1,\ Oxy}$ selectivity obtained over the K,Al-Fe and K-CuFe/Silica, *i.e.* 0.5 C% and 0.9 C% respectively, can be attributed to

the potassium promotion which enhances the formation of long chain oxygenates (Yang et al., 2004), (Ding et al., 2015).

Table 6. 5: Oxygenate selectivity (C%) as function of carbon number obtained under normal FTS conditions (FTS-Before) over the four selected catalysts.

Oxygenates class	$C_{1, Oxy}$	$C_{2, Oxy}$	$C_{3-4, Oxy}$	$C_{5-14, Oxy}$	Overall oxygenates
Fe,Mn-CuZnO	8.8	10.0	5.3	6.2	30.3
K,Al-Fe	0.5	5.0	3.6	3.6	13.0
10 wt% Fe/Al_2O_3	8.1	4.6	3.9	6.4	23.0
K-CuFe/Silica	0.9	6.0	4.6	4.50	16.0

Reaction conditions: T = 240˚C, P = 20 bar, GHSV = 6000 h^{-1}, H_2/CO ratio = 2.0.

Regarding the molar distribution of the different classes of oxygenates obtained during the three reaction stages, *i.e.* FTS-Before, NFTS, FTS-After, over the four selected catalysts, shown in Figure 6. 13, it can be observed that alcohols stayed the dominant oxygenate class while a drop in their contents occurred during the NH_3 co-feeding (NFTS). Additionally, the drop in the alcohol selectivity observed was followed by a gradual increase in aldehyde, ketone and acid contents. And after the removal of NH_3 from the feed gas (FTS-After), a molar distribution of the different classes of oxygenates, similar to the one obtained before the NH_3 co-feeding (FTS-Before), was obtained over the Fe,Mn-CuZnO and 10 wt% Fe/Al_2O_3 catalysts.

In the study performed by Sango et al. (2013), (2015) over a Fe-based catalyst promoted with potassium, significant declines in the selectivity of all oxygenate classes, *i.e.* alcohols, aldehydes and acids, were observed after the co-feeding of 2-10 vol% NH_3. Over a similar catalyst, Henkel (2013) reported, in addition to the significant drop in alcohols, the disappearance of both aldehydes and acids after the co-feeding of 2 vol% NH_3. The drop in the alcohols selectivity and the increase in the selectivity of both aldehydes and acids observed in this study may be attributed to the inhibition effect of NH_3 on the adsorption of H_2 and CO species which might have inhibited the formation of alcohols and/or favoured the occurrence of secondary reactions involving the alcohols formed (Sango, 2013), (Sango et al., 2015). Alternatively, it may be attributed to the inhibition effect of NH_3 on the adsorption of H_2 species which reduces the hydrogenation activity (Ordomsky et al., 2016) limiting the formation of hydrogenated compounds, *i.e.* alcohols and paraffins, while favouring the formation of olefins, aldehydes and acids (Cairns, 2008).

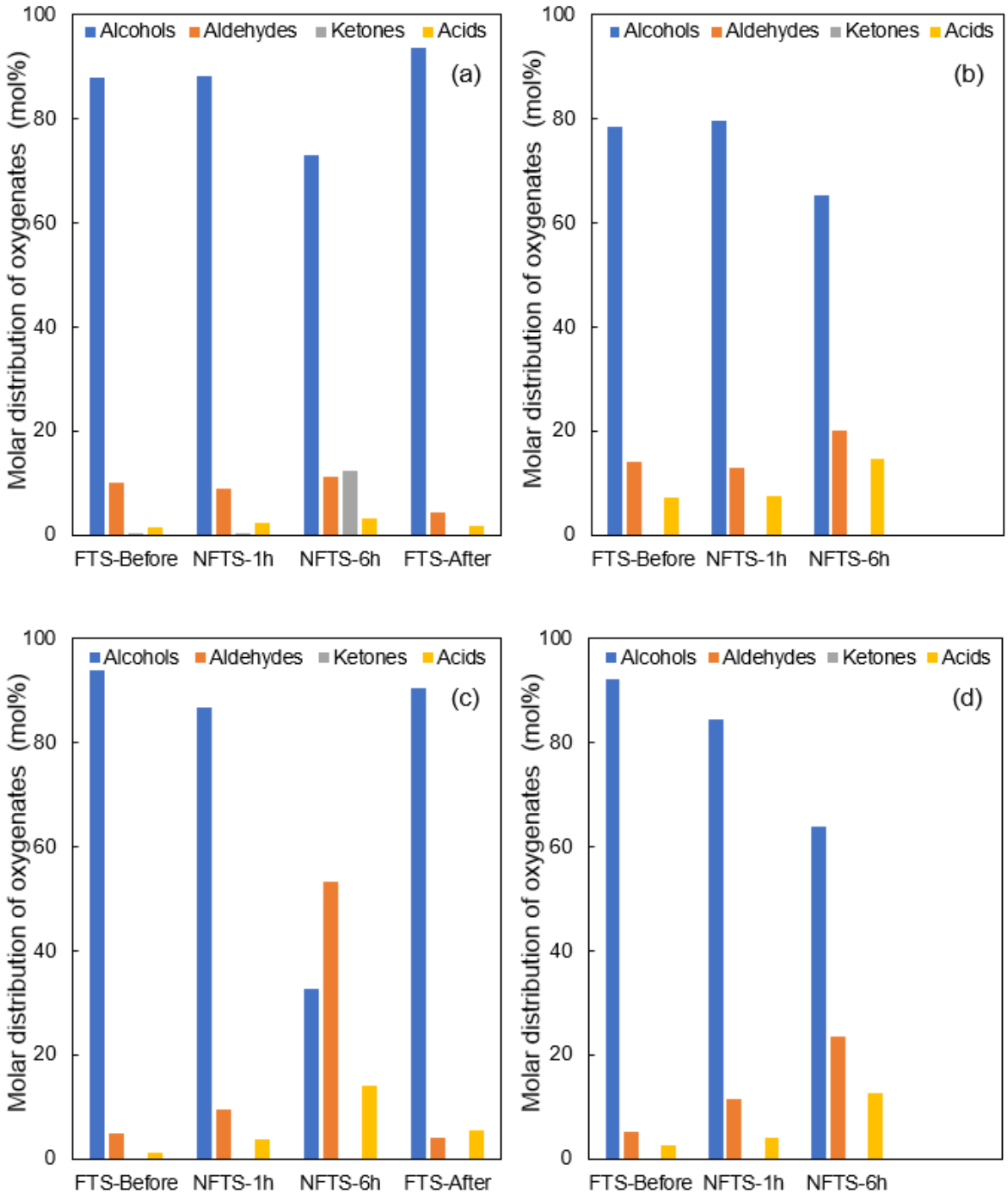

Figure 6. 13: Molar distribution of oxygenates obtained during the reaction stages over the Fe,Mn-CuZnO (a); K,Al-Fe (b); 10 wt% Fe/Al_2O_3 (c) and K-CuFe/Silica (d) catalysts (Reaction conditions: T = 240˚C, P = 20 bar, GHSV = 6000 h^{-1}, H_2/CO = 2:1, 5 vol% NH_3).

A close inspection of the overall oxygenate selectivities obtained during the reaction stages, summarised in Table 6. 6, highlights that the NH_3 co-feeding resulted in a significant decrease in the overall oxygenate selectivity obtained over the Fe,Mn-CuZnO, 10 wt% Fe/Al_2O_3 and K-CuFe/Silica while a slight decrease was observed over the K,Al-Fe catalyst. A look closed look at the oxygenate molar distribution, shown in Figure 6. 14, highlights that the decrease in the oxygenate content occurred across all carbon numbers as a result of the NH_3 co-feeding. Additionally, from the molar content of methanol in the oxygenates, summarized in Table 6. 6, it can be observed that the presence of NH_3 leads in the decrease in the methanol content over Fe,Mn-CuZnO, 10 wt% Fe/Al_2O_3 and K-CuFe/Silica catalysts while a slight increase was observed over the K,Al-Fe catalyst. Upon the removal of NH_3 from the feed gas, a partial recovery of both the oxygenate selectivity and the molar methanol content was observed over the Fe,Mn-CuZnO and 10 wt% Fe/Al_2O_3 catalysts, as shown in Table 6. 6. Regarding the oxygenate molar distribution, presented in Figure 6. 14, a higher recovery of the short chain oxygenates was obtained compared to the long chain oxygenates after the removal of NH_3, *i.e.* FTS-After, over the Fe,Mn-CuZnO and 10 wt% Fe/Al_2O_3 catalysts. It can be assumed that the systems may have not reached steady state in higher carbon numbers during 6 hours after returning under FTS (FTS-After).

Table 6. 6: Overall oxygenate, i.e. 1-alcohols and aldehydes, selectivity (C%) and molar methanol content in oxygenates (in brackets, mol%) obtained during the reaction stages over the four selected catalysts.

Reaction stage	24 hours under FTS	1 hour under NFTS	6 hours under NFTS	After returning under FTS
Fe,Mn-CuZnO	29.7 (28.7)	21.2 (21.5)	12.0 (24.8)	25.1 (25.2)
K,Al-Fe	12.0 (3.8)	12.5 (4.0)	8.2 (8.4)	-
10 wt% Fe/Al_2O_3	22.6 (35.8)	23.5 (37.7)	3.4 (7.7)	17.3 (25.1)
K-CuFe/Silica	15.5 (5.7)	13.0 (1.7)	4.6 (1.6)	-

Reaction conditions: T = 240˚C, P = 20 bar, GHSV = 6000 h^{-1}, H_2/CO ratio = 2.0, 5 vol% NH_3

The decrease in the oxygenates selectivity observed during the addition of NH_3 and the partial recovery observed after the removal of NH_3 confirmed that the presence of NH_3 has a negative effect on the formation of oxygenates over the four selected catalysts. From the results obtained, it may be assumed that the presence of NH_3 partially inhibits the primary routes of oxygenates formation through the competitive adsorption between NH_3, OH and CO species which limits the availability of CO and OH species responsible for the formation of oxygenates (Sango, 2013), (Sango et al., 2015). Alternatively, the drop in the oxygenates selectivity can be attributed to the substitution of the OH and/or CO species by NH_3 species in the last step of the oxygenates formation mechanisms leading to the formation of NCCs. Additionally, it

could also be speculated that the decrease of oxygenates selectivity observed upon NH_3 co-feeding might be due to the secondary reactions occurring between the oxygenates formed and NH_3 species leading to the formation of the corresponding NCCs (Sango, 2013), (Sango et al., 2015), (De Vries, 2017), (Rawoot, 2017).

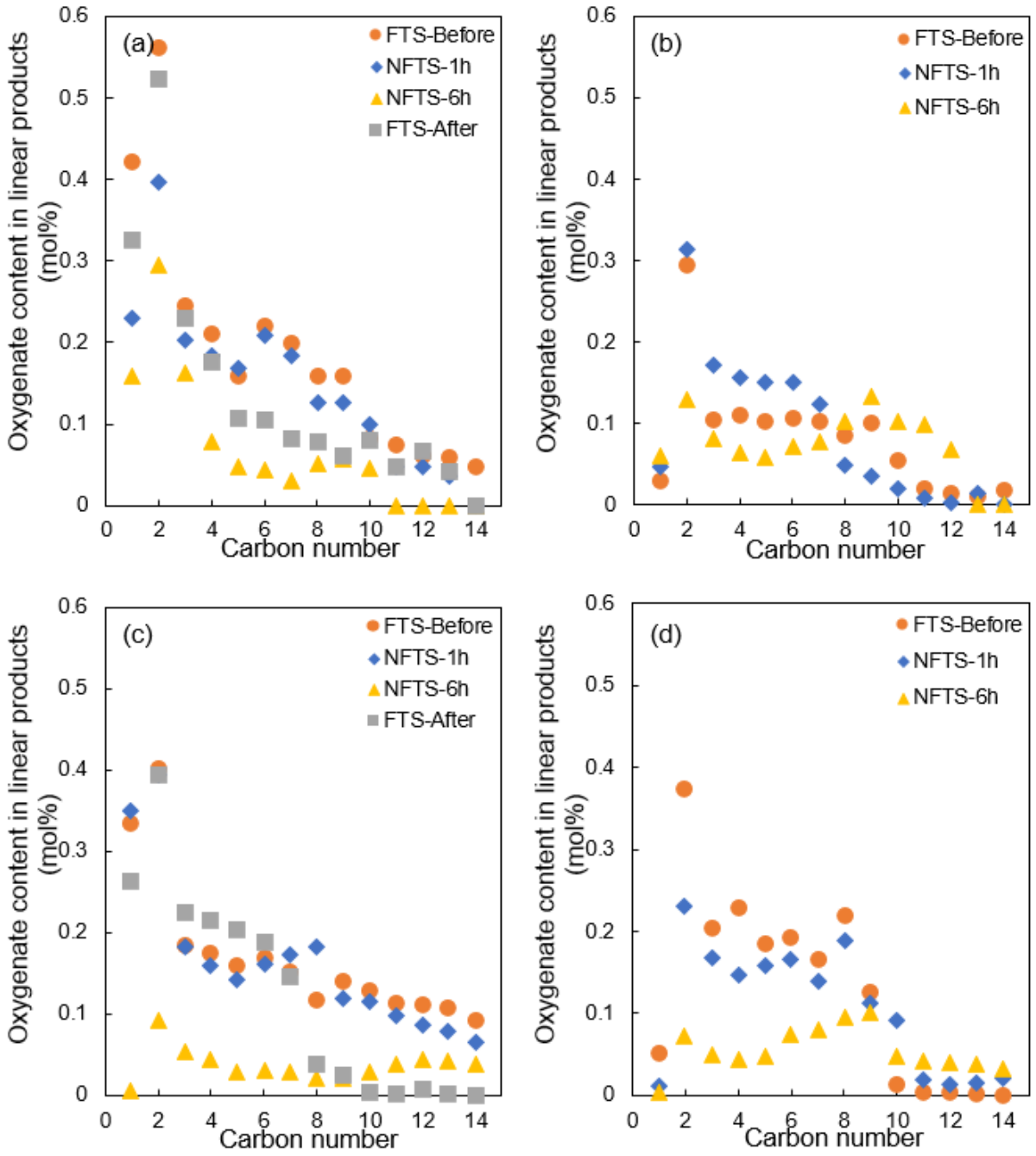

Figure 6. 14: Molar content of 1-alcohols plus aldehydes in fraction of linear hydrocarbon products (paraffins, olefins and oxygenates) as function of carbon number obtained during the reaction stages over the Fe,Mn-CuZnO (a); K,Al-Fe (b); 10 wt% Fe/Al_2O_3 (c) and K-CuFe/Silica (d) catalysts (Reaction conditions: T = 240˚C, P = 20 bar, GHSV = 6000 h^{-1}, H_2/CO = 2:1, 5 vol% NH_3).

6.8. Nitrogen-containing compounds (NCCs)

The formation of NCCs has also been reported in literature as a result of the co-feeding of NH_3 during the FTS (Alfred, 1950), (Brown & Maselli, 1973), (Claeys et al., 2013), (Sango, 2013), (Henkel, 2013), (De Vries, 2017).

Fischer et al. (2016) reported a complete disappearance of oxygenates and the formation of a single NCCs, *i.e.* acetonitrile with a selectivity of 37.7 C%, during the addition of 5 vol% NH_3 while a high oxygenates selectivity, *i.e.* 71.2 C%, was obtained under normal FTS conditions over an alumina supported iron-rhodium (10 wt% Rh and 5.4 wt% Fe loadings) alloy catalyst. However, over a similar catalyst with 6.3 wt% Rh and 5.2 wt% Fe loadings, Rawoot (2017) observed that the co-feeding of 5 vol% NH_3 resulted in the drop in alcohols content, the disappearance of aldehydes and the formation of trace amount of acids followed by the formation of a mixture of NCCs, *i.e.* nitriles, amides, formamides and amines, with a high acetonitrile content.

Additionally, over a Fe-based catalyst, Alfred (1950) reported the formation of aliphatic amines, while the formation of a mixture of amides, amines and nitriles were reported by Claeys et al. (2013), Sango (2013), Henkel (2013), De Vries (2017). Therefore, the type and amount of NCCs produced during the NFTS seems to be dependent of the type of catalyst, NH_3 content and reaction conditions.

In this study, to assess the formation and selectivity of the NCCs over each of the four selected catalysts, an online 2D-GC (TOF-MS and FID) in conjunction with an offline GC-FID was used and the results obtained, summarised in Table 6. 7 and Figure 6. 15, are discussed in this subsection.

Table 6. 7: NCCs selectivity (C%) obtained during the co-feeding of NH_3 over the four selected catalysts.

Reaction stage	1 hour under NFTS	6 hours under NFTS
Fe,Mn-CuZnO	5.0	17.9
K,Al-Fe	0.2	3.2
10 wt% Fe/Al_2O_3	3.1	3.3
K-CuFe/Silica	0.9	3.8

Reaction conditions: T = 240˚C, P = 20 bar, GHSV = 6000 h^{-1}, H_2/CO ratio = 2.0, 5 vol% NH_3

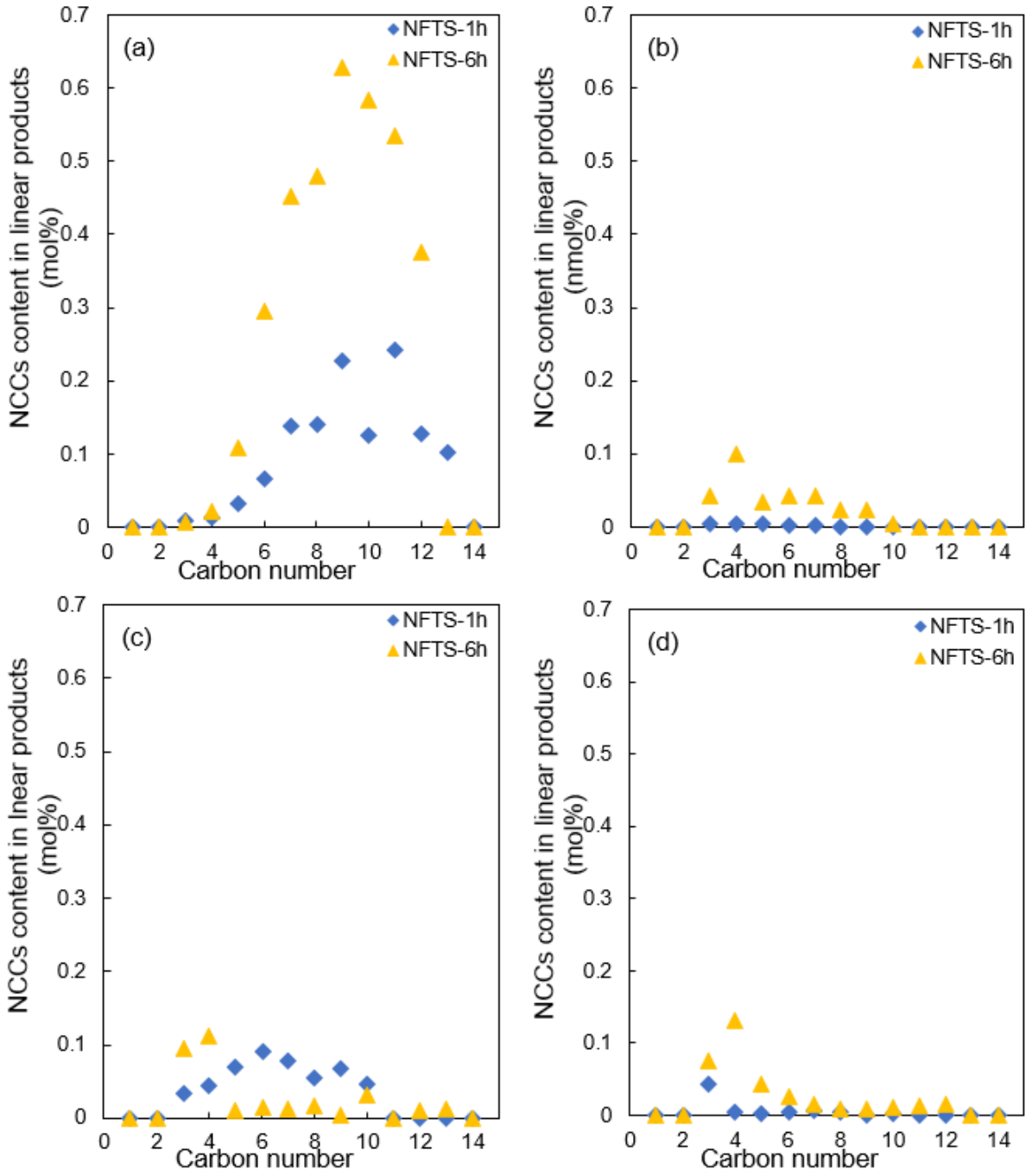

Figure 6. 15: Molar content of NCCs (nitriles, amines, amides, acetamides, formamides) in fraction of linear products (paraffins, olefins, oxygenates and NCCs) as function of carbon number obtained during the NH_3 co-feeding (NFTS) over the Fe,Mn-CuZnO (a); K,Al-Fe (b); 10 wt% Fe/Al_2O_3 (c) and K-CuFe/Silica (d) catalysts (Reaction conditions: T = 240˚C, P = 20 bar, GHSV = 6000 h^{-1}, H_2/CO = 2:1, 5 vol% NH_3).

Over the **Fe,Mn-CuZnO catalyst**, the co-feeding of NH_3 resulted in a decrease in the oxygenates selectivity and the formation of a single NCCs class, namely nitriles and a solid substance which is believed to be ammonium carbonate while a mixture of NCCs, nitriles, amides, amines, formamides and acetamides, was obtained over the three other catalysts. The formation of nitriles during the run occurred instantaneously upon addition of NH_3 and their molar content and selectivity increased gradually over time from 5.0 C% after 1 hour to 17.9 C% after 6 hours of co-feeding NH_3, as shown in Figure 6. 15(a) and Table 6. 7. An instantaneous formation of a mixture of nitriles, amides and amines was also reported by Rawoot (2017). However, after 3 hours of NH_3 co-feeding, Rawoot (2017) observed that the overall NCCs selectivity reached a maximum at 36 C% and declined to approximately 18 C% after 6 hours. The drop in the overall NCCs selectivity was also accompanied by the change in the major NCCs class. During the first hours of NH_3 co-feeding, nitriles were identified as the major NCCs, however, over time the content of amines increased and exceeded the nitriles content. Based on these observations, Rawoot (2017) speculated that the initial spike in the NCCs formation may be the result of the reaction between certain surface species formed during the normal FTS and NH_3. Furthermore, the drop in the NCCs selectivity over time was then attributed to the inhibition effect of NH_3 on the formation of these surface species considered as the precursors of NCCs (Rawoot, 2017). The formation of a single NCCs class and the gradual increase of the NCCs selectivity obtained in this present study over the Fe,Mn-CuZnO catalyst might be due to the stability of the catalyst and it may be speculated that the presence of NH_3 into the system has minimal impact on the formation of surface species responsible of the production of NCCs.

Furthermore, from Figure 6. 16, which summarises the selectivities of oxygenates and NCCs, *i.e.* only nitriles, it can be observed that after 1-hour of NH_3 co-feeding, the sum of the nitrile and oxygenate selectivities was lower than the oxygenate selectivity obtained before the NH_3 co-feeding over the Fe,Mn-CuZnO catalyst. This points out that the introduction of NH_3 might have partially inhibited the primary routes of oxygenates formation while favouring the formation of NCCs (Rawoot, 2017). Alternatively, the drop observed in the oxygenates selectivity upon addition of NH_3 can be attributed to the fact that oxygenates and/or their precursors might be the precursors of NCCs (Sango, 2013). After 6 hours under NFTS conditions, the sum of the nitriles and oxygenates was found to be higher than the oxygenates selectivity obtained prior the co-feeding of NH_3, see Figure 6. 16. It can then be hypothesised that the nitriles can also be formed via primary reaction routes. Upon removal of NH_3 from the system, a partial recovery of the oxygenates selectivity was observed while a small amount of nitriles was still been produced. This observation supports the hypothesis that the presence of NH_3 might have inhibited the primary routes of oxygenates formation (Rawoot, 2017).

A closer inspection of the selectivity of oxygenates and nitriles in the different carbon number fractions, shown in Figure 6. 16, indicates that the addition of NH_3 caused a sharp drop in the selectivity of short chain oxygenates, *i.e.* C_1-C_4, while no C_1-C_2 nitriles were detected and a very small amount of C_3-C_4 nitriles was obtained. Another interesting observation was that the higher oxygenates selectivities during the normal FTS occurred over the lowest carbon number range *i.e.* C_1-C_4, while the higher nitriles selectivity during the co-feeding of NH_3 occurred over the highest carbon number range, *i.e.* C_5-C_{14}. From these observations, it can be assumed that the short chain oxygenates, *i.e.* C_1-C_4, and/or their precursors react further with NH_3 surface species to form longer chain NCCs (Rawoot, 2017). Alternatively, due to the high content of long chain nitriles obtained, it can also be hypothesised that the nitriles are formed via the secondary reactions of long chain FTS products (Sango, 2013) due to their increasing retention on the catalyst surface (Schulz & Claeys, 1999b).

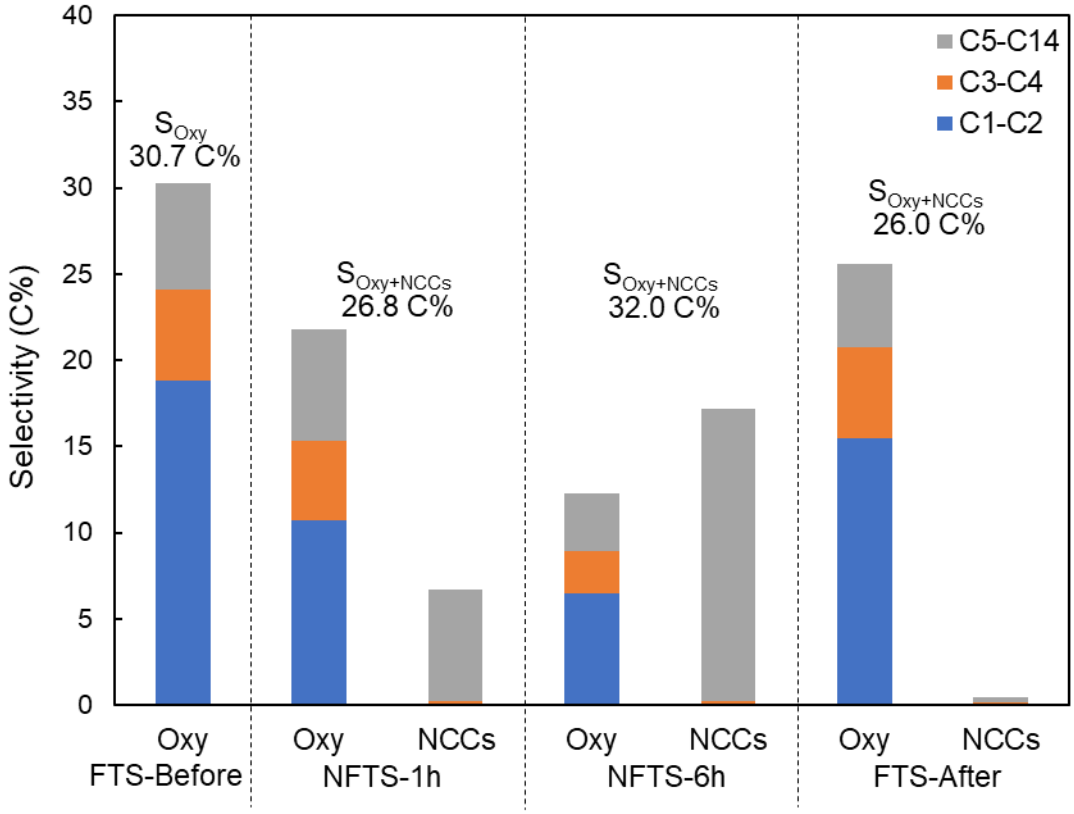

Figure 6. 16: Oxygenates and nitriles selectivities obtained during the reaction stages over the Fe,Mn-CuZnO catalyst (Reaction conditions T = 240˚C, P = 20 bar, GHSV = 6000 h-1, H_2/CO = 2:1, 5 vol% NH_3).

Over the **K,Al-Fe catalyst**, the co-feeding of NH_3 resulted in the formation of a mixture of NCCs, *i.e.* nitriles, amines, amides, acetamides and formamides. An increase in the overall NCCs selectivity, from 0.2 C% after 1 hour to 3.2 C% after 6 hours, was observed over time, as shown in Table 6. 7. Additionally, the NCCs molar content in the linear products also increased over time, as shown in Figure 6. 15(b).

Regarding the molar distribution of the different classes of the NCCs produced, shown in Figure 6. 17, small amount of nitriles and amines were produced while a relatively large amount of amides, formamides and acetamides were obtained during the co-feeding of 5 vol% NH_3 over the K,Al-Fe catalyst. Henkel (2013) only observed the formation of nitriles and amines upon the addition of 2 vol% NH_3 during the FTS over Fe-based catalysts promoted with potassium. Over a similar catalyst, small amounts of amides and formamides were detected in addition of the formation of amines and nitriles during the study performed by Sango (2013) after the addition of 2-10 vol% NH_3. Sango (2013) suggested that the formation of amides and formamides may occur through the secondary reaction of primarily formed acids. The large content of amides, formamides and acetamides obtained in this study over the K,Al-Fe catalyst, might be due to the secondary reactions of oxygenated compounds. Interestingly, an increase in acids and aldehydes contents was also observed during the NH_3 co-feeding while a decrease of alcohols content was observed, see Figure 6. 13(b). These results suggested that due to the inhibition of H_2 adsorption, the alcohols and/or their precursors might have further reacted to form aldehydes and acids. It can then be assumed that some of the acids formed reacted further with NH_3 to amides, formamides and acetamides (Sango, 2013).

Furthermore, the summary of the oxygenates and NCCs selectivity, presented in Figure 6. 18, highlights the unexpected slight increase in the oxygenate selectivity, *i.e.* from 12.0 to 12.5 C%, after 1-hour co-feeding NH_3 and a decrease in the oxygenates selectivity followed by the increase in the NCCs selectivity after 6 hours co-feeding NH_3. Another interesting observation made from Figure 6. 15, was that the sum of both oxygenates and NCCs produced after 6 hours co-feeding NH_3, *i.e.* 12.8 C%, equalled the oxygenates selectivity obtained before the co-feeding of NH_3, *i.e.* 12.9 C%.

Additionally, from the oxygenates and NCCs selectivities in the different carbon number fractions, shown in Figure 6. 18, it can be observed that the drop in the oxygenates selectivity over the C_3-C_4 and C_5-C_7 carbon number ranges occurred simultaneously with the increase in the selectivity of NCCs over the same carbon number ranges. These observations point out a strong correlation between the formation of NCCs and the decrease in oxygenates formation during the co-feeding of NH_3 during the FTS over the K,Al-Fe catalyst. It can then be assumed that the oxygenates and/or their precursors are involved in the formation of NCCs during the

co-feeding of NH_3 over the K,Al-Fe catalyst (Sango, 2013), (Henkel, 2013), (De Vries, 2017), (Rawoot, 2017).

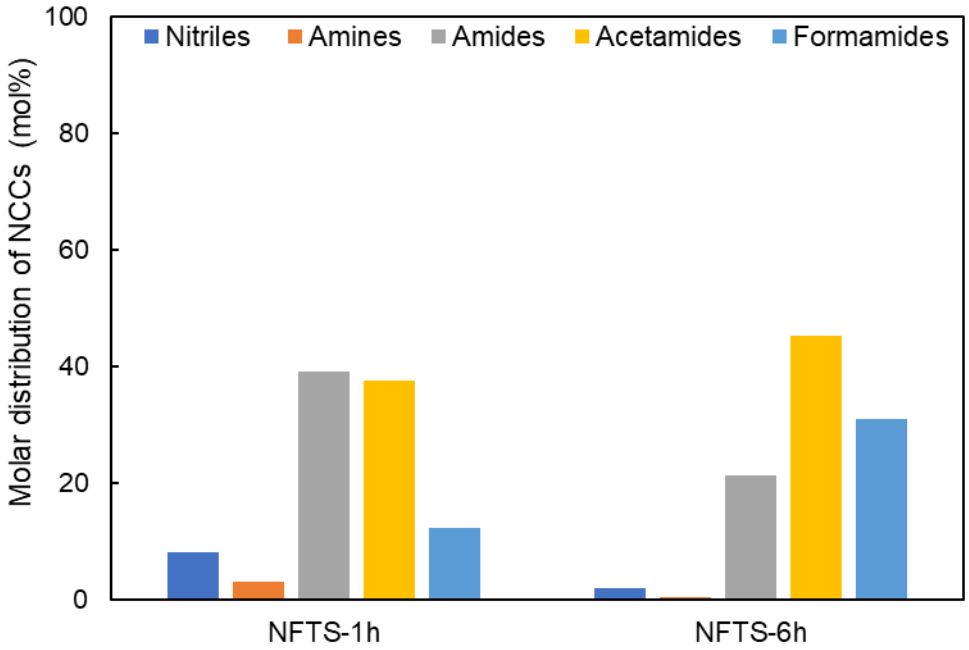

Figure 6. 17: Molar distribution of NCCs obtained during the reaction stages over the K,Al-Fe catalyst (Reaction conditions T = 240˚C, P = 20 bar, GHSV = 6000 h^{-1}, H_2/CO = 2:1, 5 vol% NH_3).

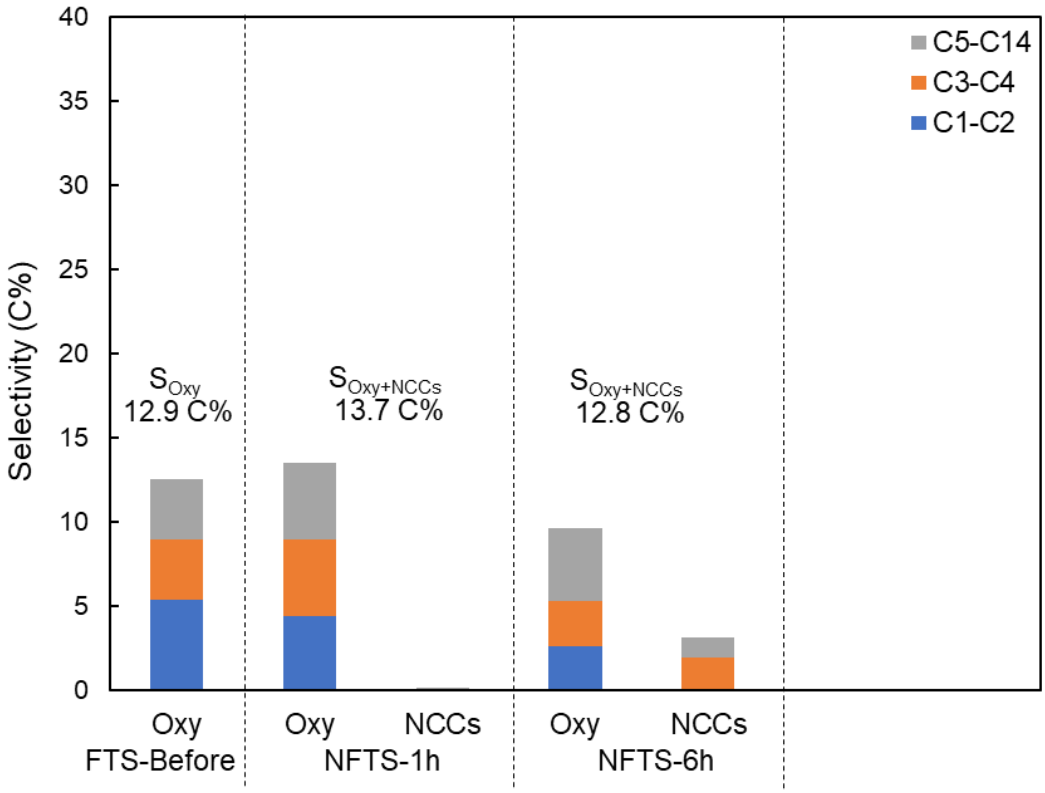

Figure 6. 18: Oxygenates and NCCs selectivities obtained during the reaction stages over the K,Al-Fe catalyst (Reaction conditions: T = 240˚C, P = 20 bar, GHSV = 6000 h-1, H_2/CO = 2:1, 5 vol% NH_3).

Over the **10 wt% Fe/Al_2O_3 catalyst**, the co-feeding of 5 vol% NH_3 resulted in the formation of a mixture of NCCs, *i.e.* nitriles, amines, amides, acetamides and formamides. As presented in Table 6. 7, the co-feeding NH_3 led to the immediate formation of NCCs which reached a selectivity of 3.1 C% after 1 hours. After 6 hours co-feeding NH_3, a minimal increase in the NCCs selectivity, *i.e.* 3.3 C%, was observed.

A closer look at the molar distribution of the different classes of the NCCs and the molar content of NCCs in the linear products, shown in Figure 6. 19 and Figure 6. 15(c) respectively, revealed a change in both the composition and distribution of the NCCs over time. After 1-hour co-feeding NH_3, the NCCs mixture made of nitriles, amides, acetamides and formamides was dominated by amides and has a high molar content over the long chain fraction, as shown Figure 6. 19 and Figure 6. 15(c). After 6 hours co-feeding NH_3, a considerable drop in the nitriles content followed by the appearance of amines was observed and formamides were found to be the dominant NCCs, as shown on Figure 6. 19. Additionally, an increase in the content of the short chain NCCs accompanied by a significant drop in the long chain NCCs content was observed after 6 hours co-feeding NH_3, as shown in Figure 6. 15(c). The opposite trend observed in the amines and nitriles content suggests that the amines are formed from the hydrogenation of the nitrile species (Sango, 2013), (Sango et al., 2015). The increase in the formation of both formamides and acetamides can be attributed to the secondary reactions of either acids formed and/or their precursors and/or amides formed (Sango, 2013), (Sango et al., 2015).

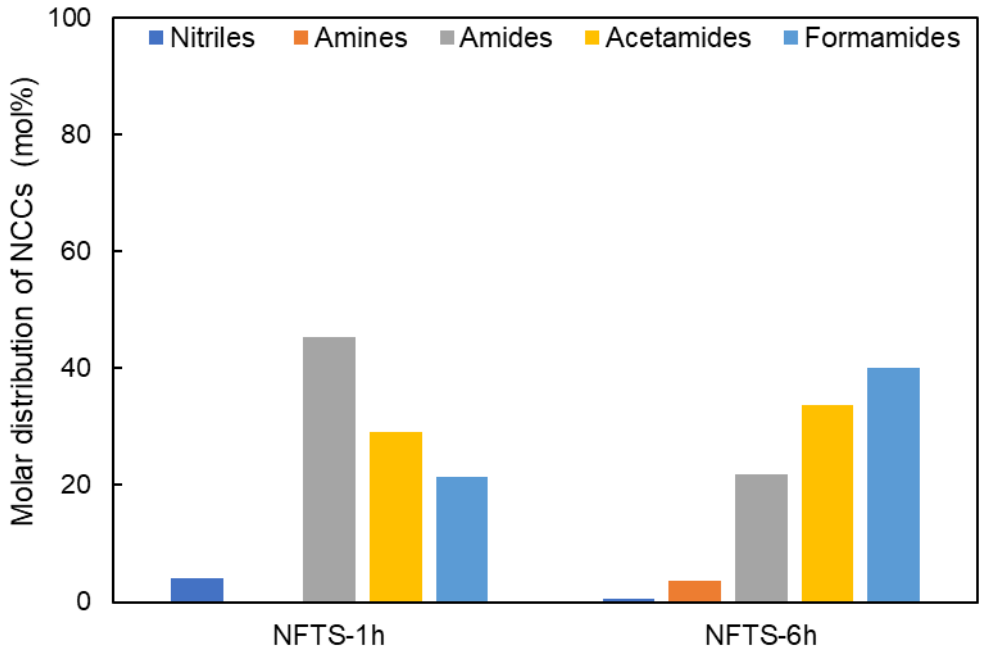

Figure 6. 19: Molar distribution of NCCs obtained during the reaction stages over the 10 wt% Fe/Al_2O_3 catalyst (Reaction conditions T = 240˚C, P = 20 bar, GHSV = 6000 h^{-1}, H_2/CO = 2:1, 5 vol% NH_3).

From Figure 6. 20, which summarises the oxygenate and NCCs selectivities, it can be clearly observed that the sum of oxygenate and NCCs selectivities obtained after 1-hour co-feeding was higher than the oxygenate selectivity obtained under normal FTS conditions. This may imply that the presence of NH_3 during the first hour favoured the formation of both oxygenates and NCCs as a slight increase in the overall oxygenate selectivity, *i.e.* from 22.6 to 23.5 C%, as observed. This could be attributed to the initial inhibition effect of NH_3 on the secondary oxygenates hydrogenation (Sango, 2013), (Sango et al., 2015). However, after 6-hours co-feeding NH_3, a drastic drop in the oxygenates selectivity followed by a minimal increase in the NCCs selectivity was obtained resulting in the sum of both selectivities, *i.e.* oxygenates and NCCs, being much lower than the oxygenates selectivity obtained under normal FTS conditions. Furthermore, upon the removal of NH_3 from the feed gas, no NCCs formation was observed while the oxygenates selectivity obtained was lower than the selectivity obtained before the co-feeding of NH_3. These observations suggest that the adsorption of NH_3 on 10 wt% Fe/Al_2O_3 catalyst surface strongly inhibits the formation of oxygenates. Additionally, it can be assumed that the formation of NCCs during the NH_3 co-feeding over the 10 wt% Fe/Al_2O_3 catalyst may occur via primary routes which do not involve oxygenates and/or their precursors as a drastic drop in the oxygenates content did not correlate to the NCCs formation.

Looking at the selectivity of oxygenates and nitriles in the different carbon number fractions, shown in Figure 6. 20, it can be observed that the significant drop in the oxygenates selectivity did not correlate to the increase in the NCCs selectivity across all carbon numbers except over the C_3-C_4 carbon number range. This indicates that the decrease in the oxygenates selectivity may not be caused by the formation of the NCCs via the secondary reactions of the corresponding oxygenates. This supported the hypothesis that the NH_3 species strongly inhibit the primary routes of oxygenates formation by blocking the metal sites responsible for the adsorption of OH and CO species on the 10 wt% Fe/Al_2O_3 catalyst.

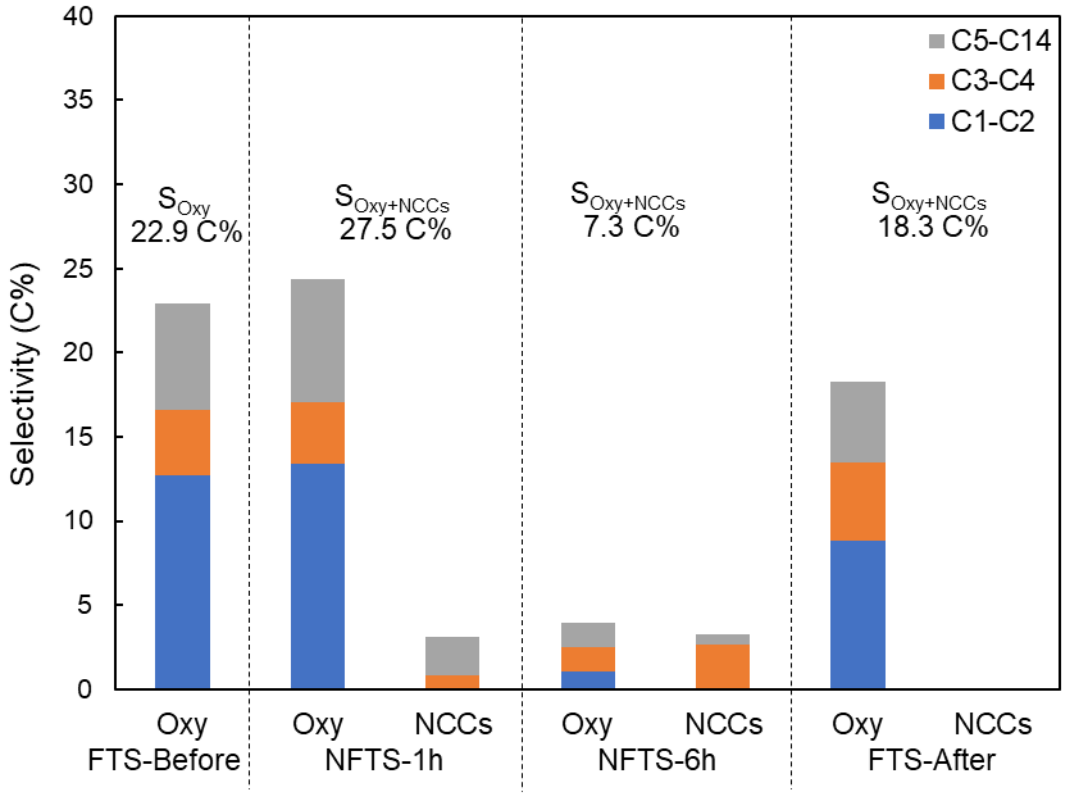

Figure 6. 20: Oxygenates and NCCs selectivities obtained during the reaction stages over the 10 wt% Fe/Al_2O_3 catalyst (Reaction conditions: T = 240˚C, P = 20 bar, GHSV = 6000 h^{-1}, H_2/CO = 2:1, 5 vol% NH_3).

Over the **K-CuFe/Silica catalyst**, the co-feeding of 5 vol% NH_3 resulted in the formation of a mixture of NCCs, *i.e.* nitriles, amines, amides, acetamides and formamides. After 1-hour, the NH_3 co-feeding led to the formation of a small amount of NCCs, *i.e.* 0.9 C%, see Table 6. 7, which was dominated by amines, as shown Figure 6. 21. Over time on stream, the content, and composition of the NCCs formed changed significantly. After 6 hours co-feeding, the overall NCCs increased to 3.8 C%, see Table 6. 7, leading to the increase in the NCCs molar content across all carbon numbers as presented in Figure 6. 15(d). Additionally, the formation of acetamides and formamides was detected after 6 hours co-feeding, as shown in Figure 6. 21. Regarding the NCCs composition, shown in Figure 6. 21, a sharp decrease in the amines content followed by the increase in the other NCCs, *i.e.* nitriles, amides, acetamides and formamides, were also observed. This highlights that over time the increasing amount of adsorbed NH_3 species on the K-CuFe/Silica catalyst surface might have enhanced the secondary reactions of nitrogen-containing products formed and/or the addition of NH_3 species to the terminal surface species leading to the formation of NCCs (Sango, 2013), (Sango et al., 2015).

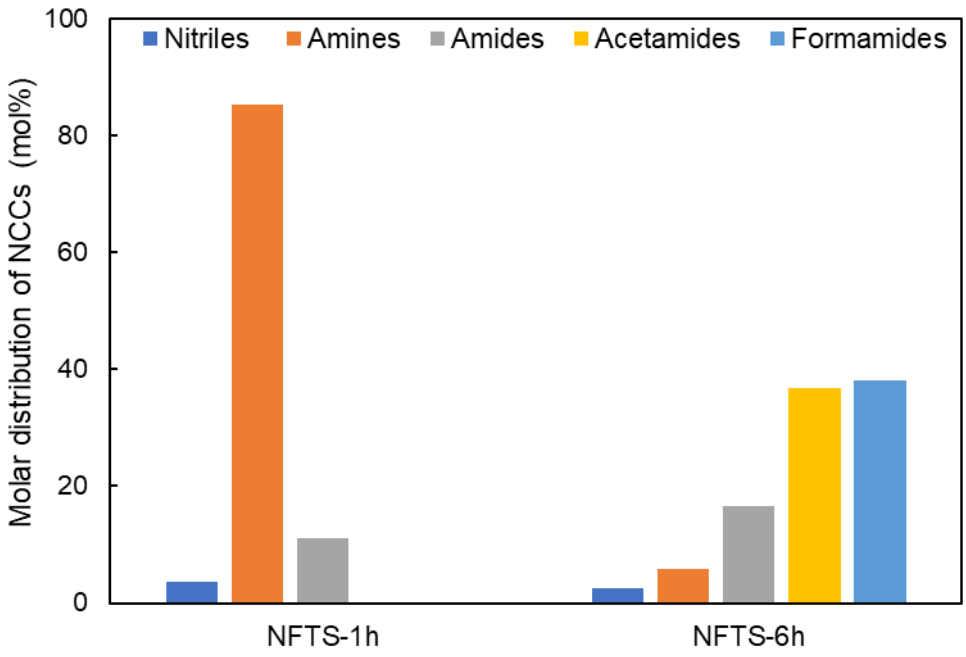

Figure 6. 21: Molar distribution of NCCs obtained during the reaction stages over the K-CuFe/Silica catalyst (Reaction conditions T = 240˚C, P = 20 bar, GHSV = 6000 h^{-1}, H_2/CO = 2:1, 5 vol% NH_3).

From Figure 6. 22, which summarises the oxygenates and NCCs selectivities, it can be clearly observed that the co-feeding of NH_3 led to a gradual decline in the oxygenates selectivity while the NCCs selectivity increased over time. However, the sum of the selectivity of both oxygenates and NCCs obtained during the NH_3 co-feeding was found to be lower than the selectivity of oxygenates obtained initially under normal FTS conditions. From these observations, it may be assumed that the drop in the oxygenates content might not be necessary the result of their involvement in the secondary reactions leading to the formation of NCCs. Additionally, it can be suggested that the presence of NH_3 species block the metal sites responsible of the primary routes of oxygenates and/or their precursors. In this regard, the formation of NCCs during the co-feeding of NH_3 over the K-CuFe/Silica catalyst could therefore occur either through the secondary reactions of oxygenates and/or their precursors or through primary reaction routes.

From the selectivity of oxygenates and nitriles in the different carbon number fractions, shown in Figure 6. 22, a significant drop in the C_1-C_2 oxygenates selectivity was observed upon NH_3 co-feeding while the formation of C_1-C_2 NCCs was not detected. From this observation, it can be assumed that the presence of NH_3 species either inhibits the formation of short chain oxygenates or favours the re-incorporation of the short chain oxygenates formed in the chain growth which results in the formation of longer chain oxygenates or NCCs. Furthermore, it was also observed that the drop in the oxygenates selectivity seemed to correlate to the increase in the NCCs selectivity over the other carbon number ranges, *i.e.* C_3-C_4 and C_5-C_{14}.

This indicates that the decrease in the oxygenates selectivity may not be caused by the secondary reactions involving the oxygenates formed and/or their precursors and NH_3 species leading to the formation of the corresponding NCCs during the co-feeding of NH_3 over the K-CuFe/Silica catalyst (Sango, 2013), (Sango et al., 2015), (Henkel, 2013), (De Vries, 2017), (Rawoot, 2017).

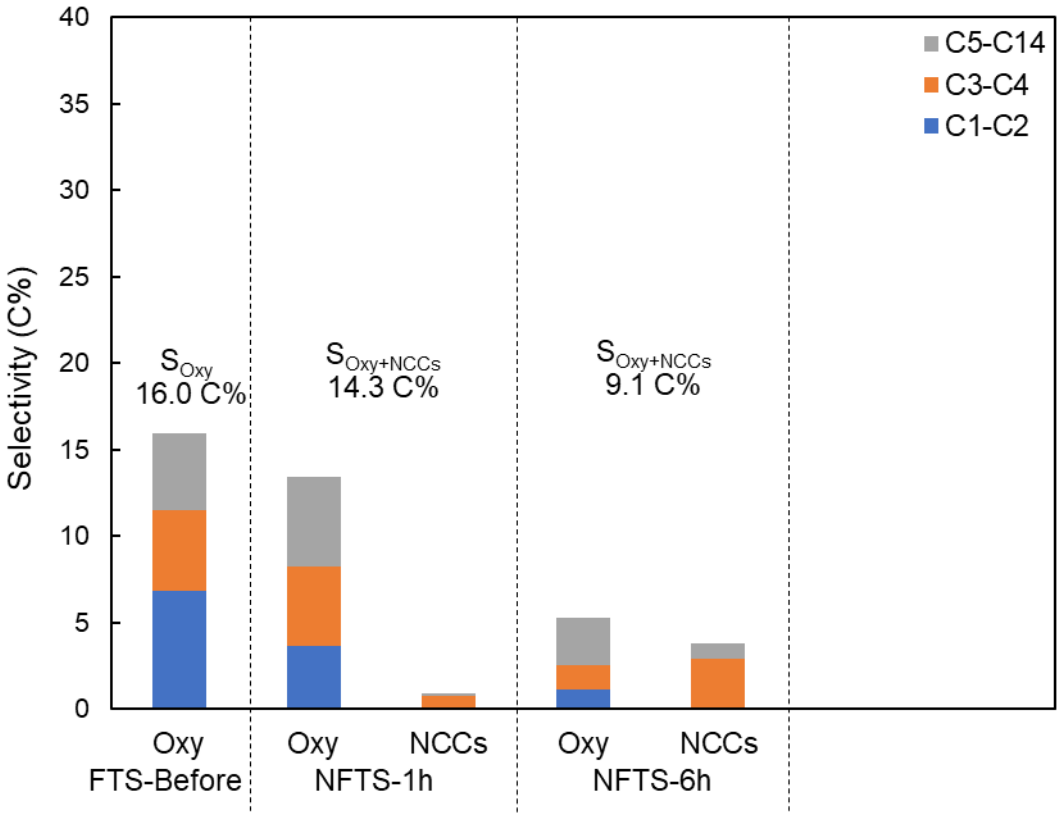

Figure 6. 22: Oxygenates and NCCs selectivities obtained during the reaction stages over the K-CuFe/Silica catalyst (Reaction conditions T = 240˚C, P = 20 bar, GHSV = 6000 h-1, H_2/CO = 2:1, 5 vol% NH_3).

6.9. Discussion on the formation of nitrogen-containing compounds during NH_3 co-feeding over the four selected catalysts and proposed mechanisms

In this study, the formation of nitrogen-contained compounds (NCCs) upon the addition of ammonia (NH_3) during the FTS was investigated over four selected catalysts, *i.e.* Fe,Mn-CuZnO; K,Al-Fe; 10 wt% Fe/Al_2O_3 and K-CuFe/Silica.

A selective production of nitriles with a NCCs selectivity of 17.9 C% and a resulting oxygenates selectivity of 12.0 C% were obtained over the Fe,Mn-CuZnO catalyst during the co-feeding of 5 vol% NH_3. Additionally, the co-feeding of 5 vol% NH_3 led to the formation of NCCs mixtures consisting of nitriles, amines, amides, acetamides and formamides with an overall NCCs selectivity of 3.2 C%, 3.3 C% and 3.8 C% and resulting oxygenate selectivity of 8.2 C%, 3.4 C% and 4.6 C% over K,Al-Fe, 10 wt% Fe/Al_2O_3 and K-CuFe/Silica catalysts respectively. From the experiments performed and the results gathered, it is evident that the catalyst composition influences the distribution and the production of both oxygenates and NCCs. Without further investigations, the mechanism of formation of the NCCs obtained over each of the four selected catalysts cannot be conclusively identified. However, based on the results and observations gathered in this present study, few possible mechanisms can be suggested.

Fe,Mn-CuZnO catalyst

The NH_3 co-feeding over the Fe,Mn-CuZnO catalyst resulted in the immediate formation of a single NCCs class, *i.e.* nitriles. The significant and gradual decrease observed in the oxygenate, *i.e.* made predominately of alcohols, formation and selectivity during the NH_3 co-feeding suggested that the NH_3 species might have inhibited the primary route of oxygenate formation and/or that the precursors of oxygenates might have reacted with the NH_3 species for the formation of NCCs obtained. However, a closed look at the sum of the selectivity of both oxygenates and nitriles obtained during the NH_3 co-feeding revealed that the nitriles might have also been produced via primary routes as the sum of the selectivity of the oxygenates and nitriles was found to be much higher than the overall oxygenate selectivity obtained under normal FTS conditions. From these results and observations, two mechanisms for the selective formation of nitriles over the Fe,Mn-CuZnO catalyst can be proposed. The proposed mechanism of the formation of nitriles via the secondary reaction of oxygenates and/or the reaction of the oxygenate precursors with the surface NH_3 species is schematised in Figure 6. 23.

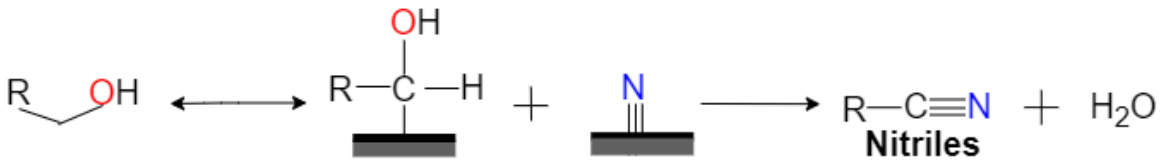

Figure 6. 23: Proposed mechanism of the formation of nitriles via the oxygenates secondary reactions. Adapted from Sango et al. (2013), (2015).

The proposed mechanism of the formation of nitriles via primary routes involves the reaction between the surface CN species, formed via the reaction between surface carbides and surface nitrides, and the surface alkyl species in a chain termination step as illustrated in Figure 6. 24.

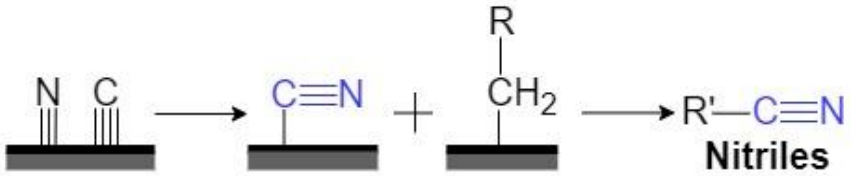

Figure 6. 24: Proposed mechanism of the formation of nitriles via the primary reaction routes. Adapted from Sango et al. (2013), (2015).

K,Al-Fe catalyst

The NH_3 co-feeding over the K,Al-Fe catalyst resulted in the formation of a mixture of NCCs made of nitriles, amines, amides, formamides and acetamides. In the NCCs mixture obtained, amide products, *i.e.* amides, formamides and acetamides, were found to be have the highest content. A close look at the selectivity of the oxygenated compounds during the NH_3 co-feeding highlighted the decrease in the alcohol selectivity which was accompanied with an increase in the selectivity of aldehydes and acids. This was then attributed to the inhibition effect of NH_3 on the adsorption of H_2 which might have favoured the secondary of alcohols precursors leading to the formation of aldehydes and acids. Some of the aldehydes and acids formed might have further reacted with the surface NH_3 species to produce the amides, formamides and acetamides, as illustrated on the proposed mechanism presented in Figure 6. 25.

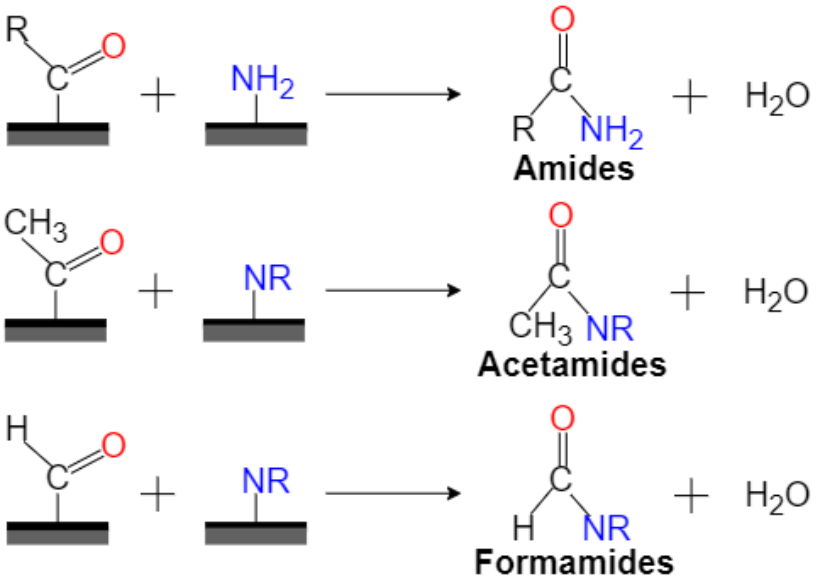

Figure 6. 25: Proposed mechanism of the formation of amides, acetamides and formamides via the secondary reactions of oxygenates, i.e. acids and aldehydes. Adapted from (De Vries, 2017).

10 wt% Fe/Al_2O_3 catalyst

The NH_3 co-feeding over the 10 wt% Fe/Al_2O_3 catalyst resulted in the immediate formation of a mixture of NCCs made of nitriles, amines, amides, formamides and acetamides. Over time on stream, the overall selectivity towards NCCs remained relatively constant however the change in the composition and distribution of NCCs and a significant decrease in the overall oxygenates was observed. The opposite trend observed between the nitriles and amines content suggested that the amines are formed from the hydrogenation of the nitrile species.

The increase in the formation of both formamides and acetamides observed over time on stream during the NH_3 co-feeding over the 10 wt% Fe/Al_2O_3 catalyst can be attributed to the secondary reactions of either acids formed and/or their precursors or to amides formed, which proposed mechanisms are presented in Figure 6. 25.

K-CuFe/Silica catalyst

The NH_3 co-feeding over the K-CuFe/Silica catalyst resulted in the formation of a mixture of NCCs made of nitriles, amines, amides, formamides and acetamides. During the first hours of NH_3 co-feeding, a small content of NCCs was detected and mostly composed of amines which can been explained by the addition of the surface NH_2 species to the alkyl species at the chain termination stage, as shown in the proposed mechanism presented in Figure 6. 26.

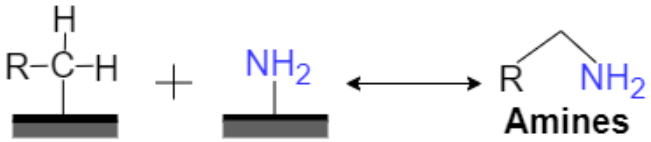

Figure 6. 26: Proposed mechanism of the formation of amines via the addition of surface NH_2 specie to surface alkyl specie at the chain termination step. Adapted from Sango et al. (2013), (2015).

Over time on stream, a significant decrease in the oxygenate selectivity accompanied by an increase in both the overall NCCs selectivity and the content of amides, acetamides and formamides were observed. These results and observations then suggested that the presence of NH_3 species on the surface of the K-CuFe/Silica catalyst may have inhibited the formation of the oxygenates while enhancing the formation of NCCs by reacting with the oxygenated precursors, as shown in the proposed mechanism presented in Figure 6. 27.

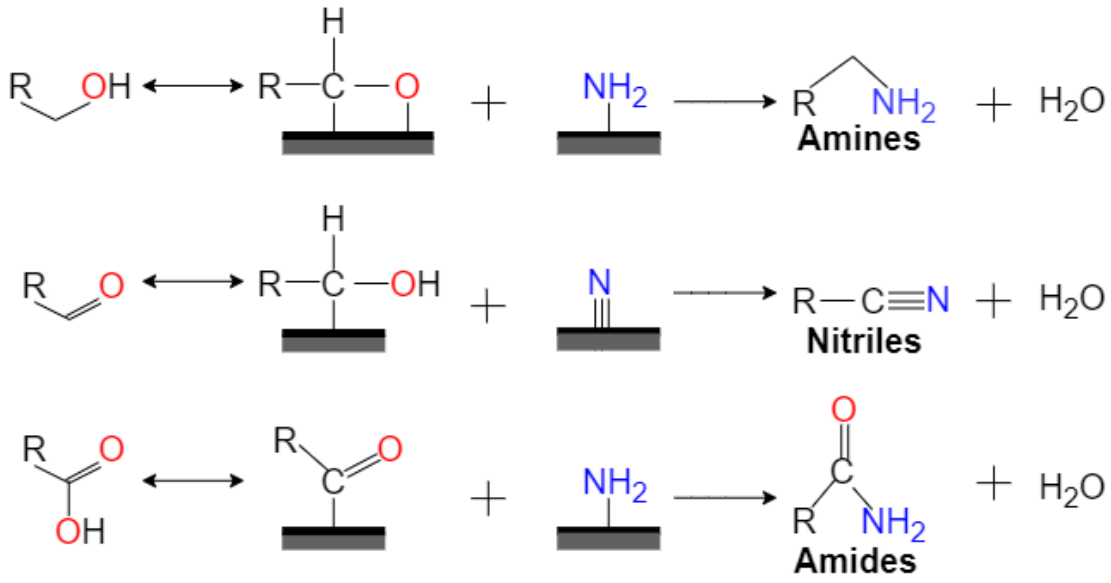

Figure 6. 27: Proposed mechanisms of the NCCs formation via the oxygenates secondary reactions and/or the reaction between their precursors and NH_3 species. Adapted from (De Vries, 2017).

Chapter 7: Conclusions

Based on previous studies, it was speculated that oxygenates and/or their precursors are the precursors of nitrogen containing compounds (NCCs) during the NFTS. Therefore, it was hypothesised that the use of a catalyst yielding a high oxygenates content under FTS conditions may be a suitable catalyst for the formation of NCCs under NFTS. This study was then conducted to verify this hypothesis and investigate the effects of the co-feeding of ammonia (NH_3) on the overall catalytic performance, *i.e.* the catalyst activity and products formation, of four catalysts which were selected based on their relatively high oxygenates selectivity.

The catalysts used in this study, *i.e.* Fe,Mn-CuZnO; K,Al-Fe; 10 wt% Fe/Al_2O_3; K-CuFe/Silica catalysts were synthesised via a (co)precipitation and/or wet impregnation techniques described by Ding et al. (2013), Schaller et al. (2018), Pijolat & Perrichon (1985), and Ding et al. (2012b) respectively. The XRD and in-situ XRD analyses allowed to determine the different phases present in each of the catalysts in their calcined state and to investigate the phases reduction behaviour, respectively. Due to the presence of copper (Cu), the reduction of phases present in the calcined Fe,Mn-CuZnO catalyst, namely Fe_2O_3 and CuO, occurred at a relatively low temperature, *i.e.* 150˚C, leading to the formation of the metallic Cu and an iron manganese oxide ($(FeO)_{0.3}(MnO)_{0.7}$) phase. The Fe_2O_3 phase present in the K,Al-Fe, 10 wt% Fe/Al_2O_3 and K-CuFe/Silica catalysts underwent a two-step reduction to form a metallic Fe phase. However, due to the low loading of potassium (K) and aluminium (Al) in the K,Al-Fe and K-CuFe/Silica catalysts, no K and Al phases were detected via both XRD analyses. Furthermore, the ICP-OES and BET analyses of all four catalysts confirmed their actual composition and the presence of mesopores, respectively.

The catalyst testing was conducted in a fixed bed reactor at 240˚C with a total pressure of 20 bar, a space velocity of 6000 h^{-1}, a H_2/CO ratio of 2 and 10 vol% of the total flowrate being the reference gas, argon. The catalyst testing was performed in three stages, *i.e.* 24 hours under normal FTS conditions (FTS-Before) followed by 6 hours of NH_3 co-feeding (NFTS) and 6 hours after returning to normal FTS conditions (FTS-after). To assess the effects of NH_3 co-feeding on the catalytic activity and the products formation, an online GC-TCD analysis was performed continuously during all three stages while the products analysis was conducted via the offline GC-FID and an online 2D-GC (TOF-MS & FID).

In this study, the co-feeding of NH_3 during the FTS over the four selected catalysts affected the catalytic activity and the formation of FTS products while enhancing the formation of NCCs.

The co-feeding of NH_3, over the unsupported catalysts, *i.e.* Fe,Mn-CuZnO and K,Al-Fe, resulted in a significant deactivation of the catalysts as a drastic decrease of around 50% in

the CO conversion was observed while minimal changes in the CO conversion were observed over the supported catalysts, *i.e.* 10 wt% Fe/Al_2O_3 and K-CuFe/Silica. This indicates that the poisonous effect of NH_3 on the catalytic activity through the inhibition of the CO adsorption by the NH_3 species is less pronounced over the supported catalysts due to their stability compared to the unsupported catalysts. This may also be attributed to the interaction of the NH_3 species with the support leading to less effect on the reactions.

Additionally, the co-feeding of NH_3 resulted in a complete disappearance of CO_2 over all four selected catalysts, which indicates that the presence of NH_3 might have suppressed the formation of CO_2 via the water gas shift (WGS) reaction. However, the formation of a white solid, which was believed to be ammonium carbonate, and the occurrence of a pressure build-up during the NFTS conditions in two of the experiments, suggested that the CO_2, formed via the WGS reaction, reacts further with the NH_3 species in presence of water to form ammonium carbonate as postulated by Alfred (1950) and (Sango, 2013). After returning to normal FTS conditions over the Fe,Mn-CuZnO catalyst, a partial recovery of both CO conversion and CO_2 selectivity were obtained which highlighted the partially reversible deactivation of the catalyst as the result of the co-feeding of NH_3.

The co-feeding of NH_3 led to an increase in the CH_4 selectivity over the Fe,Mn-CuZnO and K-CuFe/Silica catalysts while a drop was obtained over the K,Al-Fe and 10 wt% Fe/Al_2O_3 catalysts. The increase in CH_4 selectivities observed upon the co-feeding of NH_3 over the Fe,Mn-CuZnO and K-CuFe/Silica catalysts suggested that the NH_3 species compete and limit the adsorption of the CO while favouring the desorption of methyl surface species to form methane. From the drop in CH_4 selectivities observed upon the co-feeding of NH_3 over K,Al-Fe and 10 wt% Fe/Al_2O_3 catalysts, it can be assumed that the presence of NH_3 over these two catalysts competes and limits the adsorption of both CO and H_2 species while restricting the desorption of methyl species and favouring their incorporation in the chain growth.

Minimal changes in the α-values of linear hydrocarbons were observed upon the co-feeding of NH_3 over all four selected catalysts which suggested that the presence of NH_3 has a limited impact on the chain growth probability.

An increase in the olefins content was also observed as a result of the NH_3 co-feeding over the selected catalysts which suggested that the presence of NH_3 inhibits the hydrogenation reaction by reducing the amount of H_2 species available on the catalyst surface due to the competitive adsorption between NH_3 and H_2 species. Alternatively, the adsorption of the NH_3 species might have favoured the desorption and inhibited the re-adsorption of the olefins resulting in the inhibition of olefins secondary reactions and the high olefins content.

Over all four selected catalysts, the co-feeding of NH_3 during the FTS resulted in the significant decrease in the oxygenates selectivity. It could then be assumed that the competitive adsorption between NH_3, CO and H_2 species limits the availability of CO and OH species, *i.e.* species responsible for the oxygenates formation, which inhibits the primary routes of oxygenates formation. Alternatively, the drop in the oxygenates selectivity could be attributed to the substitution of the CO and OH species by the NH_3 species into the final step of the oxygenates formation mechanism leading to the formation of NCCs while limiting the oxygenates formation. Furthermore, it could be assumed that the drop in the oxygenates selectivity might be due to the secondary reactions involving the oxygenates formed and the NH_3 species leading to the formation of NCCs. The partial recovery of the oxygenates selectivity observed after returning under normal FTS conditions over the Fe,Mn-CuZnO and K-CuFe/Silica catalysts confirmed that the presence of NH_3 leads to a reversible inhibition of the oxygenates formation.

The co-feeding of NH_3 during the FTS over the four selected catalysts led to the formation of a variety of NCCs. Over the Fe,Mn-CuZnO catalyst, a selective production of nitriles was obtained while the formation of a mixture of NCCs made of nitriles, amines, amides, acetamides and formamides was obtained during the NFTS over the other three catalysts. Additionally, over all four catalysts, changes in the composition and distribution of both NCCs and oxygenates were observed over time on stream. Over all four catalysts, a significant drop in the C_1-C_4 oxygenates was observed while only a small content of C_1-C_4 NCCs was obtained. This suggested that in the presence of NH_3 the short chain oxygenates might have undergone secondary reactions or been incorporated in a growing chain leading to the formation of long chain NCCs and/or other FTS products. Over the Fe,Mn-CuZnO catalyst, a gradual increase in the nitriles selectivity accompanied by a sharp drop in the oxygenates selectivity was observed. This suggested that the oxygenates and/or their precursors are the precursors of NCCs and confirmed the inhibition effect of NH_3 on the oxygenates formation. Over the other three catalysts, the sharp decrease in the oxygenates selectivity was accompanied with the formation of a mixture of NCCs, the composition of which varied over time. Over the K,Al-Fe and 10 wt% Fe/Al_2O_3 catalysts, a drop in both nitriles and amides contents followed by an increase in amines and acetamides/formamides was observed over time on stream. This suggested that the nitriles formed undergo further hydrogenation reactions leading to the formation of the corresponding amines. The increase in the content of acetamides and formamides was attributed to the reaction between the oxygenates, namely acids and aldehydes, and/or their precursors with the surface NH_3 species. Furthermore, the sum of oxygenates and NCCs selectivities obtained during the NFTS over the K,Al-Fe catalyst was found to be similar to the oxygenates selectivity obtained under normal FTS conditions. This

may indicate that NCCs are formed via the secondary reactions of oxygenates and/or their precursors during the NFTS over the K,Al-Fe catalyst. However, over the 10 wt% Fe/Al_2O_3 and K-CuFe/Silica catalysts, the sum of oxygenates and NCCs selectivities obtained during the NFTS was found to be less than the oxygenates selectivity obtained under normal FTS conditions. After the removal of NH_3 from the feed gas, a partial recovery of the oxygenates selectivity was observed. This suggested that the presence of NH_3 indeed has a negative impact on the formation of oxygenates and that the formation of NCCs may occur through secondary reactions of oxygenates and/or the primary routes.

The present study provides promising results and highlights the great potential of the NFTS for the direct production of valuable chemicals*, i.e.* NCCs and oxygenates. Moreover, the study highlighted the possibility of the selective production of valuable compounds, *i.e.* nitriles, via the co-feeding of ammonia during the Fischer-Tropsch process over a Fe,Mn-CuZnO catalyst. The production of a mixture of NCCs composed of amines, amides, acetamides and formamides can also be obtained during the co-feeding of ammonia during the Fischer-Tropsch process over K,Al-Fe, 10 wt% Fe/Al_2O_3 and K-FeCu/Silica catalysts. Furthermore, the presence of oxygenates after 6 hours under the NFTS conditions indicate the need to optimise the reaction conditions and/or the catalyst formulation to further maximise the production of the NCCs.

Additionally, from the results and observations obtained from the present study, it can be concluded that the occurrences on catalysts surfaces leading to the NCCs formation are highly dependent on the catalyst formulation. Therefore, the development of improved catalysts suitable for the NFTS should be investigated.

Chapter 8: Recommendations/Future work

Based on the general conclusions made for the results and observations obtained during the present study the following recommendations have been made in order to shed further light on the new questions and findings that developed throughout the study.

One of the major issues encountered during the NH_3 co-feeding runs was the pressure build-up which prevented to run the reactions over a long time on stream and this was attributed to the formation of the white solid, believed to be ammonium carbonate. Thus, further research into the characterization of the white solid should be performed as if the white solid found is ammonium carbonate, it may be considered as a valuable product whilst capturing any CO_2 formed during the process. Additionally, the development and implementation of strategies should be done in order to ensure that the formation of the white solid does not affect the process so that the runs can be performed over a longer time on stream, to ensure that a steady state is achieved under the NFTS conditions.

All four catalysts investigated in this study, *i.e.* Fe,Mn-CuZnO; K,Al-Fe; 10 wt% Fe/Al_2O_3 and K-CuFe/Silica, show great potential for the production of nitrogen-containing compounds (NCCs) via the NH_3 co-feeding. The selective production of nitriles obtained over the Fe,Mn-CuZnO catalyst highlights the need to further investigate its catalytic performance under the NFTS conditions to gather more information on the NCCs products formation over this catalyst. Additionally, over the Fe,Mn-CuZnO catalyst, the formation of oxygenates during the NH_3 co-feeding is a good indication that the NCCs (nitriles) selectivity can be further optimised. Therefore, the optimization of the reaction conditions should also be performed over the Fe,Mn-CuZnO catalyst in order to maximise the NCCs selectivity. It is evident that the nature of the catalyst, *i.e.* (un) promoted and/or (un) supported, impacts both the class of NCCs formed as well as their content. Thus, further studies will be needed to provide insights on the effect of the nature of the catalyst to improve the catalyst formulations and obtain efficient catalysts for higher selective production of NCCs under NFTS conditions. More comprehensive studies of these selected catalysts to investigate the effect of the reaction temperature, ammonia concentration and other reaction parameters such as the space velocity and H_2/CO ratio under the NFTS conditions are needed in order to gather more information about the different routes of formation of the NCCs, which will allow to provide more conclusive mechanisms.

Lastly, the NH_3 co-feeding in the present study was all performed under steady-state reaction conditions. Further investigations should also consider the intermittent addition of ammonia which may yield even higher NCCs selectivities than the ones obtained under steady-state conditions.

References

Alfred, C. 1950. *Process of synthesizing aliphatic amines*. US. Patent 2,518,754.

Anderson, R., Friedel, R. & Storch, H. 1951. Fischer-Tropsch reaction mechanism involving stepwise growth of carbon chain. *The Journal of Chemical Physics.* 19(3):313-319.

Anderson, R.B., Feldman, J. & Storch, H.H. 1952. Synthesis of alcohols by hydrogenation of carbon monoxide. *Industrial & Engineering Chemistry.* 44(10):2418-2424.

Auvil, S.R. & Penquite, C.R. 1981. *Process for preparing acetonitrile*. US. Patent 4,272,452.

Bartholomew, C.H. 2001. Mechanisms of catalyst deactivation. *Applied Catalysis A: General.* 212(1):17-60.

Bartley, W.J. 1981. *Production of methyl and ethylamines with rhodium-iron catalysts*. US. Patent 4,250,116.

Bradley, M.J., Ananth, R., Willauer, H.D., Baldwin, J.W., Hardy, D.R. & Williams, F.W. 2017. The Effect of copper addition on the activity and stability of iron-based CO2 hydrogenation catalysts. *Molecules.* 22(9):1579.

Brown, P. & Maselli, J. 1973. *Process for preparing n-alkylamines*. US. Patent 3,726,926.

Bukur, D.B. & Sivaraj, C. 2002. Supported iron catalysts for slurry phase Fischer–Tropsch synthesis. *Applied Catalysis A: General.* 231(1):201-214.

Bukur, D.B., Patel, S.A. & Lang, X. 1990. Fixed bed and slurry reactor studies of Fischer-Tropsch synthesis on precipitated iron catalyst. *Applied catalysis.* 61(1):329-349.

Bukur, D.B., Lang, X., Akgerman, A. & Feng, Z. 1997. Effect of process conditions on olefin selectivity during conventional and supercritical Fischer−Tropsch synthesis. *Industrial & Engineering Chemistry Research.* 36(7):2580-2587.

Cairns, P. 2008. Oxygenates in iron Fischer-Tropsch synthesis: is copper a selectivity promoter? PhD dissertation. University of Cape Town.

Chaumette, P., Courty, P., Kiennemann, A. & Ernst, B. 1995. Higher alcohol and paraffin synthesis on cobalt based catalysts: comparison of mechanistic aspects. *Topics in Catalysis.* 2(1-4):117-126.

Claeys, M. & Van Steen, E. 2008. Fischer-Tropsch catalysts for the biomass-to-liquid (BTL)-process. *Chemical Engineering & Technology: Industrial Chemistry‐Plant Equipment‐Process Engineering‐Biotechnology.* 31(5):655-666.

Claeys, M.C.M. & Van Steen, E.W.J. 2004. Chapter 8: Basic studies. In *Studies in Surface Science and Catalysis* A. Steynberg and M. Dry, Eds. 601-680.

Claeys, M.C.M. & Fischer, N.F. 2013. *Sample presentation device for radiation-based analytical equipment*. U.S. Patent 8597598.

Claeys, M.C.M., Van Steen, E.W.J., Roessner, F. & Sango, T.S. 2013. *Process for the production of nitrogen or phosphorus containing compounds from synthesis gas*. US. Patent 8,513,463.

da Silva Maciel, G.P., da Silva, J.M., Bispo, M.D., Krause, L.C., Jacques, R.A., Zini, C.A. & Caramão, E.B. 2017. Comprehensive two-dimensional gas chromatography and its application to the Investigation of pyrolytic liquids. *Pyrolysis.*89.

Dallüge, J., Beens, J. & Udo, A. 2003. Comprehensive two-dimensional gas chromatography: a powerful and versatile analytical tool. *Journal of Chromatography A.* 1000(1-2):69-108.

Davis, B.H. 2003. Fischer-Tropsch synthesis: relationship between iron catalyst composition and process variables. *Catalysis Today.* 84(1):83-98.

De Klerk, A., Dancuart, L. & Leckel, D. 2005. Chemicals Refining From Fischer-Tropsch Synthesis. *18th World Petroleum Congress*. Johannesburg, South Africa, 2005/1/1/ 2005. 7.

De Vries, C. 2017. Adding ammonia during Fischer-Tropsch synthesis: pathways to the formation of N-containing compounds. PhD disssertation. University of Cape Town.

Dictor, R.A. & Bell, A.T. 1986. Fischer-Tropsch synthesis over reduced and unreduced iron oxide catalysts. *Journal of Catalysis.* 97(1):121-136.

Ding, M., Qiu, M., Wang, T., Ma, L., Wu, C. & Liu, J. 2012a. Effect of iron promoter on structure and performance of CuMnZnO catalyst for higher alcohols synthesis. *Applied Energy.* 97:543-547.

Ding, M., Liu, J., Zhang, Q., Tsubaki, N., Wang, T. & Ma, L. 2012b. Preparation of copper-iron bimodal pore catalyst and its performance for higher alcohols synthesis. *Catalysis Communications.* 28:138-142.

Ding, M., Tu, J., Qiu, M., Wang, T., Ma, L. & Li, Y. 2015. Impact of potassium promoter on Cu–Fe based mixed alcohols synthesis catalyst. *Applied Energy.* 138:584-589.

Ding, M., Ma, L., Zhang, Q., Wang, C., Zhang, W. & Wang, T. 2017. Enhancement of conversion from bio-syngas to higher alcohols fuels over K-promoted Cu-Fe bimodal pore catalysts. *Fuel processing technology.* 159:436-441.

Ding, M., Qiu, M., Liu, J., Li, Y., Wang, T., Ma, L. & Wu, C. 2013. Influence of manganese promoter on co-precipitated Fe–Cu based catalysts for higher alcohols synthesis. *Fuel.* 109:21-27.

Donnelly, T.J. & Satterfield, C.N. 1989. Product distributions of the Fischer-Tropsch synthesis on precipitated iron catalysts. *Applied catalysis.* 52(1):93-114.

Dry, M.E. 1981. The fischer-tropsch synthesis. *Catalysis science and technology.* 1:159-255.

Dry, M.E. 1996. Practical and theoretical aspects of the catalytic Fischer-Tropsch process. *Applied Catalysis A: General.* 138(2):319-344.

Dry, M.E. 2002. The Fischer–Tropsch process: 1950–2000. *Catalysis Today.* 71(3):227-241.

Dry, M.E. 2004a. Chapter 3: Chemical concepts used for engineering purposes. In *Studies in Surface Science and Catalysis.* A. Steynberg and M. Dry, Eds.: Elsevier. 196-257.

Dry, M.E. 2004b. Chapter 7: FT catalysts. In *Studies in surface science and catalysis.* A. Steynberg and M. Dry, Eds.: Elsevier. 533-600.

Dry, M.E. & Steynberg, A.P. 2004. Commercial FT process applications. In *Studies in Surface Science and Catalysis.* Elsevier. 406-481.

Dry, M.E., Shingles, T., Boshoff, L.J. & van H. Botha, C.S. 1970. Factors influencing the formation of carbon on iron Fischer-Tropsch catalysts: II. The effect of temperature and of gases and vapors present during Fischer-Tropsch synthesis. *Journal of Catalysis.* 17(3):347-354.

Edwards, M., Mostafa, A. & Górecki, T. 2011. Modulation in comprehensive two-dimensional gas chromatography: 20 years of innovation. *Analytical and Bioanalytical Chemistry.* 401(8):2335-2349.

Erley, W., McBreen, P. & Ibach, H. 1983. Evidence for CHx surface species after the hydrogenation of CO over an Fe (110) single crystal surface. *Journal of Catalysis.* 84(1):229-234.

Fang, K., Li, D., Lin, M., Xiang, M., Wei, W. & Sun, Y. 2009. A short review of heterogeneous catalytic process for mixed alcohols synthesis via syngas. *Catalysis Today.* 147(2):133-138.

Fischer, F. & Tropsch, H. 1926. The synthesis of petroleum at atmospheric pressures from gasification products of coal. *Brennstoff-Chemie.* 7:97-104.

Fischer, N., Henkel, R., Kotzé, H., Fürst, M., Olivier, J., Neethling, J. & Claeys, M. 2016. Acetonitrile via CO hydrogenation in the presence of NH3. *Catalysis Communications.* 87:14-17.

Flory, P.J. 1936. Molecular size distribution in linear condensation polymers. *Journal of the American Chemical Society.* 58(10):1877-1885.

Glasser, D., Hildebrandt, D., Liu, X., Lu, X. & Masuku, C.M. 2012. Recent advances in understanding the Fischer–Tropsch synthesis (FTS) reaction. *Current Opinion in Chemical Engineering.* 1(3):296-302.

Gredig, S.V., Koeppel, R. & Baiker, A. 1996. Comparative study of synthesis of methylamines from carbon oxides and ammonia over Cu/A12O3. *Catalysis Today.* 29(1-4):339-342.

Gredig, S.V., Koeppel, R. & Baiker, A. 1997. Synthesis of methylamines from CO2, H2 and NH3. Catalytic behaviour of various metal-alumina catalysts. *Applied Catalysis A: General.* 162(1):249-260.

Grobler, T. 2008. Two-dimensional gas chromatography: a novel technique for iron low temperature Fischer-Tropsch selectivity studies. PhD dissertation University of Cape Town.

Grobler, T., Claeys, M., van Steen, E. & Janse van Vuuren, M.J. 2009. GC×GC: A novel technique for investigating selectivity in the Fischer–Tropsch synthesis. *Catalysis Communications.* 10(13):1674-1680.

Henkel, R. 2013. The influence of ammonia on Fischer-Tropsch synthesis and formation of N-containing compounds. PhD dissertation Universität Oldenburg.

Herington, E. 1946. Fischer-Tropsch synthesis considered as a polymerization reaction. *Chem. Ind.(London).*

Herranz, T., Rojas, S., Pérez-Alonso, F., Ojeda, M., Terreros, P. & Fierro, J. 2006. Carbon oxide hydrogenation over silica-supported iron-based catalysts: Influence of the preparation route. *Applied Catalysis A: General.* 308:19-30.

Iglesia, E. 1997. Design, synthesis, and use of cobalt-based Fischer-Tropsch synthesis catalysts. *Applied Catalysis A: General.* 161(1):59-78.

Iglesia, E., Reyes, S.C., Madon, R.J. & Soled, S.L. 1993. Selectivity control and catalyst design in the Fischer-Tropsch synthesis: sites, pellets, and reactors. In *Advances in Catalysis.* D.D. Eley, H. Pines and P.B. Weisz, Eds.: Academic Press. 221-302.

Johnston, P. & Joyner, R. 1993. Structure-function relationships in heterogeneous catalysis: the embedded surface molecule approach and its applications. In *Studies in Surface Science and Catalysis.* Elsevier. 165-180.

Kuipers, E.W., Scheper, C., Wilson, J.H., Vinkenburg, I.H. & Oosterbeek, H. 1996. Non-ASF product distributions due to secondary reactions during Fischer–Tropsch synthesis. *Journal of Catalysis.* 158(1):288-300.

Kurtz, A.N. 1969. *Production of methylamines*. US. Patent 3,444,203.

Lappas, A. & Heracleous, E. 2016. Production of biofuels via Fischer–Tropsch synthesis: biomass-to-liquids. In *Handbook of Biofuels Production (Second Edition).* R. Luque, C.S.K. Lin, K. Wilson and J. Clark, Eds.: Woodhead Publishing. 549-593.

Li, S., Krishnamoorthy, S., Li, A., Meitzner, G.D. & Iglesia, E. 2002. Promoted iron-based catalysts for the Fischer–Tropsch synthesis: design, synthesis, site densities, and catalytic properties. *Journal of Catalysis.* 206(2):202-217.

Lin, M., Fang, K., Li, D. & Sun, Y. 2008. CO hydrogenation to mixed alcohols over co-precipitated Cu–Fe catalysts. *Catalysis Communications.* 9(9):1869-1873.

Liu, Z. & Phillips, J.B. 1991. Comprehensive two-dimensional gas chromatography using an on-column thermal modulator interface. *Journal of Chromatographic Science.* 29(6):227-231.

Liu, Z., Shi, S. & Li, Y. 2010. Coal liquefaction technologies—Development in China and challenges in chemical reaction engineering. *Chemical Engineering Science.* 65(1):12-17.

Lohitharn, N. & Goodwin, J.G. 2008. Impact of Cr, Mn and Zr addition on Fe Fischer–Tropsch synthesis catalysis: Investigation at the active site level using SSITKA. *Journal of Catalysis.* 257(1):142-151.

Ma, W.-P., Zhao, Y.-L., Li, Y.-W., Xu, Y.-Y. & Zhou, J.-L. 1999. An investigation of chain growth probability in Fischer-Tropsch synthesis over an industrial Fe− Cu− K catalyst. *Reaction Kinetics and Catalysis Letters.* 66(2):217-223.

Mabaso, E.I. 2005. Nanosized iron crystallites for Fischer-Tropsch synthesis. PhD dissertation. University of Cape Town.

Mahmoudi, H., Mahmoudi, M., Doustdar, O., Jahangiri, H., Tsolakis, A., Gu, S. & LechWyszynski, M. 2017. A review of Fischer Tropsch synthesis process, mechanism, surface chemistry and catalyst formulation. *Biofuels Engineering.* 2(1):11-31.

Maitlis, P.M. & de Klerk, A. 2013. *Greener Fischer-Tropsch Processes: For Fuels and Feedstocks.* John Wiley & Sons.

Maitlis, P.M., Quyoum, R., Long, H.C. & Turner, M.L. 1999. Towards a chemical understanding of the Fischer–Tropsch reaction: alkene formation. *Applied Catalysis A: General.* 186(1-2):363-374.

Mosallanejad, S., Dlugogorski, B., Kennedy, E. & Stockenhuber, M. 2018. On the Chemistry of Iron Oxide Supported on γ-Alumina and Silica Catalysts. *ACS Omega.* 3:5362-5374.

Olive, G. & Olive, S. 1979. *Process for preparing acetonitrile*. US. Patent 4,179,462.

Ordomsky, V.V., Carvalho, A., Legras, B., Paul, S., Virginie, M., Sushkevich, V.L. & Khodakov, A.Y. 2016. Effects of co-feeding with nitrogen-containing compounds on the performance of supported cobalt and iron catalysts in Fischer–Tropsch synthesis. *Catalysis Today.* 275:84-93.

Patzlaff, J., Liu, Y., Graffmann, C. & Gaube, J. 1999. Studies on product distributions of iron and cobalt catalyzed Fischer–Tropsch synthesis. *Applied Catalysis A: General.* 186(1):109-119.

Phillips, J.B., Gaines, R.B., Blomberg, J., van der Wielen, F.W.M., Dimandja, J.-M., Green, V., Granger, J., Patterson, D. et al. 1999. A Robust Thermal Modulator for Comprehensive Two-Dimensional Gas Chromatography. *Journal of High Resolution Chromatography.* 22(1):3-10.

Pichler, v.H. & Schulz, H. 1970. Recent findings in the field of synthesis of hydrocarbons from CO and H2. *Chemical Engineering Technology.* 42(18):1162-1174.

Pijolat, M. & Perrichon, V. 1985. Synthesis of alcohols from CO and H2 on a Fe/Al203 catalyst at 8-30 bars pressure. *Applied catalysis.* 13(2):321-333.

Pollak, P., Romeder, G., Hagedom, F. & Gelbke, H. 2012. Nitriles In *Ullmann's Encyclopedia of Industrial Chemistry.* 251-265.

Rahman, M.M., Abd El-Aty, A., Choi, J.H., Shin, H.C., Shin, S.C. & Shim, J.H. 2015. Basic overview on gas chromatography columns. *Analytical Separation Science.*823-834.

Rausch, A.K., Schubert, L., Henkel, R., van Steen, E., Claeys, M. & Roessner, F. 2016. Enhanced olefin production in Fischer–Tropsch synthesis using ammonia containing synthesis gas feeds. *Catalysis Today.* 275:94-99.

Rawoot, A. 2017. The production of nitrogen-containing compounds via a modified Fischer-Tropsch process. Master thesis. University of Cape Town

Roose, P., Eller, K., Henkes, E., Rossbacher, R. & Höke, H. 2000. Amines, aliphatic. *Ullmann's Encyclopedia of Industrial Chemistry.*1-55.

Sango, T. 2013. Nitrogen-containing compounds from ammonia co-feed to the Fischer-Tropsch synthesis. Master thesis. University of Cape Town.

Sango, T., Fischer, N., Henkel, R., Roessner, F., van Steen, E. & Claeys, M. 2015. Formation of nitrogen containing compounds from ammonia co-fed to the Fischer–Tropsch synthesis. *Applied Catalysis A: General.* 502:150-156.

Schaller, M., Reichelt, E. & Jahn, M. 2018. Iron-based Fischer-Tropsch catalysts for higher alcohol synthesis. *Chemie Ingenieur Technik.* 90(5):713-720.

Schulz, H. 1999. Short history and present trends of Fischer–Tropsch synthesis. *Applied Catalysis A: General.* 186(1):3-12.

Schulz, H. & Gokcebay, H. 1984. Fischer-Tropsch CO-hydrogenation as a means for linear olefins production. *Catalysis of organic reactions.*153-169.

Schulz, H. & Claeys, M. 1999a. Kinetic modelling of Fischer–Tropsch product distributions. *Applied Catalysis A: General.* 186(1):91-107.

Schulz, H. & Claeys, M. 1999b. Reactions of α-olefins of different chain length added during Fischer–Tropsch synthesis on a cobalt catalyst in a slurry reactor. *Applied Catalysis A: General.* 186(1-2):71-90.

Schulz, H., Van Steen, E. & Claeys, M. 1994. Selectivity and mechanism of Fischer-Tropsch synthesis with iron and cobalt catalysts. In *Studies in Surface Science and Catalysis.* Elsevier. 455-460.

Schulz, H., Steen, E. & Claeys, M. 1995. Specific inhibition as the kinetic principle of the Fischer-Tropsch synthesis. *Topics in Catalysis.* 2:223-234.

Shen, Y. & Lee, M.L. 1998. General equation for peak capacity in column chromatography. *Analytical Chemistry.* 70(18):3853-3856.

Snel, R. 1986. On-line gas chromatographic analysis of light Fischer-Tropsch synthesis products. *Chromatographia.* 21(5):265-268.

Steynberg, A. 2004. Introduction to fischer-tropsch technology. In *Studies in surface science and catalysis.* Elsevier. 1-63.

Steynberg, A., Dry, M., Davis, B. & Breman, B. 2004. Fischer-Tropsch reactors. In *Studies in Surface Science and Catalysis.* Elsevier. 64-195.

Surisetty, V.R., Dalai, A.K. & Kozinski, J. 2011. Alcohols as alternative fuels: an overview. *Applied Catalysis A: General.* 404(1):1-11.

Todic, B., Nowicki, L., Nikacevic, N. & Bukur, D.B. 2016. Fischer–Tropsch synthesis product selectivity over an industrial iron-based catalyst: effect of process conditions. *Catalysis Today.* 261:28-39.

Van de Loosdrecht, J., Botes, F., Ciobica, I., Ferreira, A., Gibson, P., Moodley, D., Saib, A., Visagie, J. et al. 2013. Fischer-Tropsch synthesis: catalysts and chemistry. In *Comprehensive Inorganic Chemistry II: from elements to applications.* Elsevier. 525-557.

Van Der Laan, G.P. & Beenackers, A.A.C.M. 1999. Kinetics and selectivity of the Fischer–Tropsch synthesis: a literature review. *Catalysis Reviews.* 41(3-4):255-318.

van der Westhuizen, R., Crouch, A. & Sandra, P. 2008. The use of GC× GC with time-of-flight mass spectrometry to investigate dienes and Diels–Alder polymerisation products in high-temperature Fischer–Tropsch-based fuels. *Journal of separation science.* 31(19):3423-3428.

van der Westhuizen, R., Ajam, M., De Coning, P., Beens, J., de Villiers, A. & Sandra, P. 2011. Comprehensive two-dimensional gas chromatography for the analysis of synthetic and crude-derived jet fuels. *Journal of Chromatography A.* 1218(28):4478-4486.

Walter, R. 1958. *Catalytic hydrogenation of carbon monoxide with addition of ammonia or methylamine*. US. Patent 2,821,537.

Xu, J., Yang, Y. & Li, Y.-W. 2013. Fischer–Tropsch synthesis process development: steps from fundamentals to industrial practices. *Current Opinion in Chemical Engineering.* 2(3):354-362.

Xu, J., Yang, Y. & Li, Y.-W. 2015. Recent development in converting coal to clean fuels in China. *Fuel.* 152.

Yang, J., Liu, Y., Chang, J., Wang, Y.-N., Bai, L., Xu, Y.-Y., Xiang, H.-W., Li, Y.-W. et al. 2003. Detailed kinetics of Fischer−Tropsch synthesis on an industrial Fe−Mn catalyst. *Industrial & Engineering Chemistry Research.* 42(21):5066-5090.

Yang, Y., Xiang, H.-W., Xu, Y.-Y., Bai, L. & Li, Y.-W. 2004. Effect of potassium promoter on precipitated iron-manganese catalyst for Fischer–Tropsch synthesis. *Applied Catalysis A: General.* 266(2):181-194.

Zhang, Q., Kang, J. & Wang, Y. 2010. Development of novel catalysts for Fischer–Tropsch synthesis: tuning the product selectivity. *ChemCatChem.* 2(9):1030-1058.

Zhang, Q., Deng, W. & Wang, Y. 2013. Recent advances in understanding the key catalyst factors for Fischer-Tropsch synthesis. *Journal of Energy Chemistry.* 22(1):27-38.

Zhu, M., Rocha, T.C., Lunkenbein, T., Knop-Gericke, A., Schlögl, R. & Wachs, I.E. 2016. Promotion mechanisms of iron oxide-based high temperature water–gas shift catalysts by chromium and copper. *ACS Catalysis.* 6(7):4455-4464.

Appendix

A.1. GC-TCD calibration gas composition and the TCD response factors

Gas	Mixed gas concentration [%]	TCD response factor
i	C_i	$f_{TCD,i}$
Ar	14.9	1.00
CH_4	14.9	0.83
CO	10.0	0.96
CO_2	19.9	1.03
H_2	40.3	2.14

A.2. FID response factors

	FID Response Factors		
Carbon number	Nitriles	Amines	Amides
C3	0.95	1.22	1.50
C4	0.96	1.16	1.33
C5	0.97	1.12	1.25
C6	0.98	1.10	1.20
C7	0.98	1.08	1.17
C8	0.98	1.07	1.14
C9	0.98	1.06	1.13
C10	0.99	1.06	1.11
C11	0.99	1.05	1.10
C12	0.99	1.05	1.09
C13	0.99	1.04	1.08
C14	0.99	1.04	1.08

A.3. Hydrocarbons and oxygenates ASF distribution plots

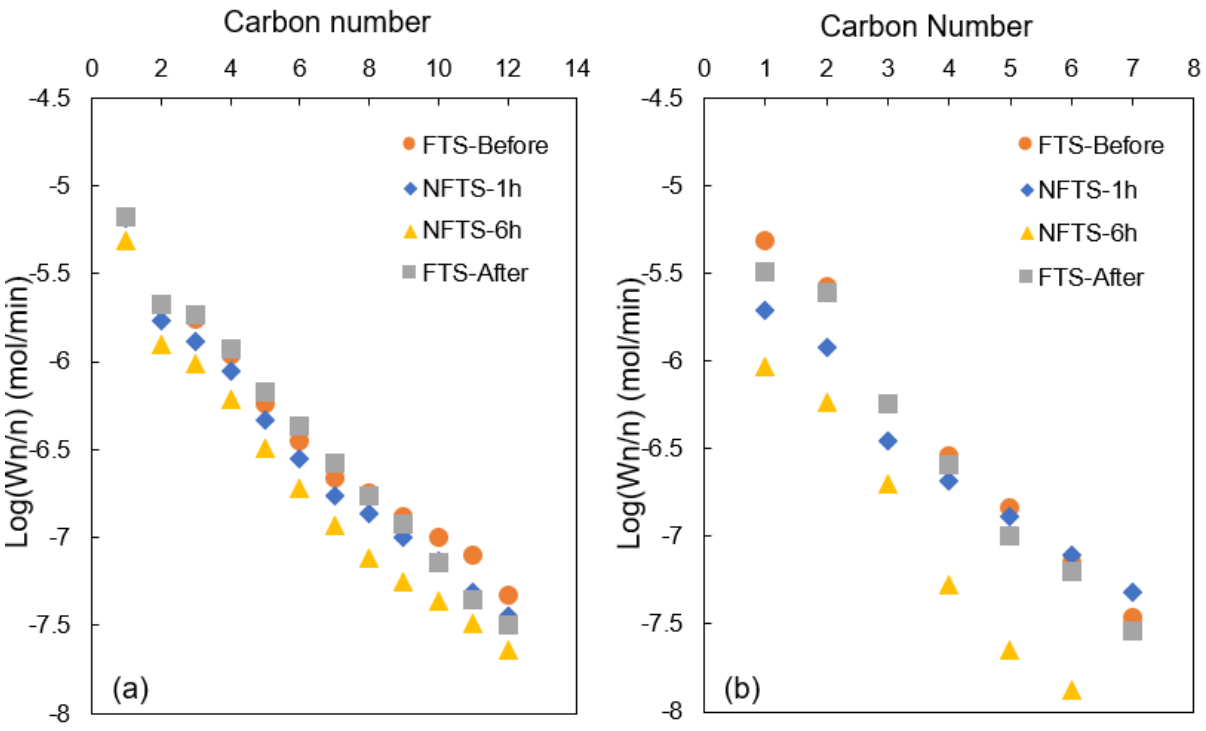

Figure A. 1: Hydrocarbons (a) and oxygenates (b) ASF distribution plots obtained during the reaction stages over the Fe,Mn-CuZnO catalyst.

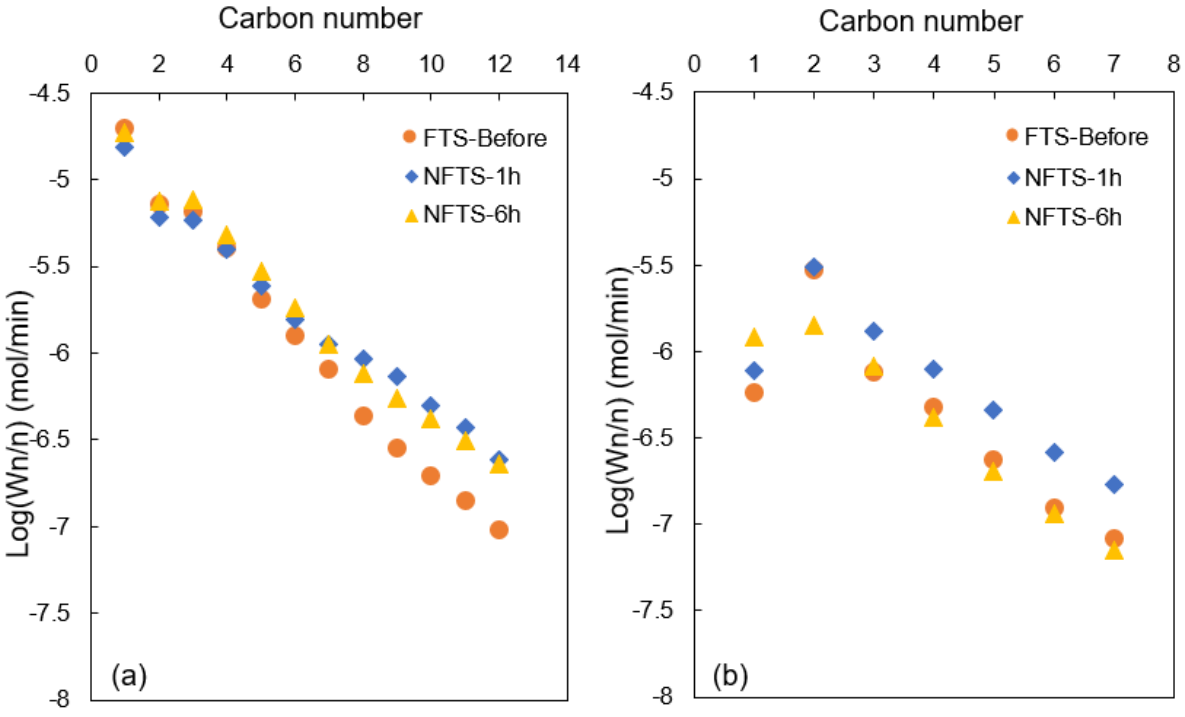

Figure A. 2: Hydrocarbons (a) and oxygenates (b) ASF distribution plots obtained during the reaction stages over the K,Al-Fe catalyst.

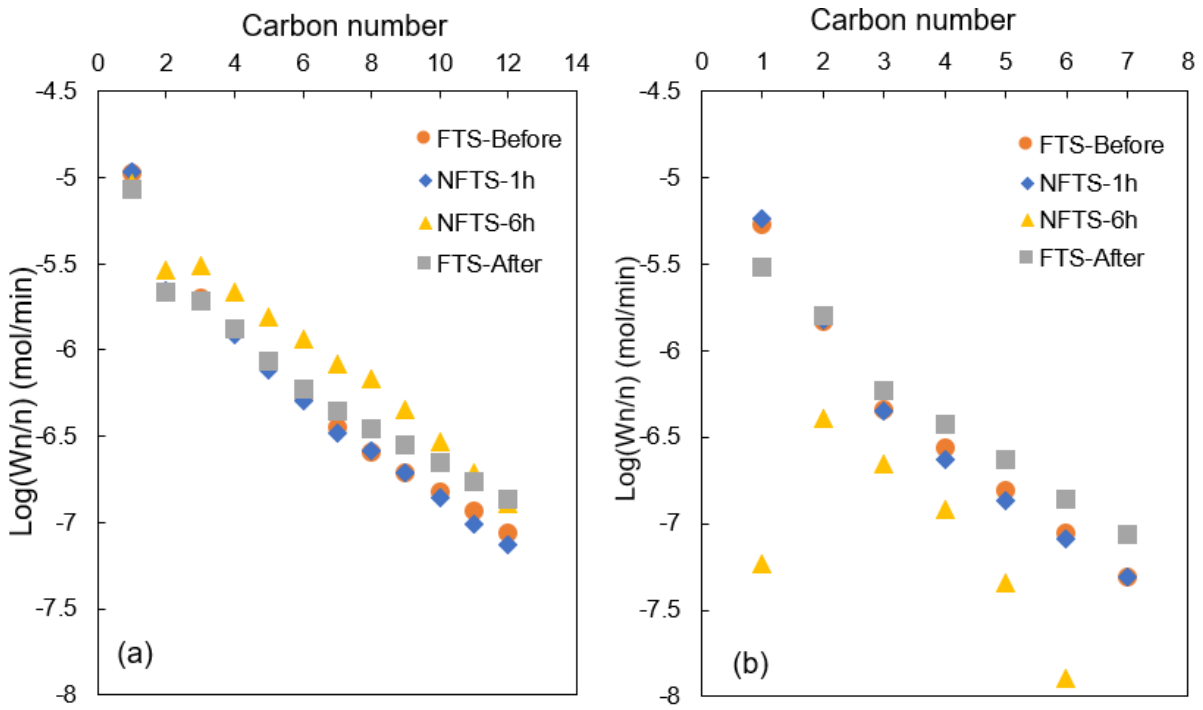

Figure A. 3: Hydrocarbons (a) and oxygenates (b) ASF distribution plots obtained during the reaction stages over the 10 wt% Fe/Al_2O_3 catalyst.

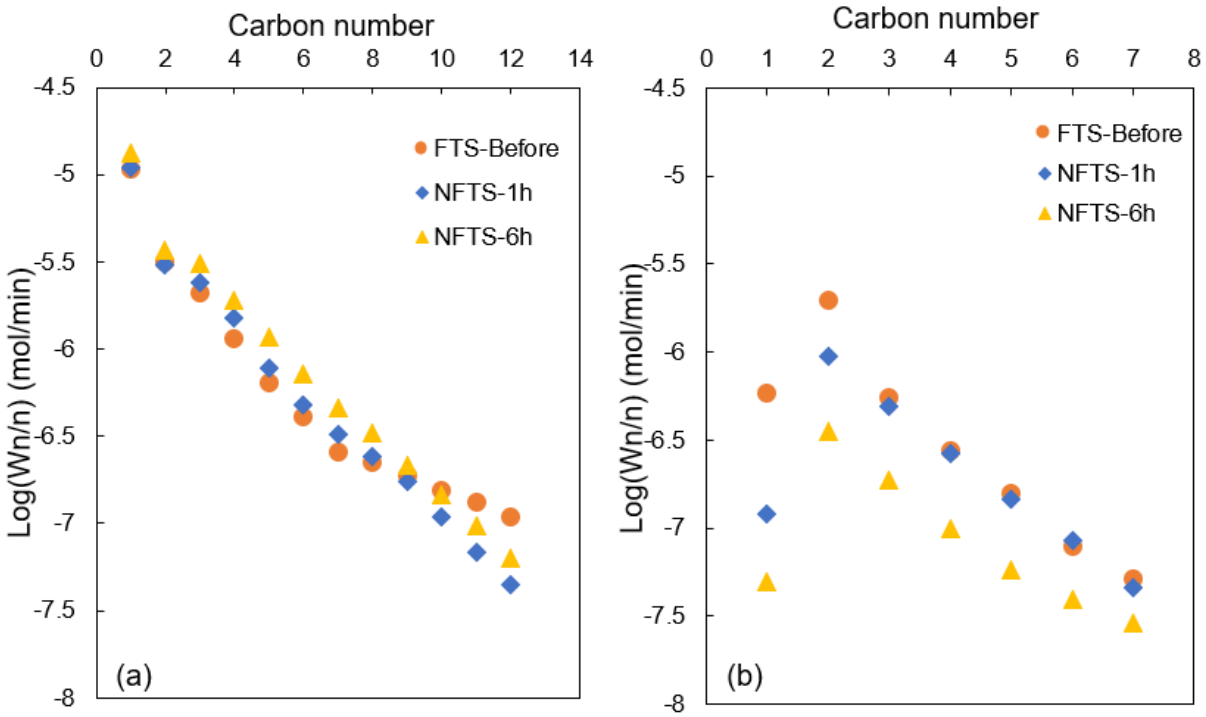

Figure A. 4: Hydrocarbons (a) and oxygenates (b) ASF distribution plots obtained during the reaction stages over the K-$CuFe/Al_2O_3$ catalyst.

A.4. Ethics Form

Application for Approval of Ethics in Research (EiR) Projects
Faculty of Engineering and the Built Environment, University of Cape Town

APPLICATION FORM

Please Note:
Any person planning to undertake research in the Faculty of Engineering and the Built Environment (EBE) at the University of Cape Town is required to complete this form **before** collecting or analysing data. The objective of submitting this application *prior* to embarking on research is to ensure that the highest ethical standards in research, conducted under the auspices of the EBE Faculty, are met. Please ensure that you have read, and understood the **EBE Ethics in Research Handbook** (available from the UCT EBE, Research Ethics website) prior to completing this application form: http://www.ebe.uct.ac.za/ebe/research/ethics1

APPLICANT'S DETAILS		
Name of principal researcher, student or external applicant		Danielle Sympathie Goho
Department		Chemical Engineering
Preferred email address of applicant:		Ghxdan001@myuct.ac.za
If Student	Your Degree: e.g., MSc, PhD, etc.	MSc In Chemical Engineering
	Credit Value of Research: e.g., 60/120/180/360 etc.	120
	Name of Supervisor (if supervised):	Prof Michael Claeys
If this is a researchcontract, indicate the source of funding/sponsorship		Click here to enter text.
Project Title		The selective production of nitrogen containing compounds via a modified Fischer-Tropsch

I hereby undertake to carry out my research in such a way that:

- there is no apparent legal objection to the nature or the method of research; and
- the research will not compromise staff or students or the other responsibilities of the University;
- the stated objective will be achieved, and the findings will have a high degree of validity;
- limitations and alternative interpretations will be considered;
- the findings could be subject to peer review and publicly available; and
- I will comply with the conventions of copyright and avoid any practice that would constitute plagiarism.

SIGNED BY	Full name	Signature	Date
Principal Researcher/ Student/External applicant	Danielle Sympathie Goho	Signature Removed	**09 Jan 2019**

APPLICATION APPROVED BY	Full name	Signature	Date
Supervisor (where applicable)	Prof Michael Claeys	Signature Removed	Click here to enter a date.
HOD (or delegated nominee) Final authority for all applicants who have answered NO to all questions in Section1; and for all Undergraduateresearch (Including Honours).	AJ ISAFIADE Click here to enter text.	Signature Removed	16 JAN 2019 Click here to enter a date.
Chair : Faculty EIR Committee For applicants other than undergraduate students who have answered YES to any of the above questions.			